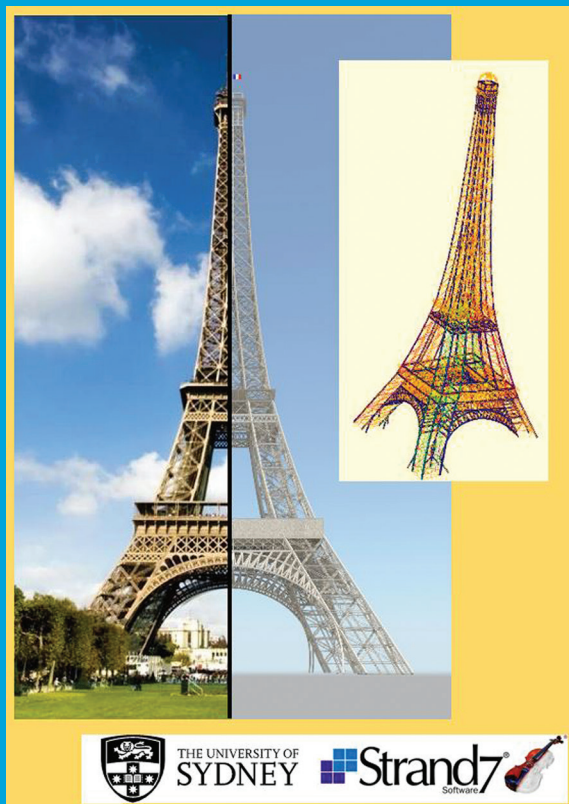


Volume 1762

 **Conference collection**

Numerical Methods in Civil Engineering Dynamics of Structures



Sydney, Australia

23 May-1 June 2016

Editor

Fernando Alonso-Marroquin

AIP | Conference Proceedings

proceedings.aip.org



AIP Proceedings: A name your community will know and respect

40 years' experience • 100,000+ papers • 1,600+ volumes

A world-class proceedings service for all events: From workshops to the largest international conference

- Online-only proceedings
- Optional printed copies or CDs for participants
- Rapid online and print publication

Our wealth of experience and expertise will ensure an outstanding publication experience.

Publication fees which work with your budget

- **Simple online publication fees:** Completely independent of page counts, publish substantial papers at no extra cost.
- **Options for online access:** 1-year conference access or select perpetual open access for the entire community.

Flexibility in the printed medium

Choose from these options to print all papers or just a selection of articles from the conference:

Conference collection

- Printed copies containing all papers published in the online proceedings.
- For editors who want to reproduce all online papers for their participants.

Selected papers

- Printed copies containing a selection of papers chosen by the editors.
- Choose to print just the best work, avoid the cost of printing everything.

Workshops and summer schools

- Printed copies designed especially for summer schools and workshops.
- Visibility and identity for events publishing tutorials and reviews.

Get a proposal for your proceedings in 3 simple steps

Step 1.

Obtain a proceedings questionnaire by writing to us at confproc@aip.org or download from proceedings.aip.org

Step 2.

Fill in the questionnaire with details of your conference and return it to confproc@aip.org

Step 3.

We'll review the questionnaire and your requirements and write to confirm if we can offer a proposal.



ISBN 978-0-7354-1420-4
ISSN 0094-243X

AIP

Numerical Methods in Civil Engineering

Vol. 1762

Numerical Methods in Civil Engineering

Dynamics of Structures

Sydney, Australia

23 May–1 June 2016

Editor

Fernando Alonso-Marroquin

The University of Sydney, Sydney, Australia

Sponsoring Organizations

Strand7 Pty Limited

The University of Sydney

All papers have been peer reviewed.



Melville, New York, 2016
AIP Conference Proceedings

Volume 1762

To learn more about AIP Conference Proceedings visit <http://proceedings.aip.org>

Editor

Fernando Alonso-Marroquin

The University of Sydney
School of Civil Engineering J05
Sydney NSW 2006
Australia

Email: fernando@sydney.edu.au

Authorization to photocopy items for internal or personal use, beyond the free copying permitted under the 1978 U.S. Copyright Law (see statement below), is granted by the AIP Publishing LLC for users registered with the Copyright Clearance Center (CCC) Transactional Reporting Service, provided that the base fee of \$30.00 per copy is paid directly to CCC, 222 Rosewood Drive, Danvers, MA 01923, USA: <http://www.copyright.com>. For those organizations that have been granted a photocopy license by CCC, a separate system of payment has been arranged. The fee code for users of the Transactional Reporting Services is: 978-0-7354-1420-4/16/\$30.00



© 2016 AIP Publishing LLC

No claim is made to original U.S. Government works.

Permission is granted to quote from the AIP Conference Proceedings with the customary acknowledgment of the source. Republication of an article or portions thereof (e.g., extensive excerpts, figures, tables, etc.) in original form or in translation, as well as other types of reuse (e.g., in course packs) require formal permission from AIP Publishing and may be subject to fees. As a courtesy, the author of the original proceedings article should be informed of any request for republication/reuse. Permission may be obtained online using RightsLink. Locate the article online at <http://proceedings.aip.org>, then simply click on the RightsLink icon/"Permissions/Reprints" link found in the article abstract. You may also address requests to: AIP Publishing Office of Rights and Permissions, 1305 Walt Whitman Road, Suite 300, Melville, NY 11747-4300, USA; Fax: 516-576-2450; Tel.: 516-576-2268; E-mail: rights@aip.org.

ISBN 978-0-7354-1420-4

ISSN 0094-243X

Printed in the United States of America

AIP Conference Proceedings, Volume 1762
Numerical Methods in Civil Engineering
Dynamics of Structures

Table of Contents

Preface: Numerical Methods in Civil Engineering: Dynamics of Structures	010001
Transient dynamic analysis of the Bao'An Stadium David Knight, Rowan Whitefield, Eric Nhieu, Faham Tahmasebinia, Peter Ansourian, and Fernando Alonso-Marroquin	020001
Dynamic analysis of the BMW tower in Munich Joaquin Indacochea-Beltran, Pearl Elgindy, Elaine Lee, Thiviya Vignesh, Peter Ansourian, Faham Tahmasebinia, and Fernando Alonso Marroquin	020002
Blasting response of the Eiffel Tower Lachlan Horlyck, Kieran Hayes, Ryan Caetano, Faham Tahmasebinia, Peter Ansourian, and Fernando Alonso-Marroquin	020003
Façade Greening: High-rise apartment building in Milan using pre-stressed concrete slab Wenning Sun, Mingxin Li, Yinong Han, Moqi Wang, and Peter Ansourian	020004
Full dynamic model of Golden Gate Bridge Thomas Game, Cameron Vos, Rafid Morshedi, Rebecca Gratton, Fernando Alonso-Marroquin, and Faham Tahmasebinia	020005
Dynamic analysis of the Milad Tower Edwin Wilhelm, Mitchell Ford, Darren Coelho, Lachlan Lawler, Peter Ansourian, Fernando Alonso-Marroquin, and Faham Tahmasebinia	020006
Energy balance in the WTC collapse Kaiqi Zhu, Kang Xu, Peter Ansourian, Faham Tahmasebinia, and Fernando Alonso-Marroquin	020007

PREFACE: Numerical Methods in Civil Engineering: Dynamics of Structures

We proudly present our new edition of the work by our Civil Engineering students of The University of Sydney on finite element modelling using Strand7 software. Our focus this year is the modelling of the response of landmark buildings under dynamics actions.

Since 1988, the Strand7-Finite Element Analysis Software has been developed by Strand7 Pty Limited in Sydney, Australia. Early development on a predecessor of Strand7 was undertaken by academics of the University of Sydney and University of New South Wales in the mid 80's. Today Strand7 is an internationally renowned, well-established, finite element software. Strand7 has strong and versatile capabilities for dynamics analysis. Extremely efficient in-built solvers in Strand7 allows linear and non-linear transient dynamics, natural frequency, spectral response, quasistatic analysis, and linear and non-linear transient heat transfer analysis.

Here we present a selection of the Strand7 dynamic analyses performed on highly complex civil engineering structures. We start with a dynamics analysis of the Bao'an stadium in Shenzhen, China. The transient dynamics solver allows calculations of the earthquake response in this particular structure where standard spectral analysis shows slow convergence. We perform a fully dynamics analysis of the BMW Tower. This emblematic suspending structure in Munich, Germany proved the capabilities of Strand7 to model highly complex geometries in buildings under fire and wind loads. The Golden Gates Bridge's paper provides an excellent investigation of the bridge response to dead load, static load, wind load, and spectral seismic loads. The response of the cables of this enormous structure is investigated in detail using dedicated cable elements available in Strand7. The project on the Milad Tower in Tehran, Iran, provides the dynamics response of this tall building under wind load. The analysis is based on the Davenport spectral response formulation, which is much less expensive than computational fluid dynamics calculations.

Some contributions aim to face current challenges in our society: we present a blasting analysis on the iconic Eiffel Tower in Paris, France. A superb investigation based on original construction drawings largely replicates the existing tower. Aiming to bring wilderness to large cities, we explore the use of prestresses concrete slabs in vertical forests such as the Green Façade in Milan, Italy. Finally, the energy balance analysis of the collapse of the Twin Towers in New York, USA, confirms that the energy released by the aircraft fuel was sufficient to produce a localised buckling collapse after 2hrs of heat exposure.

Special thanks to Coraline Chiew for designed the cover.

Fernando Alonso-Marroquin

School of Civil Engineering, The University of Sydney

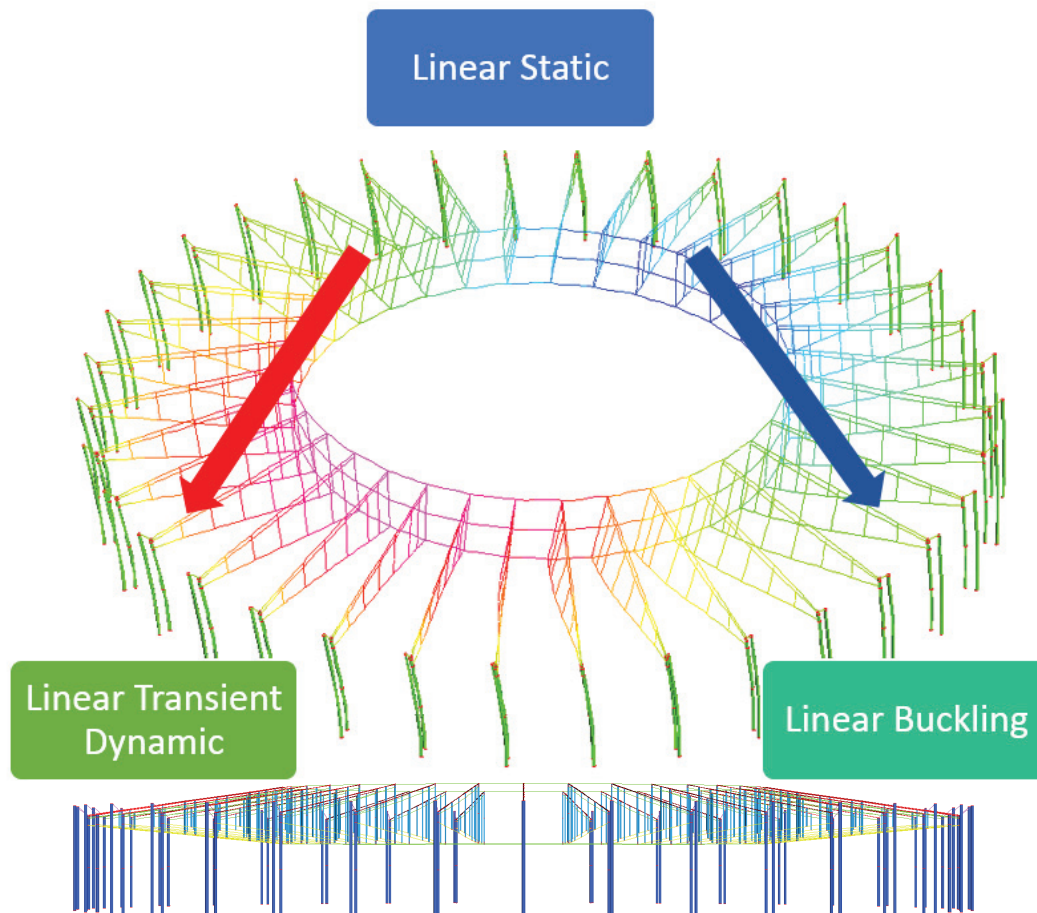
Transient Dynamic Analysis of the Bao'An Stadium

David Knight, Rowan Whitefield, Eric Nhieu, Faham Tahmasebinia, Peter Ansourian, and Fernando Alonso-Marroquin ^{a)}

School of Civil Engineering, the University of Sydney, Sydney NSW 2006 Australia

^{a)}Corresponding author: fernando@sydney.edu.au

Abstract. Bao'An Stadium is a unique structure that utilises 54m span cantilevers with tensioned members to support the roof. This report involves a simplified finite element model of Bao'An stadium using Strand7 to analyse the effects of deflections, buckling and earthquake loading. Modelling the cantilevers of the original structure with a double curvature was problematic due to unrealistic deflections and no total mass participation using the Spectral Response Solver. To rectify this, a simplified symmetrical stadium was created and the cable free length attribute was used to induce tension in the inner ring and bottom chord members to create upwards deflection. Further, in place of the Spectral Response Solver, the Transient Linear Dynamic Solver was inputted with an El-Centro earthquake. The stadium's response to a 0.20g earthquake and self-weight indicated the deflections satisfied AS1170.0, the loading in the columns was below the critical buckling load, and all structural members satisfied AS4100.



INTRODUCTION

Bao'An stadium is an iconic structure that has structural columns inspired by local bamboo forests, intended to create a prominent feature in Shenzhen China. The structure has a circular shape with an outer diameter of 236m and an inner diameter of 128m. A lightweight roof structure with a polytetrafluoroethylene membrane is cantilevered 54m to provide shelter for spectators. The stadium is a complex structure due to the inclusion of the inner ring cables that have a pre tension of 3600 kN in the top cable, and 1800 kN in the bottom cable. These cables are supported through a lightweight truss system comprising of thin cables that extend to the external columns which also support a large compression ring. The columns are large circular hollow sections ranging in sizes from 550 mm to 800 mm. The stadium behaves similar to a bicycle wheel, the trusses equivalent to tension spokes of the wheel and the rim representing the outer compression ring (Guo et al., 2011; Tian et al., 2011). The stadium has a gross floor area of 88,500 m² and was constructed over a 2 year period. TABLE 1 shows the main details.

The key structural components supporting the stadium roof are long span cantilevered members. This is achieved through the use of tensioned cables as the bottom chord and a tapered truss geometry that creates upward deflection (Guo et al., 2013). This report investigates how the cantilevers of Bao'An stadium prevent deflections under self-weight and dynamic earthquake loading.

TABLE 1. Building details

Location: Shenzhen China	The year of build: 2009-2011
Architects: GMP Architekten	Overall height: 39.65m
Structural Engineers: Schlaich Bergermann Und Partner	Floor area: 88,500 m ²
Function: Sports stadium primarily constructed for the Universiade	Car spaces: 750
The structure of the plan: A large circular roof structure with a circular rings at the centre supported on a complicated external column geometry ranging from 550 mm to 800 mm	Occupant capacity: 40,050

PRELIMINARY STRUCTURAL MEMBERS

There is a lack of detailed information in the literature on the member sizing and properties. This resulted in the majority being estimated from pictures. The members chosen for the Strand7 model were based on images from Ferguson (2011) and structural journals (Guo et al., 2011; Guo et al., 2013; Tian et al., 2011). TABLE 2 shows the members chosen for the structure. The detailed member selection process is contained in APPENDIX 1. The key criteria for the selection of the members was vertical deflection limits, ideally stiff, light weight members. This is achieved with the selection of circular hollow sections for majority of the structural members.

TABLE 2. Structural elements

Structural Element	Size of elements (mm)	Dead Load (kN/m)
External Columns	800x50 CHS	9.07
Box Girder	200 x 100	1.54
Top Chord	250 x 30 CHS	1.60
Bottom Chord	200 x 5 CHS	0.24
Cables	10 mm Cable	-
Vertical Truss Members	400 x 10 CHS	-
Roof Membrane - polytetrafluoroethylene	1mm	0.20

STRUCTURAL SYSTEM

Bao'An stadium consists of a complex structural system to resist vertical and lateral loads. Vertical loads are resisted as shear flows through the roof truss. These are then transferred to the columns as bending moments through a fixed connection, and then transferred to the foundations. The membrane roof is connected continuously to the top chord to completely suppress all buckling modes. Vertical truss members also act as spring stiffeners to reduce the effective length to the lower chord to prevent large buckling modes. The ring cables are pre tensioned to prevent any compressive stresses causing sagging catenary actions. Lateral loads are resisted by the very stiff columns which are stabilised by the outer compression rings.

Long Span Cantilever

To demonstrate how the cantilevers can resist deflection, a single column-roof section has been analysed. The self-weight of all the roof members are treated as an applied uniformly distributed load on the top chord. The bottom chord is pre-tensioned to prevent compressive stresses while the inner ring is in tension to limit deflections. FIGURE 1(a) shows the overall action of the tensioned cables in the bottom chord and bottom inner ring. The net resultant force is acting inwards because the inner ring is tensioned higher. FIGURE 1(b), shows a free body diagram of a typical column-roof section with the applied tensile force 'T' as the resultant action of cable tension, this tensile force T may be chosen to minimise the deflection of the cantilever. FIGURE 1(c) shows how this effectively creates an applied moment that resists deflection.

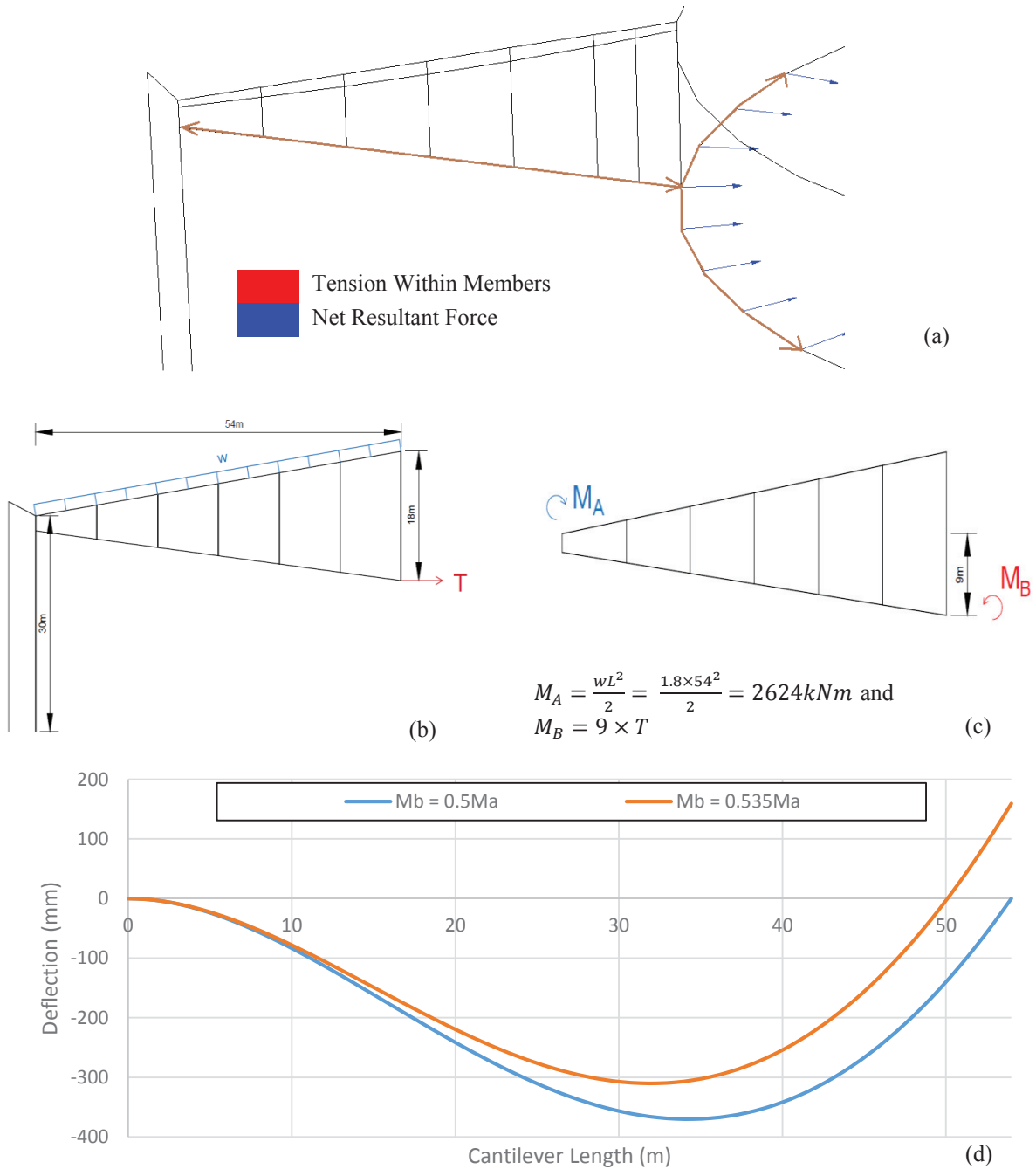


FIGURE 1. (a) Net resultant force of single section (b) Free body diagram of a column-roof section (c) Free body diagram of a truss cantilever (d) Comparison of deflected shape with applied end moment

The truss is treated as a cantilevered beam with constant second moment of area, it can be shown that the moment EQUATION (1) can be integrated twice (2) for deflection:

$$M(x) = \frac{w}{2}(x^2 - 2L) - M_b \quad (1)$$

$$v(x) = \iint -\frac{M}{EI} dx = -\frac{wx^2}{24EI}(x^2 - 4xL + 6L^2) + \frac{M_b x^2}{EI} \quad (2)$$

The cantilevered beam is assumed to have a depth of 9m as shown in FIGURE 1(b). The stiffness was then calculated using the parallel axis theorem. A model was created to visualise the deflected shape and optimised the applied moment M_B to an appropriate value. In FIGURE 1(d) it was found that zero deflection at the free end of the cantilever occurred when the end moment was half the support moment, $M_B = 0.5M_A$. Further, through trial and error the sagging and hogging deflections were minimised, at a value of $M_B = 0.535M_A$. The resulting deflections were -295.6 mm downward and 230.9 mm upward with a theoretical tensile value of 156.00 kN.

$$M_B = 0.535M_A = 0.535 \times 2624 = 1403 \text{ kNm} \quad (3)$$

$$T = \frac{M_B}{9m} = \frac{1404 \text{ kNm}}{9m} = 156.00 \text{ kN} \quad (4)$$

DESIGN AIMS

Deflection

The key parameter in the design was to limit the deflections experienced in the 54m cantilever. The process involved modelling a singular column section and optimising the structure with cable elements to effectively reduce the deflections. Once the deflections were satisfied, the stresses were checked and a buckling analysis was done. The structure was then copied every 10° about the vertical axis to complete the model. The guide for acceptable deflections is stated in AS1170.0 as EQUATION 5;

$$\delta = \frac{L}{120} = \frac{54}{120} = 0.45m \quad (5)$$

Buckling Analysis

Perfect Euler

The column was assumed to be a vertical cantilever with restraints at the top to be free and the bottom to be translation and rotation fixed. The buckling length of the column was assumed to be half in EQUATION 6:

$$P = \frac{\pi^2 EI}{4L^2} = \frac{\pi^2 \times 200000 \times 8.32 \times 10^9}{4 \times (32000)^2} = 4010 \text{ kN} \quad (6)$$

Strand7 – Linear Buckling Analysis

The first mode of buckling was done with no gravity and then gravity applied. The eigenvalue and critical buckling loads were found by strand7 using EQUATION 7.

$$P_{applied} \times \lambda = P_{crit} \quad (7)$$

Earthquake Analysis

For a transient solver with damping, the global matrix equation is listed as EQUATION 8 below where M, C, and K are the mass, damping and stiffness matrices respectively. $Mrg(t)$ represents the external force (base acceleration) acting on the mass where r is an arbitrary vector and g(t) is the earthquake acceleration.

$$M\ddot{U} + C\dot{U} + KU = Mrg(t) \quad (8)$$

Before applying an earthquake, the structure was observed to be oscillating. To reduce oscillations, Rayleigh damping was applied and the earthquake was run at 600 seconds after the initial vibrations were sufficiently damped. It was found that the spectral response solver solutions produced mass participation factors of zero. The assumption of a combination of modal shapes was not applicable hence the need for a Transient Dynamic Solver.

METHODOLOGY

Cylindrical Coordinates & Online Editor for 3D Model

In Strand7, a single 2D column was created according to the nodes and elements in FIGURE 2. To create a 3D model, the online editor tool was used to import the coordinates of the nodes for the columns and inner ring beams from a spreadsheet. The nodes for the columns and ring beams were set every 10° and the appropriate beam elements were selected as per (Guo et al., 2013). Using this process, the column section in FIGURE 2 was copied around a central axis to form the completed 3D model of the stadium as shown in FIGURE 3.

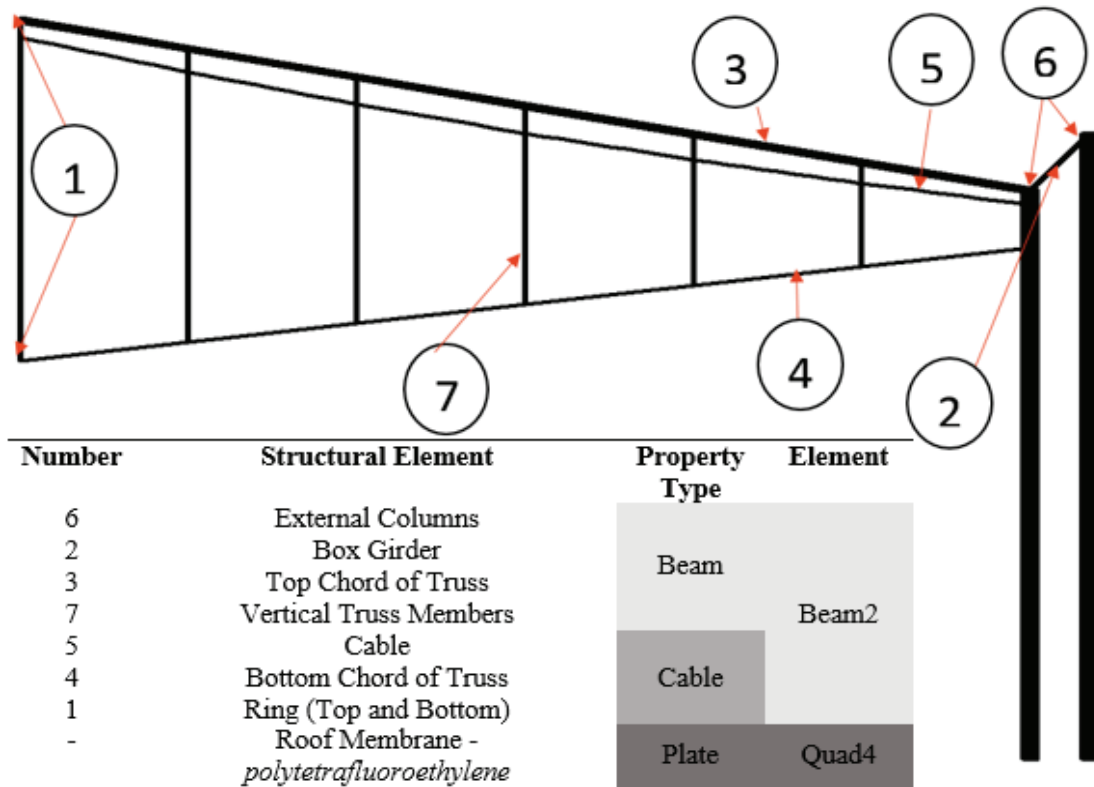


FIGURE 2. Schematic of structural members

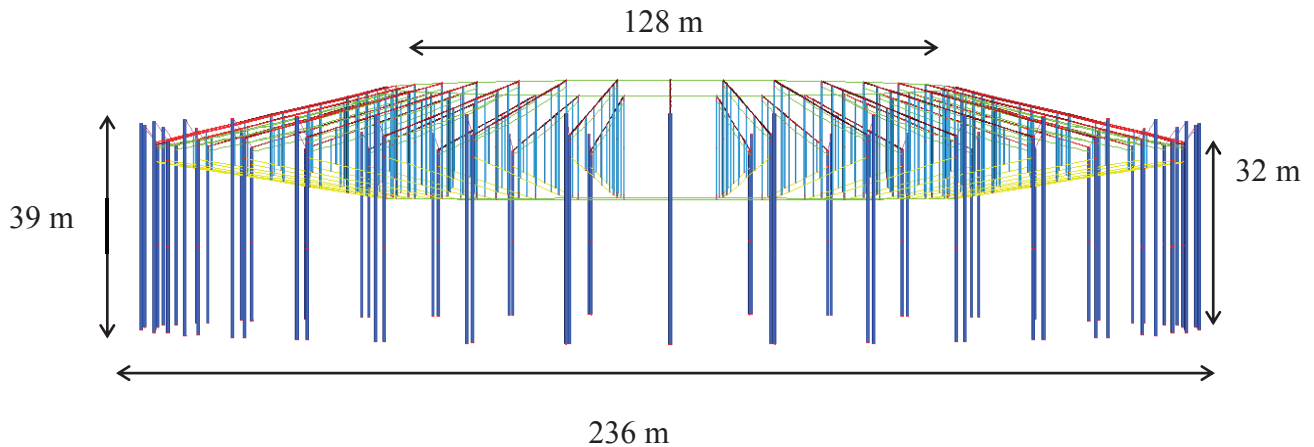


FIGURE 3. Section view

Modelling Limitations

In this model, the roof was lighter than the actual stadium due to purlins that are supporting the Teflon roof not being modelled. It could be expected that the required cable tension would be higher than the value obtained from Strand7.

The double curvature of the roof was ignored to allow for a simple structure resembling a cantilever spanning 54m. The flat roof allowed for each cantilever section to deflect equally. In an initial model, incorporating the curves in the roof resulted in collapse.

The outer ring beams were not included in the model since they proved to be redundant in minimising deflections. The columns are significantly large and the box girder connecting the beams provided sufficient restraint.

Cable Elements

Cable elements required a non-linear analysis due to the deformed geometry of the cable. In the linear static analysis, the load in the cable acted in the vertical direction only. In the nonlinear analysis the load is applied on the deformed shape so it has orthogonal and parallel components to the cable. The effect of having the parallel component is that axial shortening occurs. When running the nonlinear solver, the vertical deflection increased by 2mm and was not significant.

To reduce deflections, the Cable Free Length attribute is a key parameter that can be modified to induce tension in the cable elements. The Cable Free Length of the bottom chord was chosen to be 8m with the original cable length as 8.55m. The Cable Free Length of the bottom inner ring beam was chosen to be 9.5m given the actual length is 11.5m.

The second method for inducing tension in cable members is applying point loads. Radial point loads were applied which effectively mimicked the pre tension within the members as shown in FIGURE 1(a). Through this method, a loading of 565 kN was applied which resulted in a similar deflection of 140mm. The reason this method was not selected as it made the inner cables redundant as no load was being carried.

Linear Transient Dynamic Solver

To model the stadium's response to an earthquake, the El Centro earthquake data was used. The ground acceleration was similar to that expressed in the Chinese standard GB 50011-2011 which specified 0.2g. The acceleration vs time graphs for x, y and z were inputted as the base acceleration in the solver. The earthquake was applied at 600 seconds after the initial vibrations were sufficiently damped.

NUMERICAL ANALYSIS

Linear Buckling

A load case without gravity was computed to compare with the Perfect Euler mode of buckling. The eigenvalue converged on the first iteration as expected and P_{crit} was found to be 4039 kN. To find P_{crit} with gravity an initial load of 1 kN was applied and followed by six iterations. The results are summarised in the TABLE 3. Gravity induces extra compressive stresses so the column buckles earlier than perfect Euler.

TABLE 3. Buckling Analysis

Iteration	Force (kN)	Eigenvalue for Mode 1
1	1.0	27.650
2	27.6	23.384
3	646.6	5.103
4	3299.4	1.173
5	3869.6	1.006
6	3893.8	1.000
Buckling (Perfect Euler) 4010 kN	Buckling (Strand7 Gravity) 3894 kN	Buckling (Strand7 No Gravity) 4039 kN

Linear Static Solver

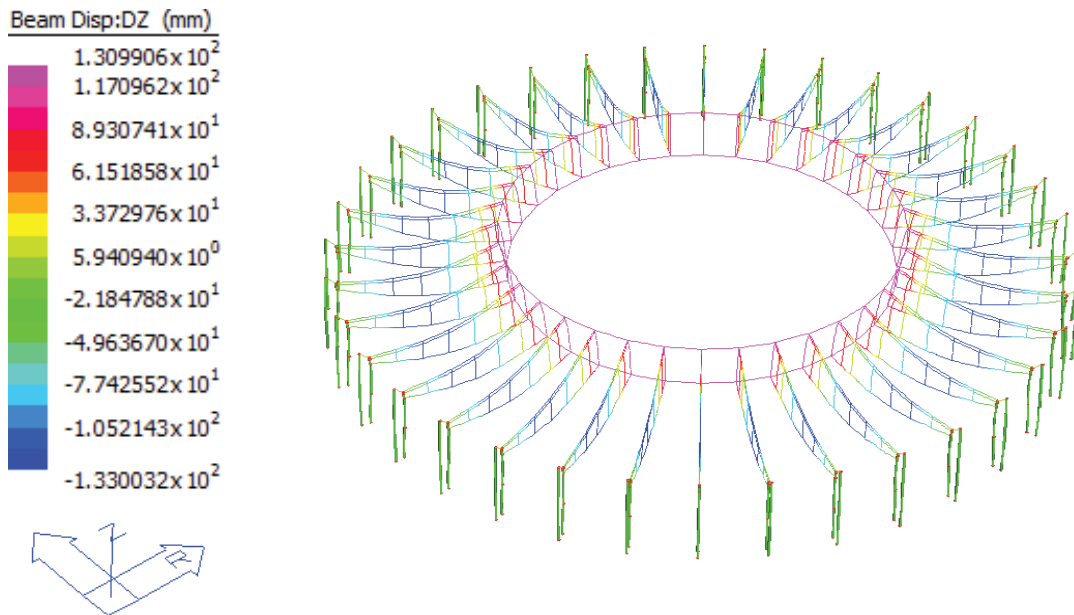


FIGURE 4. Vertical displacements for linear static

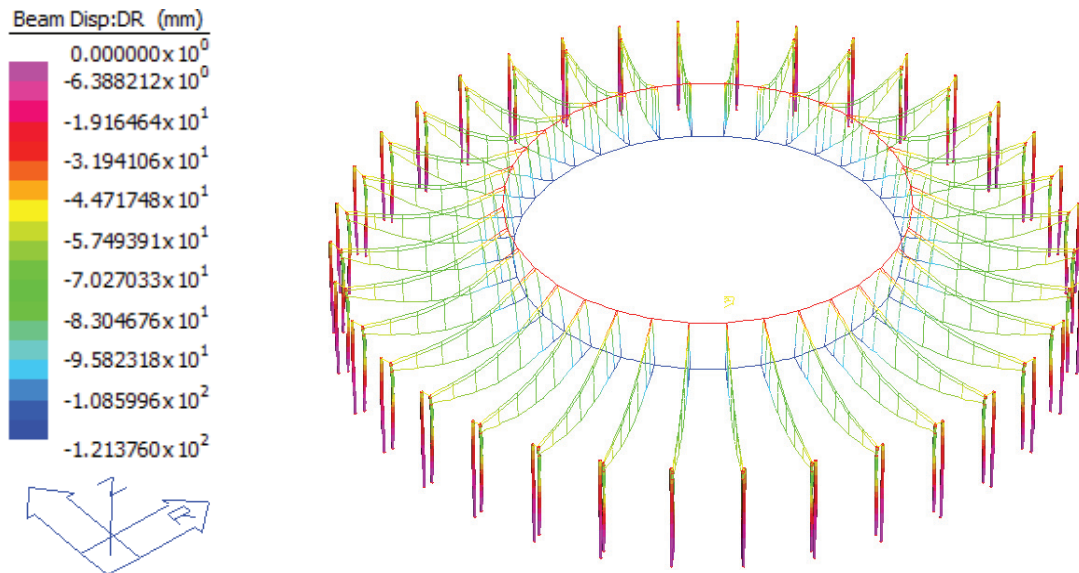


FIGURE 5. Radial displacements for linear static

FIGURE 4 shows a maximum deflection of 133 mm downward under self-weight and post-tension, well under the design limit of 450mm for serviceability. There is also an upward deflection of 131 mm induced by the tension in the bottom chord cable. FIGURE 5 shows the inner ring contracting inwards 121 mm in equilibrium. This contraction is due to the net resultant force of the inner ring in tension.

Linear Transient Dynamic Solver

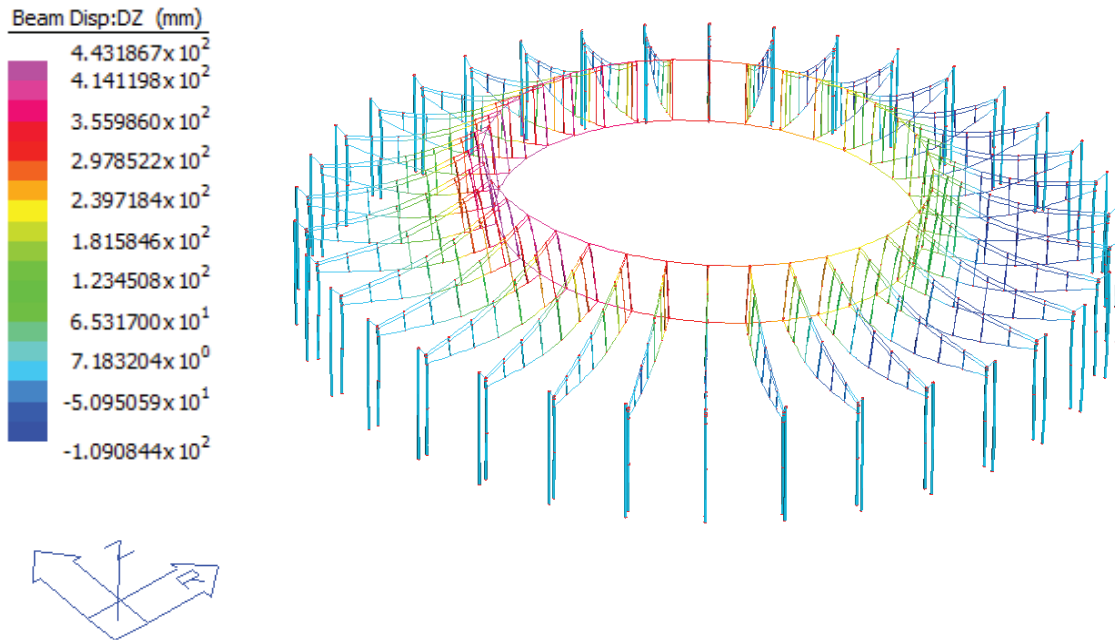


FIGURE 6. Vertical displacement for Linear Transient Dynamic Solver

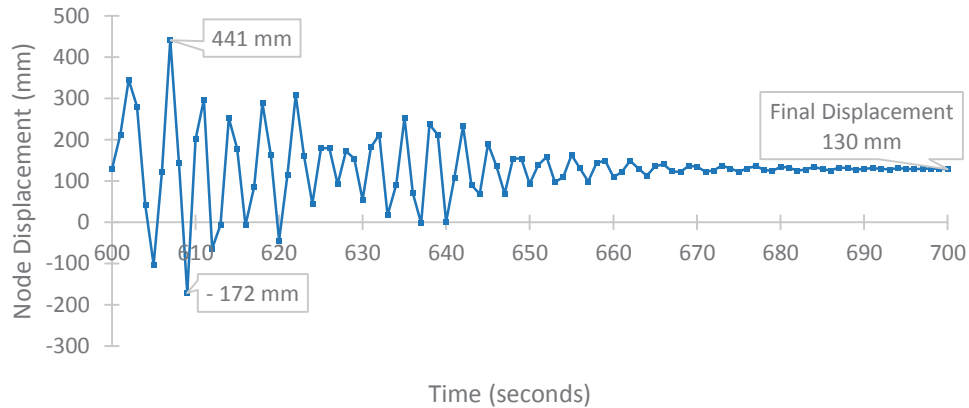


FIGURE 7. Vertical displacement El Centro

It was found no members reached yield capacity. The worst case base acceleration for El-Centro Earthquake occurred in the vertical direction, other directions were not critical. Due to symmetry, the maximum displacement is expected at the free end of the cantilever. FIGURE 6 shows this maximum beam displacement to be -109 mm in the Z direction. Note that this is different from the node displacement in FIGURE 7 of -172 mm. The final node displacements after the earthquake were equivalent to the linear static solver of 130 mm where the structure was in equilibrium as shown in FIGURE 7. These are below the AS1170.0 limit of 450 mm.

A Non-Linear Transient Dynamic Solver would account for deformed geometry. However following an initial simulation, this was found to be a time-consuming computation with non-convergence of time steps. A Linear Transient Dynamic Solver was chosen as it was time efficient.

STRUCTURAL DESIGN

TABLE 4 compares theoretical loadings using AS4100 with the Strand7 results. The calculations for AS4100 theoretical maximums are listed in APPENDIX 1.

TABLE 4. Strand7 results compared with AS4100 Serviceability requirements

Loading Type	Critical Member	Size	AS 4100 Maximum	Strand7 Results
Flexure	Top Chord	250x30 CHS	$M_i = 284 \text{ kNm}$	$M^* = 226 \text{ kNm}$
Axial	Column	800x50 CHS	$\phi N_c = 15624 \text{ kN}$	$N_c^* = 490 \text{ kN}$
Compression				
Axial Tension (Cables)	Inner Ring	10 mm Cable	$\phi N_t = 2142 \text{ kN}$	$N_t^* = 1551 \text{ kN}$
Axial Tension (Beams)	Top chord	250x30 CHS	$\phi N_t = 5971 \text{ kN}$	$N_t^* = 225 \text{ kN}$
Deflection	Top Chord	250x30 CHS	$\delta = 450 \text{ mm}$	$\delta^* = 133 \text{ mm}$
Critical Buckling Case	Column	800x50 CHS	$P_{crit} = 3894 \text{ kN}$	$P^* = 710 \text{ kN}$

CONCLUSIONS

The complex column structure was successfully simplified into a 2D model and rotated through 360° to create the 3D structure. The deflection of the cantilevers was the key criteria of design. Design aims for deflection, buckling and earthquake were satisfied. Axial loads and bending moments were checked after deflection was satisfied. Net upward deflections at the end of the cantilever were achieved with the use of tensioned cable elements and tapered out truss geometry which allowed flexibility of the bottom chord of the truss. The Teflon roof membrane was an efficient choice as a roof membrane as it fully restrained the top chord without contributing a large dead load. The combined action of buckling and axial load proved to be critical for the columns. There was sufficient capacity to handle self-weight and the El-Centro earthquake. The innovation of using tensioned cables in a bottom inner ring allowed for a long span cantilever roof.

REFERENCES

- CMC (2010). *Code for Seismic Design of Buildings (GB50011-2010)*. China Ministry of Construction, China Architecture and Building Press: Beijing, China. (in Chinese)
- Frearson, A., 2011. De Zeen Magazine. [Online]. Available at: <http://www.dezeen.com/2011/08/16/baoan-stadium-by-gmp-architekten>. [Accessed 12 May 2016].
- Guo, Y., Tian, G., Wang, K., Zhang, B., & Zhao, S. (2011). Tensioning experiment on spoke structural roof of Bao'An Stadium. *Journal of Building Structures*, 32(3), 1-10.
- Guo, Y., Wang, K., Sun, W., Tian, G., & Zhang, B. (2013). Research on key structural design problems of the Bao'An Stadium. *Journal of Building Structures*, 5 (1) 11-20.
- Ronstan (2011). *RPA112 Structural Cable Catalogue*. Adelaide, Australia.
- Standards Association of Australia (1998). *AS 4100 Steel Structures*, Sydney, Australia.
- Standards Association of Australia (2002). *AS1170.0 Structural Design Actions Part 0: General Principles*. Sydney, Australia.
- Strand 7 (2011). *ST7-1.40.35.3 Analysing Membrane Structures*. Sydney, Australia
- Strand 7 (2011). *ST7-1.40.35.8 Modelling Tension-Only or Compression-Only Structural Members*. Sydney, Australia
- Tian, G., Guo, Y., Zhang, B., Wang, K., & Zhao, S. (2011). Experiment on sensitivity to construction tolerance and research on tolerance control criteria in spoke structural roof of Bao'An Stadium. *Journal of Building Structures*, 32(3), 11-18.

APPENDIX 1

External Column

Axial Compression

Member subjected to axial compression design as per AS 4100

$A_g = 117810 \text{ mm}^2$, $I = 8.32 \times 10^9 \text{ mm}^4$, $k_f = 1$, $f_{yf} = 320 \text{ MPa}$, $f_u = 440 \text{ MPa}$

For compression $\phi = 0.9$ (Table 3.4)

Nominal Section Capacity (Clause 6.2.1)

$$\phi N_s = \phi k_f A_g f_y = 0.9 \times 1 \times 117810 \times 320 = 32,929.3 \text{ kN}$$

Nominal Member Capacity (Clause 6.3.3)

$$\lambda_n = \frac{l_e}{r} \sqrt{k_f} \sqrt{\frac{f_y}{250}} = \frac{30000}{\sqrt{\left(\frac{8.32 \times 10^9}{117810}\right)}} \sqrt{1} \left(\sqrt{\frac{320}{250}} \right) = 127.38$$

$\alpha_b = -1.0$ $\alpha_c = 0.4605$ (Table 6.3.3.3)

$$\therefore \phi N_{cx} = 0.4605 \times 32,929.3 = 15624.4 \text{ kN}$$

$$\therefore \phi N_s = 32,929.3 \text{ kN and } \phi N_c = 15624.4 \text{ kN}$$

Axial Tension

Yield capacity (Clause 7.2)

$$\phi N_y = \phi A_g f_y = 0.9 \times 117810 \times 320 = 32,929.3 \text{ kN}$$

Combined Actions

$$Z_e = \frac{I}{y_{max}} = \frac{8.32 \times 10^9}{400} = 20.8 \times 10^6 \text{ mm}^3 \quad S = \frac{\pi(d_{out}^4 - d_{in}^4)}{32 d_{out}} = \frac{\pi(800^4 - 700^4)}{32 \times 800} = 20.8 \times 10^9 \text{ mm}^3$$

$Z_c = \min[S, 1.5Z_e] = 20.8 \times 10^9$, $k_f = 1$, $f_{yf} = 320 \text{ MPa}$, $f_u = 440 \text{ MPa}$, $N^* = 710 \text{ kN}$, $M^* = 1298 \text{ kNm}$

$$M_s = f_y Z_e = 320 \times 20.8 \times 10^6 = 6656 \text{ kNm}$$

Section capacity (Clause 8.3.2) and in-plane capacity (Clause 8.4.2.2)

$$\phi M_r = \phi M_s \left(1 - \frac{N^*}{\phi N_s} \right) = 0.9 \times 6656 \left(1 - \frac{710}{32,929.3} \right) = 5865 \text{ kNm}$$

$$\phi M_i = \phi M_s \left(1 - \frac{N^*}{\phi N_c} \right) = 0.9 \times 6656 \left(1 - \frac{710}{15624.4} \right) = 5718.2 \text{ kNm}$$

SATSIFACTORY

Top Chord

Axial Compression

Member subjected to axial compression design as per AS 4100

$A_g = 20734.5 \text{ mm}^2$, $I = 1.2778 \times 10^8 \text{ mm}^4$, $k_f = 1$, $f_{yf} = 320 \text{ MPa}$, $f_u = 440 \text{ MPa}$

For compression $\phi = 0.9$ (Table 3.4)

Nominal Section Capacity (Clause 6.2.1)

$$\phi N_s = \phi k_f A_g f_y = 0.9 \times 1 \times 20734.5 \times 320 = 5971 \text{ kN}$$

Nominal Member Capacity (Clause 6.3.3)

$$\lambda_n = \frac{l_e}{r} \sqrt{k_f} \sqrt{\frac{f_y}{250}} = \frac{8630}{\sqrt{\left(\frac{1.2778 \times 10^8}{20734.5}\right)}} \sqrt{1} \left(\sqrt{\frac{320}{250}} \right) = 124$$

$\alpha_b = -1.0$ $\alpha_c = 0.476$ (Table 6.3.3.3)

$$\therefore \phi N_{cx} = 0.476 \times 5971 = 2842.2 \text{ kN}$$

$$\therefore \phi N_s = 5971 \text{ kN and } \phi N_c = 2842.2 \text{ kN}$$

Axial Tension

Yield capacity (Clause 7.2)

$$\phi N_y = \phi A_g f_y = 0.9 \times 20734.5 \times 320 = 5971 \text{ kN}$$

Combined Actions

$$Z_e = \frac{I}{y_{max}} = \frac{1.2778 \times 10^8}{125} = 1022 \times 10^3 \text{ mm}^3 \quad S = \frac{\pi(d_{out}^4 - d_{in}^4)}{32 d_{out}} = \frac{\pi(250^4 - 190^4)}{32 \times 250} = 1022 \times 10^3 \text{ mm}^3$$

$Z_c = \min[S, 1.5Z_e] = 1022 \times 10^3$, $k_f = 1$, $f_{yf} = 320 \text{ MPa}$, $f_u = 440 \text{ MPa}$, $N^* = 225 \text{ kN}$, $M^* = 226 \text{ kNm}$

$$M_s = f_y Z_e = 320 \times 1022 \times 10^3 = 327 \text{ kNm}$$

Section capacity (Clause 8.3.2) and in – plane capacity (Clause 8.4.2.2)

$$\phi M_r = \phi M_s \left(1 - \frac{N^*}{\phi N_s}\right) = 0.9 \times 327 \left(1 - \frac{225}{5971}\right) = 290 \text{ kNm}$$

$$\phi M_i = \phi M_s \left(1 - \frac{N^*}{\phi N_c}\right) = 0.9 \times 327 \left(1 - \frac{225}{2842.2}\right) = 284 \text{ kNm}$$

SATISFACTORY

Box Girder

Axial Compression

Member subjected to axial compression design as per AS 4100

$A_g = 20000 \text{ mm}^2$, $I_x = 1.667 \times 10^7 \text{ mm}^4$, $I_y = 6.667 \times 10^7 \text{ mm}^4$, $k_f = 1$, $f_{yf} = 320 \text{ MPa}$, $f_u = 440 \text{ MPa}$

For compression $\phi = 0.9$ (Table 3.4)

Nominal Section Capacity (Clause 6.2.1) X AXIS

$$\phi N_s = \phi k_f A_g f_y = 0.9 \times 1 \times 20000 \times 320 = 5760 \text{ kN}$$

Nominal Member Capacity (Clause 6.3.3)

$$\lambda_{nx} = \frac{l_e}{r} \sqrt{k_f} \sqrt{\frac{f_y}{250}} = \frac{4243}{\sqrt{\left(\frac{1.667 \times 10^7}{20000}\right)}} \sqrt{1} \left(\sqrt{\frac{320}{250}}\right) = 5.76$$

$$\alpha_b = -1.0 \quad \alpha_c = 1 \text{ (Table 6.3.3.3)}$$

$$\therefore \phi N_{cx} = \phi N_{sx} = 5760 \text{ kN}$$

Y AXIS

$$\lambda_{ny} = \frac{l_e}{r} \sqrt{k_f} \sqrt{\frac{f_y}{250}} = \frac{4243}{\sqrt{\left(\frac{6.667 \times 10^7}{20000}\right)}} \sqrt{1} \left(\sqrt{\frac{320}{250}}\right) = 83.14$$

$$\alpha_b = -1.0$$

$$\alpha_c = 0.7885 \text{ (Table 6.3.3.3)}$$

$$\therefore \phi N_{cy} = 0.7885 \times 5760 = 4541.76 \text{ kN}$$

$$\therefore \phi N_s = 5760 \text{ kN}, \phi N_{cx} = 5760 \text{ kN} \text{ and } \phi N_{cy} = 4541.76 \text{ kN}$$

Axial Tension

Yield capacity (Clause 7.2)

$$\phi N_y = \phi A_g f_y = 0.9 \times 20000 \times 320 = 5760 \text{ kN}$$

Combined Actions

$$Z_{ex} = \frac{I}{y_{max}} = \frac{1.667 \times 10^7}{50} = 333 \times 10^3 \text{ mm}^3$$

$$Z_{ey} = \frac{I}{y_{max}} = \frac{6.667 \times 10^7}{100} = 667 \times 10^3 \text{ mm}^3$$

$$S_x = \frac{bh^2}{6} = \frac{200 \times 100^2}{6} = 333.3 \times 10^3 \text{ mm}^3$$

$$S_y = \frac{b^2h}{6} = \frac{200^2 \times 100}{6} = 666.7 \times 10^3 \text{ mm}^3$$

$Z_{ex} = \min[S, 1.5Z_e] = 333 \times 10^3$, $Z_{ey} = \min[S, 1.5Z_e] = 666.7 \times 10^3$ $k_f = 1$, $f_{yf} = 320 \text{ MPa}$, $f_u = 440 \text{ MPa}$, $N^* = 12.8 \text{ kN}$, $M^* = 5.22 \text{ kNm}$

$$M_{sx} = f_y Z_e = 320 \times 333 \times 10^3 = 107 \text{ kNm}$$

Section capacity (Clause 8.3.2) and in – plane capacity (Clause 8.4.2.2)

$$\phi M_r = \phi M_s \left(1 - \frac{N^*}{\phi N_s}\right) = 0.9 \times 107 \left(1 - \frac{12.8}{5760}\right) = 96 \text{ kNm}$$

$$\phi M_i = \phi M_s \left(1 - \frac{N^*}{\phi N_c}\right) = 0.9 \times 107 \left(1 - \frac{12.8}{5760}\right) = 96 \text{ kNm}$$

SATISFACTORY

Vertical Truss Member

Axial Compression

Member subjected to axial compression design as per AS 4100

$A_g = 12252.2 \text{ mm}^2$, $I = 2.33 \times 10^8 \text{ mm}^4$, $k_f = 1$, $f_{yf} = 320 \text{ MPa}$, $f_u = 440 \text{ MPa}$

For compression $\phi = 0.9$ (Table 3.4)

Nominal Section Capacity (Clause 6.2.1)

$$\phi N_s = \phi k_f A_g f_y = 0.9 \times 1 \times 12252.2 \times 320 = 3528.6 \text{ kN}$$

Nominal Member Capacity (Clause 6.3.3) assume largest length **16245mm**

$$\lambda_{nx} = \frac{l_e}{r} \sqrt{k_f} \sqrt{\frac{f_y}{250}} = \frac{16245}{\sqrt{\left(\frac{2.33 \times 10^8}{12252.2}\right)}} \sqrt{1} \left(\sqrt{\frac{320}{250}}\right) = 1$$

$$\alpha_b = -1.0 \quad \alpha_c = 1 \quad (\text{Table 6.3.3.3})$$

$$\therefore \phi N_{cx} = \phi N_{sx} = 3528.6 \text{ kN}$$

Axial Tension

Yield capacity (Clause 7.2)

$$\phi N_y = \phi A_g f_y = 0.9 \times 12252.2 \times 320 = 3528.6 \text{ kN}$$

Combined Actions

$$Z_e = \frac{I}{y_{max}} = \frac{2.33 \times 10^8}{200} = 1165 \times 10^3 \text{ mm}^3 \quad S = \frac{\pi(d_{out}^4 - d_{in}^4)}{32d_{out}} = \frac{\pi(400^4 - 380^4)}{32 \times 400} = 1165 \times 10^3 \text{ mm}^3$$

$$Z_{cx} = \min[S, 1.5Z_e] = 1165 \times 10^3, \quad k_f = 1, \quad f_{yf} = 320 \text{ MPa}, \quad f_u = 440 \text{ MPa}, \quad N^* = 14 \text{ kN}, \quad M^* = 100 \text{ kNm}$$

$$M_{Sx} = f_y Z_e = 320 \times 1165 \times 10^3 = 373 \text{ kNm}$$

Section capacity (Clause 8.3.2) and in – plane capacity (Clause 8.4.2.2)

$$\phi M_r = \phi M_s \left(1 - \frac{N^*}{\phi N_s}\right) = 0.9 \times 373 \left(1 - \frac{14}{3528.6}\right) = 334 \text{ kNm}$$

$$\phi M_i = \phi M_s \left(1 - \frac{N^*}{\phi N_c}\right) = 0.9 \times 373 \left(1 - \frac{14}{3528.6}\right) = 334 \text{ kNm}$$

SATISFACTORY

Inner Ring Cable

Axial Tension

For a 50mm diameter ACS4 structural cable $f_{yf} = 1212 \text{ MPa}$ (Ronstan, 2011)

Yield capacity (Clause 7.2)

$$\phi N_y = \phi A_g f_y = 0.9 \times 1964 \times 1212 = 2142 \text{ kN}$$

Bottom Chord

Axial Compression

Member subjected to axial compression design as per AS 4100

$$A_g = 3063.05 \text{ mm}^2, \quad I = 1.457 \times 10^7 \text{ mm}^4, \quad k_f = 1, \quad f_{yf} = 320 \text{ MPa}, \quad f_u = 440 \text{ MPa}$$

For compression $\phi = 0.9$ (Table 3.4)

Nominal Section Capacity (Clause 6.2.1)

$$\phi N_s = \phi k_f A_g f_y = 0.9 \times 1 \times 3063.05 \times 320 = 882 \text{ kN}$$

Nominal Member Capacity (Clause 6.3.3)

$$\lambda_n = \frac{l_e}{r} \sqrt{k_f} \sqrt{\frac{f_y}{250}} = \frac{8550}{\sqrt{\frac{1.457 \times 10^7}{3063.05}}} \sqrt{1} \left(\sqrt{\frac{320}{250}}\right) = 140$$

$$\alpha_b = -1.0 \quad \alpha_c = 0.389 \quad (\text{Table 6.3.3.3})$$

$$\therefore \phi N_{cx} = 0.389 \times 882 = 343 \text{ kN}$$

$$\therefore \phi N_s = 882 \text{ kN and } \phi N_c = 343 \text{ kN}$$

Axial Tension

Yield capacity (Clause 7.2)

$$\phi N_y = \phi A_g f_y = 0.9 \times 3063.05 \times 320 = 882 \text{ kN}$$

Combined Actions

$$Z_e = \frac{I}{y_{max}} = \frac{1.457 \times 10^7}{100} = 146 \times 10^3 \text{ mm}^3 \quad S = \frac{\pi(d_{out}^4 - d_{in}^4)}{32d_{out}} = \frac{\pi(200^4 - 190^4)}{32 \times 200} = 146 \times 10^3 \text{ mm}^3$$

$$Z_c = \min[S, 1.5Z_e] = 146 \times 10^3, \quad k_f = 1, \quad f_{yf} = 320 \text{ MPa}, \quad f_u = 440 \text{ MPa}, \quad N^* = 53.33 \text{ kN}, \quad M^* = 30 \text{ kNm}$$

$$M_s = f_y Z_e = 320 \times 146 \times 10^3 = 47 \text{ kNm}$$

Section capacity (Clause 8.3.2) and in – plane capacity (Clause 8.4.2.2)

$$M_r = \phi M_s \left(1 - \frac{N^*}{\phi N_s}\right) = 0.9 \times 47 \left(1 - \frac{53.33}{882}\right) = 40 \text{ kNm}$$

$$M_i = \phi M_s \left(1 - \frac{N^*}{\phi N_c}\right) = 0.9 \times 47 \left(1 - \frac{53.33}{343}\right) = 35 \text{ kNm}$$

SATISFACTORY

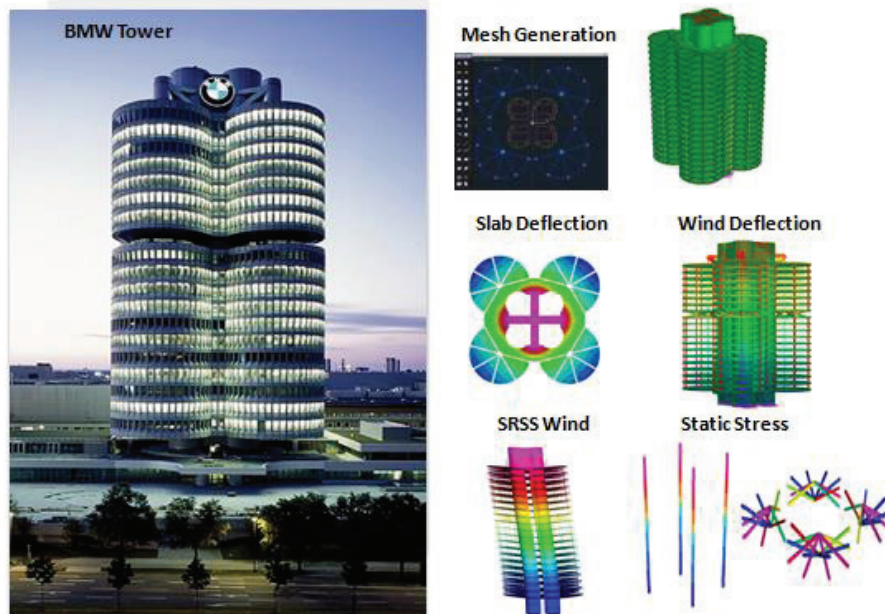
Dynamic Analysis of the BMW Tower in Munich

Joaquin Indacochea-Beltran, Pearl Elgindy, Elaine Lee, Thiviya Vignesh, Peter Ansourian, Faham Tahmasebinia, and Fernando Alonso Marroquin^{a)}.

School of Civil Engineering, The University of Sydney, Sydney NSW 2006 Australia

^{a)}Corresponding author: fernando@sydney.edu.au

Abstract. In the 1970s, world famous Austrian architect Karl Schwanzer designed an avant-garde suspended skyscraper for the new BMW headquarters. The BMW Tower was envisioned to resemble a four-cylinder motor and become a symbol for the recent flourishing success of BMW. Throughout its four decades, the BMW Tower has become the main architectural feature of modern Munich and a pride for one of the World leading car manufacturers. The structural design of the BMW Tower represented a major challenge to Germany's finest engineers because the suspended 99.5m-high structure had to withstand not only static loading but large wind dynamic loading while having deflections within appropriate serviceability limits. Strand7 has been used to determine the stresses and deflections the structure is subjected to in order to analyse its behavior under static and dynamic loadings. Ultimately, this analysis helps to understand the nature of suspended structures in relation to the Eurocode building standards. Finally, thermal resistance has also been analysed using Strand7 to simulate a fire scenario and analyse the behaviour of the cable structure, which is the most critical building component.



INTRODUCTION

The Austrian architect Karl Schwanzer, designed an award-winning multistory building for the BMW company. The design of the building was architecturally conceived to resemble the four-cylinder engine of a car. It is currently used as the headquarters for BMW.

The BMW Tower (also known as “BMW Vierzylinder”, “BMW Hochhouse”, “BMW Turm” in German) was constructed in Munich Germany between 1968 and 1972 with the engineer Helmut Bomard (Motorline, 2016). The use of suspended components makes the structure unique and iconic. Being next to a museum, the site attracts numerous international tourists to the region. This suspended structure is not only innovative but also opens numerous inspirational concepts that portray the various means of load bearing. The BMW Tower had been classified as a protected historical building since 1999 and it is a major landmark in Munich.

Being innovatively designed, the exterior has remained the same through time whilst the interior has been maintained in a futuristic manner in addition to office spaces and exhibition areas. At the shear central core, elevators and stairways are present- posing as the shortest routes to office spaces. ("BMW Four-Cylinder Building, Munich | LAMILUX Heinrich Strunz Group").

The building consists of four pre-stressed concrete cylindrical structures suspended off the ground through the use of cables connected to enormous cross-shaped steel hangers that lie on top of a shear core. With 18 suspended floors, a total of 53 000 m² of office space is available. These suspended floors consist of office space with one technical level mid building. This abundant space allowed the recentralization of staff previously dispersed around the region. A total land space of 72 000 m² was actually present, including the basement floor areas. Further details are given in Table 1.

This report presents the analyses conducted to understand the structure’s static and dynamic behaviors as well as the thermal resistance of the most critical structural components. Static behavior includes dead and live loads, while dynamic behavior comprises wind effects. Earthquake analysis was not part of this analysis as it is not required by the Eurocode for Munich because the probability of seismic activity is very low. (Solomos et al. 2008)

TABLE 1. Building Details

Location: Munich, Germany	The Year of Built: 1972
Architects: Karl Schwanzer	Approximate Cost: \$28.5 million AUD
Structural Engineer: Helmut Bomard	Overall Height: 99.5 m
Function: Commercial Office Building	Floor Area: 72000 m ² (52000 m ² useful area)
The Structure of the Plan: A circular floor plan with four segments representing a four-cylinder engine exists over 18 floors. The structure is suspended off hangers at the top of the building. The hangers are connected through the central shear core. There is also a technical floor mid-structure, containing trusses which transfer loads between the columns and the cables.	
Number of Floors: 18 Office Floors and 1 Technical Floor	

STRUCTURAL MEMBERS

Foundation: Raft slab for the shear core. Foundation over loose alluvial fine to coarse grained sediments that are the typical soil material in Munich, Germany.

Shear core: Four symmetrical reinforced-concrete cores along the entire height of the structure. Each core has a quadrant-like shape. Interior walls were used to stiffen the shear core. At each floor there is a stiffener slab used as corridor.

Hanger beams: Pre-stressed concrete cross-shaped hanger beams placed on top of the shear core structure.

- Cables: Pre-stressed steel cable structure that are connected at the top to the hanger beam and on each floor is cast-in-place to a massive rebar display to assure a fixed connection. The cables have a concrete cover to protect them from fire.
- Columns: Pre-stressed reinforced concrete columns at the edge of each radial cylindrical slab. Each column is at 7m spacing with floor-to-floor height of 4m. These columns are utilized to balanced out the loads in the steel cables. There are columns in all floors except for the technical floor.
- Beams: Pre-stressed concrete beams extend radially from the floor-to-cable junction towards the exterior columns spanning 9m. Also, 7m peripheral beams are used to join the columns.
- Truss system: Reinforced concrete 3-D truss system located on the technical floor that extends radially from the lower floor-cable junction to the base of the columns in the upper floor and from the top floor-cable junction to the top of the columns in the lower floor.
- Floor system: Reinforced concrete two-way slab.

The members of the structure are determined from the original BMW tower. The use of material and dimensions of elements are modeled as per Table 2 below.

TABLE 2. Structural Elements for the BMW Tower

Details of the Structural Elements	Structural Element Sizes (mm)	Floor Level	Material and Standard
Hanger Beam (W x D)	1500 x 1500	Top floor only	Structural Steel – Eurocode 3
Cable (ϕ)	250	All	Structural Steel – Eurocode 3
Exterior Column (W x D)	200 x 200	All except technical	R. Concrete 40MPa – Eurocode 2
Floor Beam (W x D)	600 x 600	All	R. Concrete 40MPa – Eurocode 2
Truss (W x D)	600 x 300	Technical floor	R. Concrete 40MPa – Eurocode 2
Concrete Slab (D)	300	All	R. Concrete 40MPa – Eurocode 2
Outer Shear Wall (D)	350	All	R. Concrete 40MPa – Eurocode 2
Inner Shear Wall (D)	200	All	R. Concrete 40MPa – Eurocode 2
Stiffener Shear Wall (D)	175	All	R. Concrete 40MPa – Eurocode 2

STRUCTURAL SYSTEM

The structural system of this tower is built on the connections of elements. This system is modeled as per the sketches found in Fig. 1 and Fig. 2.

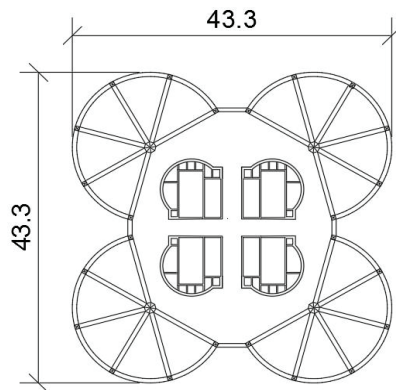


FIGURE 1. Plan of BMW Tower

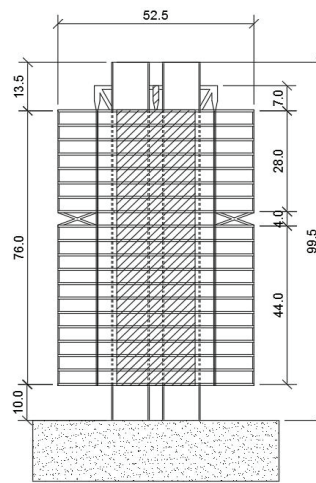


FIGURE 2. Side and Front Elevation of the BMW Tower

Construction

Initially, the concrete shear core was constructed to its full height. Steel hanger beams were then erected on top of the shear core. The steel hangers cantilever out from the shear core. The structures hang on cables that suspend from these steel hanger beams. The truss that comprises the technical floor was the first floor to be assembled. It was erected on the ground and is the most crucial structural system of the tower. All floors above the truss were then built and then the entire structure was raised one floor level by the steel cables. To construct each subsequent floor level situated beneath the truss technical floor, the floor slab was installed on-ground in the available space. The entire structure was then again elevated one floor level by the steel cables and the process was repeated. In the as-built state, the steel cables permanently suspend the structure off the ground. The truss provides a path for load redistribution between the cable and the exterior columns.

Vertical Loads

Vertical loading on this building is due to dead and live loads applied on the floor slabs. The floor slabs transfer these loads to the beams, from where it is transferred to the cables or exterior columns. The cables experience large tensile forces, which are redistributed into the exterior columns through the truss. The suspended system resists these forces by load transfer from the cables to the hangers and the shear core. The shear core is connected to the rigid foundation below therefore the suspended structure creates large compressive forces in the shear core.

Lateral Loads

Lateral loading would be produced by wind loading. While in reality, wind is applied to the exterior walls of the structure, in this model it is applied directly to the exterior columns. This lateral load is resisted by the transfer of forces from the columns through the truss, into the cables. These loads are then transferred into the hangers and shear core. In a dynamic response, the oscillating nature of the wind requires an efficient load transfer system, to reduce the warping that occurs from vibration of the structure.

Member Loads

Each member in the structure distributes load differently - depending on its property, orientation, and position.

Floor	The slab floor resists load by spreading both the dead and live loads across the floor into the beams and girders below. The rigidity of the slab floor also aids in the resistance in deflections- followed by the implementation of reinforcing bars.
Beams	Responsible for transmitting the live and dead loads to the columns and cable structure. Also, responsible for resisting the lateral loads due to dynamic wind effects and transfer such loads directly into the cable.
Columns	They transfer the floor and beam loads axially up through the structure. The columns connect through the truss to the cables, redistributing the tension and compression loads. Above the truss, the columns experience compression, and below the truss the columns experience tension.
Truss	Responsible for relieving the tensile forces in external columns by transferring loads to the cables.
Cables	The cables support the floor system of each storey. The cable can only experience tension and, therefore, all the loads on the structure are transferred through the cables to the hanger beams.
Hanger beams	Cross structure responsible for transferring loads from the cables to the shear core.
Shear core	Component that resists all the loads experienced by the structure. It experiences both axial loads imposed by the hanger beams and lateral loads imposed by wind effects on the very shear walls.

LOADS

Static Loading

In Strand7, the dead load was applied through a structural mass load case, with gravity of -9.81m/s^2 applied to the structure. The dead load on the building can be evaluated through the summary function on Strand7. The entire

structure consists of a mass of 3.52×10^7 kg. This mass averaged between the total slab areas, produces a load of 15.71 kPa acting on each slab.

$$G = 15.71 \text{ kPa} \quad (1)$$

Live loads are determined as per BS-EN-1991-1-1:2002 as 3 kPa for an office building. This force is applied on all floor slabs, except for the roof slab, as a distributed load. The Snow load was also determined from BS-EN-1991-1-1:2002 as 0.4 kPa for Munich.

$$Q = 3 \text{ kPa} \quad (2)$$

Wind actions were determined from BS-EN-1991-1-4:2005 with a base wind velocity of $v_b = 25$ m/s for Munich and an average air density of 1.25 kg/m^3 . The calculation considers the following equations to determine the wind force dependent upon the height being considered, $q_p(z)$, using curve IV as shown in Fig. 3 to calculate $c_e(z)$.

$$q_p(z) = c_e(z) \cdot q_b \quad (3)$$

$$q_b = 0.5 \cdot \rho \cdot v_b^2 \quad (4)$$

Because $c_e(z)$ was provided as a graph in BS-EN-1991-1-4:2005, the function was reproduced by graphing points into excel with an exponential trendline. This enabled the wind load to be applied as a function of the height of the structure on each column in Strand7 (Fig. 4). The equation used was:

$$c_e(z) = 0.7622 \ln(z) - 0.617 \quad (5)$$

Since the wind load was applied onto the exterior columns on one side of the structure, q_b was multiplied by the tributary width of each column. The spacing between subsequent columns differs across each half of the structure. Therefore, the loading width was taken as the sum of half the distance between columns on either side.

For the ultimate strength limit state design according to Eurocode 2 (BS EN 1992-1-1-2004), the following combination will be used for permanent, imposed and wind loads:

$$1.35 G + 1.35 Q + 1.35 W \quad (6)$$

Dynamic Wind Loading.

To determine the response of the structure to a dynamic wind loading, a spectral response was conducted with modes determined from the natural frequency analysis. Dynamic wind curves are usually derived from wind gusts in the surrounding location with a Fourier Transform to transform the gust signal into a frequency curve (Strand7 Webnotes, 2015).

The governing equation of the spectral response analysis is (Alonso-Marroquin, 2016):

$$M\ddot{U} + C\dot{U} + KU = F(t) \quad (7)$$

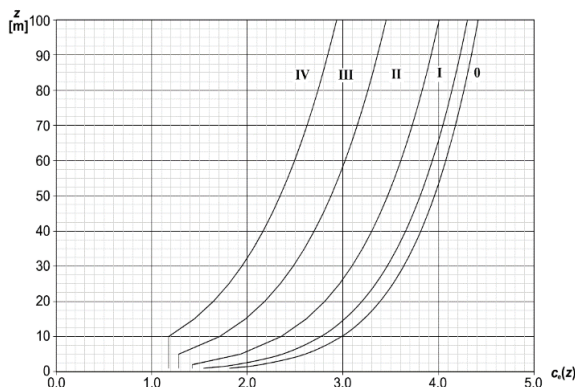


FIGURE 3. $c_e(z)$ factor for Static Wind Loading

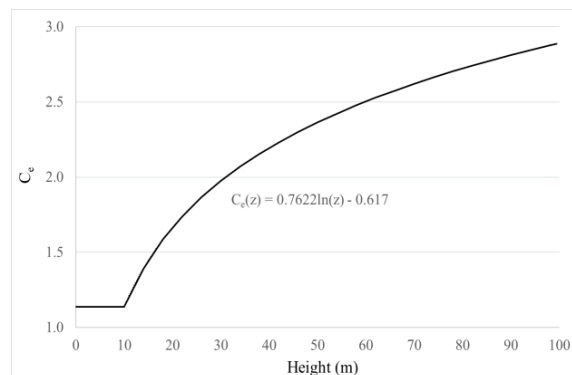


FIGURE 4. Wind load factor as a function of height

Where U is the structure displacement matrix, M is the mass matrix, C is the damping matrix, K is the stiffness matrix, and $F(t)$ is the matrix of the externally applied forces acting on the structure.

The displacement, U , is dependent upon the vibration frequencies, ω , as shown in Eq. 8 below (Alonso-Marroquin, 2016):

$$U(t) = U_0 e^{j\omega t} \quad (8)$$

Hence, in order to conduct this dynamic wind analysis, the structure's vibrational modes must be determined to find the response of the structure. The spectral response will depend upon the combination of the vibrational modes effect on the structure, and the associated load excitation for each mode.

The vibrational modes of a structure can be found by determining the natural frequencies through a Natural Frequency Analysis. This analysis removes the effect of the acting damping and external forces from the structure, resulting in the equation of the unforced-undamped vibrational motion of a multidegree of freedom (MDOF) system:

$$M\ddot{U} + KU = 0 \quad (9)$$

From Eq. 9 the natural frequencies, ω , can be determined as eigenvalues, and the mode shapes can be calculated as their corresponding eigenvectors.

The spectral response can then be determined by applying a static wind load to the structure. The static wind load is the externally applied force, $F(t)$, and was calculated as previously described in the Static Loading Section. In the Strand7 spectral response solver, this corresponds to choosing the applied load option.

The effect of the static wind loading was combined with the spectral response curve to simulate the displacement response, U , to dynamic loading experienced by the BMW Tower. It should be noted that this structure has attempted to simulate the discontinuous shear core due to elevator door openings.

A Power Spectral Density (PSD) curve is used to determine the dynamic spectral response. A PSD curve represents a typical wind gust curve. According to Davenport's approach (1961) it is assumed that "although gusts occur in a purely random sequence their statistical properties over a suitable period can be regarded as constant and independent of the origin of time." This period of time ranges from 5mins to 1 hour. Davenport determined the typical normalised PSD for along wind, which is dependent on the base wind, v_b , of the site. It produces a normalised factor vs frequency curve as follows (Cheimets, 1990).

$$Factor = 4.0 \frac{\left(\frac{1200}{V}\right)^2}{\left(1 + \left(\frac{1200n}{V}\right)^2\right)^{\frac{4}{3}}} \quad (10)$$

Where, n is frequency in Hertz and V is average velocity, which is taken as 25 m/s for Munich.

The Davenport PSD is as follows in Fig. 5 below. For a base wind velocity of 25 m/s, the normalised PSD peaks at a frequency of 0.036 Hz corresponding to a period of 27.8 s, which is expected from wind effects on buildings. This a relatively low frequency compared to peak frequencies from Earthquake loading. According to Davenport (1961), "The effect of increasing the wind speed would be to increase the intensity of the fluctuations and to sweep the spatial pattern past a point on the ground faster, but without actually altering the pattern."

In Strand7, a natural frequency analysis is conducted first to determine the vibration modes of the structure. Once the modes are determined, a Spectral Response analysis is conducted to determine the response of the structure to the applied static wind load. The normalised Davenport PSD curve is used in conjunction with the static wind load to determine the actual dynamic response of the structure due to wind loading in the direction of the main wind pressure. Additionally, 5% damping was applied to the structure.

Thermal Loading

The thermal load has been applied only to the pre-stressed steel cable of the structure. Only the cable has been considered because it is a critical feature of the structure. This is because the structure is a low-redundancy system and if the steel cable yields, it would reduce in strength and cause failure of the building. Hence, it is important to

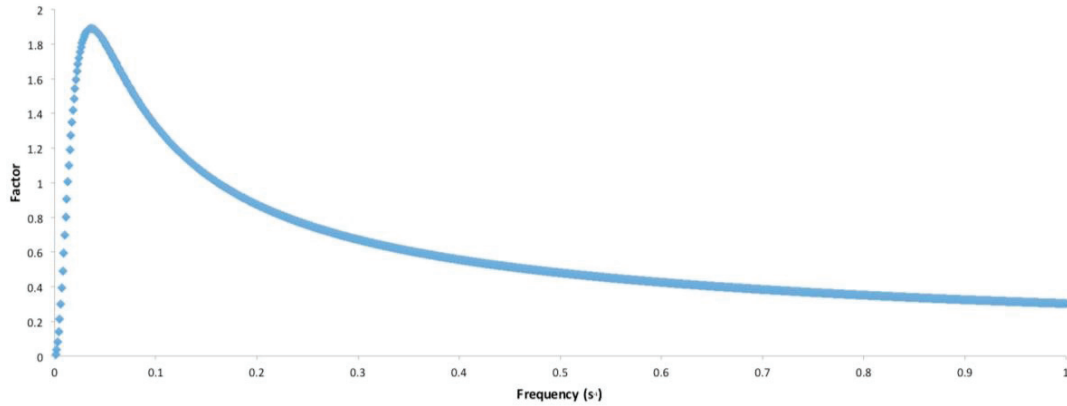


FIGURE 5. Davenport PSD Curve

ensure there is sufficient time for evacuation. The thermal load has been determined from BS-EN-1992-1-2:2004 as a maximum temperature of 1200°C for fire loading. These cables are enclosed within a thick concrete layer, which provided the thermal resistance in the steel.

In Strand7, a transient heat analysis will be conducted with calculations completed at time intervals of 15 min. An initial temperature of 25°C ambient temperature was applied to the structure to simulate the typical internal temperature of the building. The outer boundary conditions do not allow heat transfer. The heat conducts between the concrete and steel. The steel core was included to increase accuracy of the results. This accounts for the conductive effects of the steel core.

NUMERICAL ANALYSIS

Mesh Generation

A blueprint of the BMW Tower floor plan was found from recent renovations. This file was placed into AutoCAD, from where measurements were taken to determine sizing of beams, columns, floor slab and shear core. The completed AutoCAD section is shown in Fig. 1.

Once this was completed, the AutoCAD .dxf file set up was imported into Strand7. Different layers in AutoCAD (shown by different colours in Fig. 6) are automatically generated as separate groups in Strand7.

In Strand7, polylines were recognised as beams, while closed polylines were recognized as plates. Therefore, the beams, cable and column connecting plates were instantly created. From there, the column and cable plates centre nodes were extruded to become truss elements. The shear wall beam elements were extruded to become plates and formed the vertical shear wall.

To form the floor slab, the triangular sections between beams were subdivided manually to ensure the correct subdivision would produce a constant mesh across the floor slab. Once the floor slab was set-up, this was incrementally copied up the structure.

In the technical floor, the columns were deleted while beam elements were used to create the radial 3D-truss system. Also,



FIGURE 6. Modeled Structure

on the upper part of the shear core, beam elements were used to create the cross-shaped hanger structure.

Because the slabs were lifted from the ground, they have been modeled with nodes disconnected from the shear core. Finally, links were used on each floor to partially connect the slab to the shear core to simulate artificial connections that might exist in the real structure.

During the set-up of the Strand7 model, the connection between elements has been thoroughly done in order to achieve continuous results except in the case of the connection between the slab and the shear core, as previously explained. Table 3 presents a detailed summary of the elements used to model the structure. The material geometric properties were shown in Table 2. Finally, Tri3 and Quad4 plate elements were chosen in order to alleviate the computational time to run each model. However, more accurate results could be achieved with Tri6 and Quad 8 plate elements.

TABLE 3. Strand7 Elements used to Model the BMW Tower

Details of the Modelled Elements	Material	Strand7 Element	Number of Elements
Hanger Beam (W x D)	Structural Steel	Beam	24
Cable (ϕ)	Structural Steel	Truss	80
Cable Plate (W x D)	R. Concrete 40MPa	Plate/Shell Tri 3	640
Exterior Column (W x D)	R. Concrete 40MPa	Truss	432
Column Plate (D)	R. Concrete 40MPa	Plate/Shell Tri 3	1920
Floor Beam (W x D)	R. Concrete 40MPa	Plate/Shell Tri 3 & Quad 4	11040
Truss (W x D)	R. Concrete 40MPa	Beam	96
Slab (D)	R. Concrete 40MPa	Plate/Shell Quad 4	85200
Outer Shear Wall (D)	R. Concrete 40MPa	Plate/Shell Quad 4	26725
Inner Shear Wall (D)	R. Concrete 40MPa	Plate/Shell Quad 4	46204
Stiffener Shear Wall (D)	R. Concrete 40MPa	Plate/Shell Quad 4	11940

Solvers

A detailed list of solvers for each analysis is shown in Table 4.

TABLE 4. Solvers used to model the BMW Tower

Load Type	Static	Dynamic Wind	Thermal
Solver	Linear Static	Natural Frequency Spectral Response	Transient Heat
Input	Elastic Modulus Poisson's Ratio Density	Density Vibrational Modes Factor Vs. Frequency Table	Initial Temperature Specific Heat Thermal Conductivity
Output	Displacement Stresses	Displacement Stresses	Temperature as a function of time
Load	Permanent Imposed (live and snow)	Permanent Imposed (wind)	Fixed Temperature
Boundary Conditions	Fixed at Base	Fixed at Base	Fixed external nodal temperature of 1200°C

Static Deflection Results

The load combination effects on the structure under serviceability limits were analysed with an applied load combination of G + Q + W (dead, live and wind). Fig. 7 visualises the DY deflections under this serviceability state limit. The majority of these deflections are due to the applied lateral loading on the windward and leeward sides in the direction of y. The dead and live loads do not generate any lateral deflections; however a second order analysis could be done to resemble more realistic results. The structure as a whole experiences a maximum of 37mm deflecting laterally in both beams and plate elements. This maximum deflection is located at the connection between the angled hanger and the shear wall, hence representing both plate and beam elements. This point is

where the loading is transferred directly into the shear wall from the loaded columns and beams. Therefore, maximum loading causes the highest displacement in the structure.

Since the wind loads are increasing with height and are applied at the external columns, it is expected that there is a greater deflection at the top of the structure relative to the base. This deflection is evident in both the external columns and shear core as per Fig. 7. The linear deflections decrease down the vertical plane.

Vertical deflections in the DZ direction are analysed in Fig. 8. The range of plate deflections experienced within the structure varies from 7mm to 260mm. All the beam elements deflect within this range of values. Considering that beam elements are representing both the hangers and the steel cable-deflections, they will experience the same deflection as the plates at those points. The slightly larger deflections are purely due to the cantilevered extension of the slabs from the cable connection. From Fig. 8, it is also clear that the shear core experiences a uniform minimum deflection down the entire structure, as the loading transferred through the hangers affect the entire structure evenly.

It can be viewed more extensively through Fig. 9 and Fig. 10 which show deflections at the top and bottom slabs. Both images show the deflections increasing symmetrically towards the outer perimeter of the slab. This is due to the sagging experienced from the lack of support of a suspended structure. The support acts solely at the cables, and sagging will occur from this point out. It is also important to point out that the bottom slab experiences the highest deflections in the structure. This is because it is located at the bottom of the cables- which is holding up the entire structure's dead and live loads. The significant tension experienced from the cables are reflected in this large displacement. Comparing top and bottom floor slabs- there is a 251mm deflection at the bottom floor compared to 218mm at the top floor. This difference averages out to be approximately 16.5mm increase per floor due to the weight above.

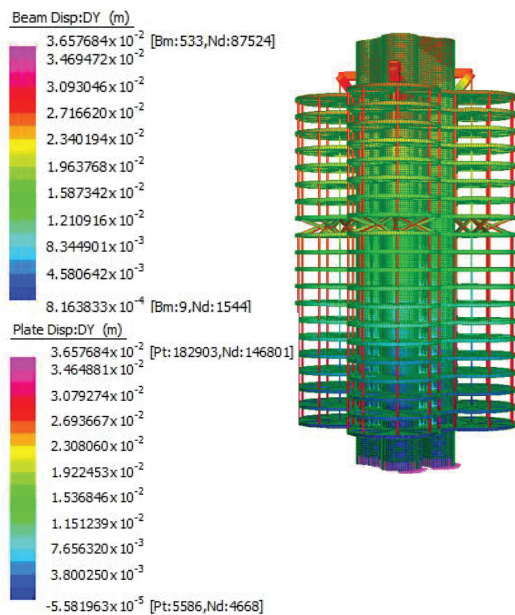


FIGURE 7. Deflection DY under Serviceability State Limit

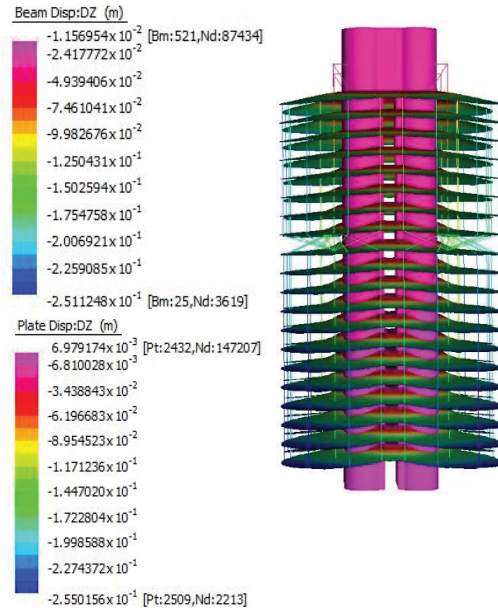


FIGURE 8. Deflection DZ under Serviceability State Limit

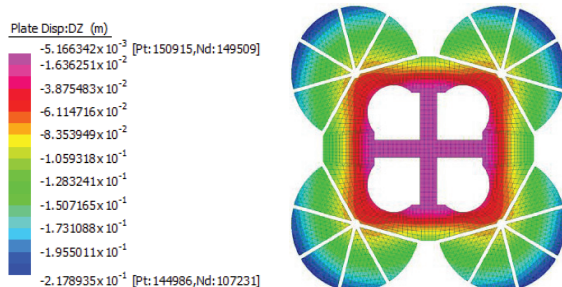


FIGURE 9. Slab Deflection at Top Floor

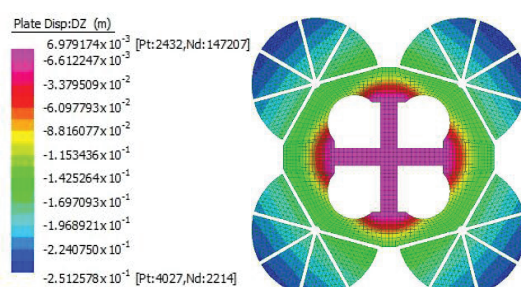


FIGURE 10. Slab Deflection at Bottom Floor

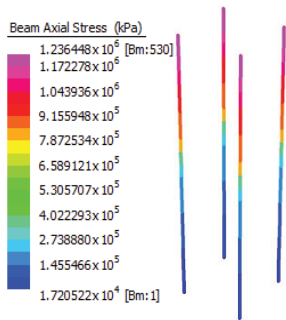


FIGURE 11. Axial stresses on cables

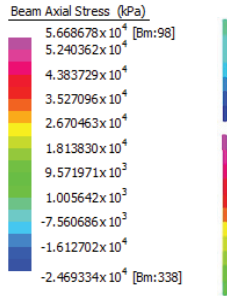


FIGURE 12. Axial stresses on a single column

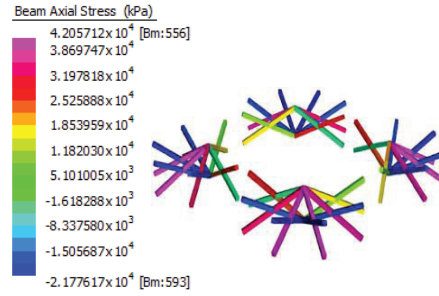


FIGURE 13. Axial stresses on Truss

Static Stress Results

The stresses are analysed for the cable, column, and truss elements of the structure as these will experience the largest stresses. These results are taking the appropriate combination for USL. Results will help further explain the transfer of loads. The cables experience the greatest axial tension in the structure due to the suspension of the slabs as shown in Fig. 11. This tension reduces further down the structure, to a minimum of 17.2MPa. The columns analysed are exterior columns at the perimeter of the slabs. It is clear that they are under compression at the upper section of the building (above the truss level) and under tension at the lower section of the building (below the truss level) as shown in Fig. 12. The maximum compression and tension values are both at the connecting points through the truss level. Therefore, it is evident to conclude that the truss functions to redistribute the loads through the columns from the cables. In the upper section, the tension in the cables is balanced out through the compression in the column, dissipating in axial stress at the top. Similarly, for the lower columns, the tensile stresses experienced dissipate away from the truss level. The truss level clearly shows a combination of tensile and compressive stresses as per Fig. 13. They successfully redistribute loads through these members, connecting through to the external column and internal steel cable, as described earlier. Evidently, the compressive truss members are linking the compressive external columns to the cable whilst the tensile truss members are linking the lower tensile columns to the cable. The inner truss members are seen to further redistribute the loads in various directions.

Dynamic Wind Deflection Results

Initially, a natural frequency analysis was conducted 25 modes converged, as shown in Table 5.

TABLE 5. Natural frequencies of the BMW Tower

Mode	Frequency (Hz)	Mode	Frequency (Hz)	Mode	Frequency (Hz)
1	0.500	9	2.440	17	3.460
2	0.531	10	2.470	18	3.480
3	0.885	11	2.600	19	3.500
4	1.160	12	2.790	20	3.510
5	1.170	13	2.850	21	3.530
6	1.340	14	3.260	22	3.740
7	1.390	15	3.310	23	3.760
8	2.240	16	3.440	24	3.820
				25	3.890

After the convergent modes were determined, a Spectral Response Analysis was conducted to investigate the effects of dynamic wind on the structure. The static wind load was applied to the structure, with the Davenport PSD as described previously in Dynamic Wind Loading.

The dynamic wind analysis determined that mode 5 was the most significant mode, with a maximum excitation amplitude of 8.82 produced. This was much greater than the other modes and the SRSS combination can be considered to represent this mode.

The dynamic wind analysis produced the deflected shape as shown in Fig. 14, at 10% exaggerated deflection. The displacement of the shear core at the height of the building is 13 cm in the along wind direction (DY). This is a relatively small deflection, but is still four times larger than the deflection determined by the static analysis, 2.8cm as shown in Fig. 7. The increase in the dynamic analysis is expected because the analysis responds to a peak wind loading from a typical wind gust curve that the PSD represents. Additionally, that these results are in a similar frame of size shows that the analysis was effective in determining the deflections.

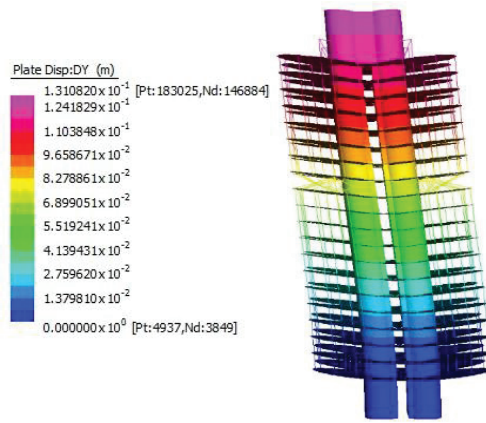


FIGURE 14. Displacement due to Dynamic Loading

Resistance to Thermal Effects

This analysis was performed through a two-dimensional model in Plain Strain, using Quad8 plate elements to model both the concrete cover and the steel cables inside. The cables had a total diameter of 250mm, and the concrete cover to this steel was 250mm thick. Fig 15 displays the Strand7 model.

Through a transient heat analysis, the resulting heat transfer through the structural element can be understood. The maximum fire loading, according to the most conservative Eurocode guidelines was 1200°C. This load was applied to the external nodes to represent a highly uncontrolled fire, whilst other nodes were subjected to an initial 25°C ambient temperature.

If considering the failure of such an important element, the entire suspended floors will collapse as a result due to the amount of load taken by these cables. Therefore, it is critical to ensure that the cables have sufficient fire protection.

As shown in Fig. 16, the prestressed concrete encased cable was subjected to different heat transfer scenarios dependant on the heating times. It is apparent that there is a linear increase in temperature through the concrete cover towards the steel cable at any one time. However, temperatures in the cable are approximately constant throughout its surface due to the elevated conductivity of steel. By including the steel cable inside the concrete cover, appropriate conduction of heat can be analysed through this cover, promoting a more accurate indication of fire resistance period (FRP). Considering a critical temperature of steel as 550°C (i.e. temperature at which the steel yield strength has been reduced to 60% of the initial yield strength), the present cable will have a FRP of up to 615min, which is equivalent to 10.25 hours. This time period is definitely sufficient for the safe evacuation of all office staff during a fire. Since the fire considered was of the worst type, generally there would be a greater time period given a smaller temperature. Regardless, it can be concluded that the cover is satisfactory for this multistorey building.

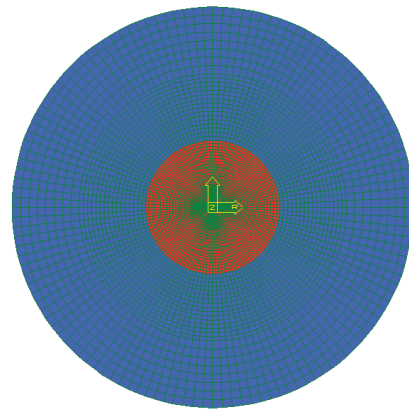


FIGURE 15. Model of Cable. Reinforced Concrete surrounds inner Steel Cable

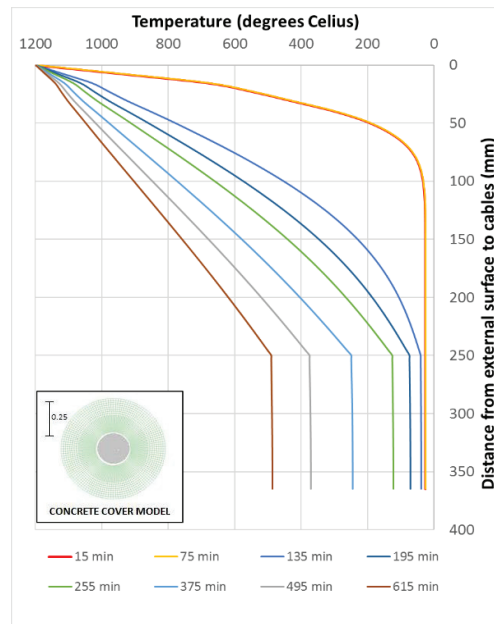


FIGURE 16. Heat dissipation through the cable's protective cover

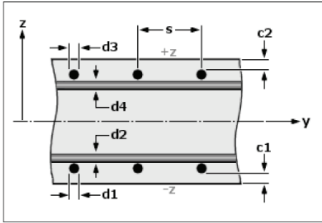
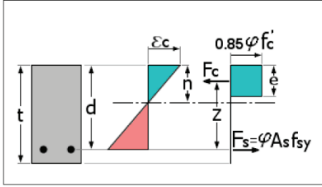
STRUCTURAL DESIGN

The initial model set-up did not consider reinforced concrete, but only plain concrete. Then, the analyses performed with Strand7 yielded the design effects on each of the structural members so it was actually possible to design each member for both ultimate strength level and serviceability strength level criteria.

Hence, a new model was run considering a first set of reinforcement layouts. This process was repeated iteratively until a solution that could satisfy the SSL criteria was determined. Table 6 shows summarizes the final rebar layouts for each type of structural element:

TABLE 6. Summary table for the reinforcement used

		Beams	Floor Slabs	Shear Walls
Cover	C1 (mm)	25	25	50
	C2 (mm)	25	25	50
Bar diameters	D1 (mm)	50	20	80
	D2 (mm)	50	20	-
	D3 (mm)	50	20	80
	D4 (mm)	50	20	-
Bar spacings	S1 (mm)	80	150	100
	S2 (mm)	80	150	-
	S3 (mm)	80	150	100
	S4 (mm)	80	150	-
Concrete properties	E_c (MPa)	32,800	32,800	32,800
	ϵ	0.003	0.003	0.003
	F'_c (MPa)	50	40	40
	ϕ	0.8	0.8	0.8
Rebar properties	E_s (MPa)	200,000	200,000	200,000
	F_{s_y} (MPa)	500	500	500
	A_{s_b} (base)	0.5 t	0.5 t	0.5 t

Special consideration was given to the structural design of cables. Initially, the cables were estimated to have the following characteristics:

Axial Force:	60690kN
Diameter:	160mm
Cross sectional Area:	20106 mm ²

To verify this, GALFAN ® Coated Steel-Fully Locked Strands, PFEIFER, were used in the following calculations, where for a single strand:

Minimum Breaking Load (MBL)	405kN
Nominal Diameter	21.0mm
Cross-section Area	281.0mm ²

Currently a 160mm diameter cable contains 71 strands, with each having a minimum breaking load of 405kN.

$$N_{design} = n_{cables} \cdot MBL \quad (11)$$

$$N_{design} = 71 \cdot 405 \text{ kN} \quad (12)$$

$$\therefore N_{design} = 28760 \text{ kN} \leq 60690 \text{ kN} \quad (13)$$

Therefore a design axial force of 28760kN does not satisfy requirements of our current analysis. Giving a failure allowance factor of $\phi = 0.85$, the cable must be able to support approximately 71400kN. From this the entire cable is increased to a diameter of 250mm in the model.

$$N^* \leq 0.85 n_{cables} \cdot 405 \text{ kN} \quad (14)$$

$$\therefore 405 \cdot n_{cables} \geq \frac{60690}{0.85} = 71400kN \quad (15)$$

$$\therefore n_{cables} \geq \frac{71400}{405} = 176 \text{ cables} \quad (16)$$

$$176 \cdot 281 = 49456 \text{ mm}^2 \quad (17)$$

$$D = \sqrt{4 \cdot \frac{area}{\pi}} = 250mm \quad (18)$$

CONCLUSIONS

This paper provides a complete dynamic analysis of the BMW Tower, situated in Munich. It provides an investigation into static loading, dynamic wind loading, and thermal loading of the steel cable.

There is little technical information available regarding the structural behaviour of the BMW Tower. Consequently it has been necessary to perform an iterative process in order to be able to determine the structural design of the main components of the building structure.

The 3D finite element model, used in conjunction to the Eurocodes has been successful in estimating the sizing of the members. Initially, the model was run to determine the design effects on each structural element. Afterwards, the structural members were progressively redesigned to comply ultimate strength levels and serviceability strength level criteria. The finite element model of the BMW Tower considered the appropriate combination for static loads (dead and live) as well as the governing wind dynamic loading case for tall buildings. Therefore the structure was determined to have satisfactory serviceability deflections, and satisfactory USL in the cable.

Further research and optimization should be performed to achieve more accurate results. These may include, but are not limited to: using higher order elements such as Tri 6 and Quad 8, analysing the settlement effect of the soil foundation due to the structure, considering the effects of across-wind on the dynamic behavior of the building, evaluating the potential effect of a blast near the cable structure and recreating the design of the structural members using the German building code that was current in the 1970s.

REFERENCES

7 Forum, (2016), BMW Hochhaus – BMW Meilenstein, retrieved from https://www.youtube.com/watch?time_continue=555&v=nVDkzqAsRd0

(2006) Renovation of the BMW Tower in Munich, retrieved from <http://www.ais-online.de/objektreferenz/sanierung-des-bmw-hochhauses-in-muenchen/11581183/?p=9&pid=9674809>

F Alonso-Marroquin (2016), Finite Element Modelling for Civil Engineering, Quantumfi Publishers, Sydney, ISBN 978-0-9944287-0-7

BMW Australia, 2016, 40 Years of the BMW Tower and Museum, retrieved from <http://www.motorline.bmw.com.au/com/en/insights/newsandevents/latest-news/40-years-of-the-bmw-tower-and-museum-.html>

BMW Group (2013). 40 years of BMW Headquarters and Museum, retrieved from <https://www.press.bmwgroup.com/global/article/detail/T0143556EN/40-years-of-bmw-headquarters-and-museum?language=en>

P Cheimets, (1990), Results of Wind Spectrum Literature Search, retrieved from <https://www.cfa.harvard.edu/sma/memos/20.pdf>.

A G Davenport, (1961). The spectrum of horizontal gustiness near the ground in high winds. [Quarterly Journal of the Royal Meteorological Society](#), 87 (372), 194-211.

European Committee for Standardisation (2002), BS EN 1991-1-1-2002, *Eurocode 1 - Actions On Structures (Part 1-1 General Actions - Densities, Self-weight, Imposed Loads For Buildings)*, European Commission, Brussels

European Committee for Standardisation (2005), BS EN 1991-1-4-2005, *Eurocode 1 - Actions On Structures (Part 1-4 General Actions - Wind Actions)*, European Commission, Brussels

European Committee for Standardisation (2004), BS EN 1992-1-1-2004, *Eurocode 2 - Design Of Concrete Structures (Part 1-1 General Rules & Rules For Buildings)*, European Commission, Brussels

European Committee for Standardisation (2004), BS EN 1992-1-2-2004, *Eurocode 2 - Design Of Concrete Structures (Part 1-2 General Rules - Structural Fire Design)*, European Commission, Brussels

D Kiley. *Driven*. (John Wiley, Hoboken New Jersey, 2004)

Meskouris - Konzepte der DIN 4149 - RWTH Aachen, Lehrstuhl für Baustatik und Baudynamik

Ronstan (2013) *Ronstan Structural Cables*, retrieved from http://www.ronstantensilearch.com/wp-content/uploads/2013/11/RPA112_Structural_Cable_Catalogue_72dpi_0.pdf, pp 9.

W Schueller, The Cable in Structures, retrieved from <http://www.slideshare.net/fullscreen/WolfgangSchueller/the-cable-in-building-structures/23>.

G Solomos, A Pinto, S Dimova (2008), *A Review of the Seismic Hazard Zonation in National Building Codes in the Context of EUROCODE 8*, (European Commission Joint Research Centre, Luxembourg)

Strand7 Webnotes (2015). "Response Spectrum and Power Spectral Density", Strand7 Pty Limited, Sydney, Australia

Y Liu and Z Lu, Seismic Performance and Storey-Based Stability of Suspended Buildings, [Advances in Structural Engineering](#) November 2014 vol. 17 no. 10 1531-1550

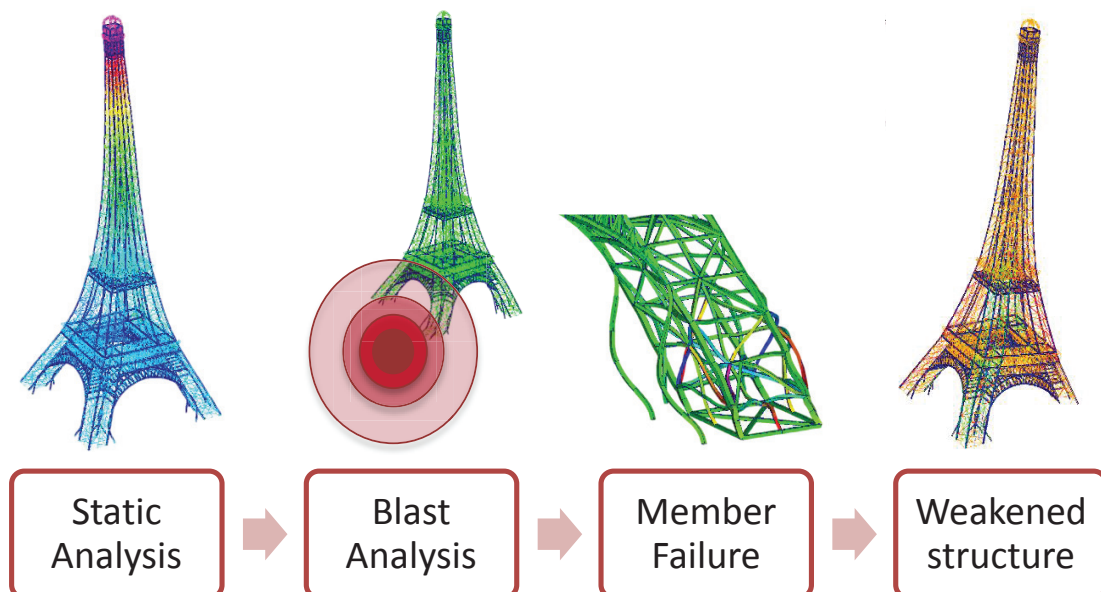
Blasting Response of the Eiffel Tower

Lachlan Horlyck, Kieran Hayes, and Ryan Caetano, Faham Tahmasebinia, Peter Ansourian, and Fernando Alonso-Marroquin ^{a)}

School of Civil Engineering, The University of Sydney, Sydney NSW 2006 Australia

^{a)} Corresponding author: fernando@sydney.edu.au

Abstract. A finite element model of the Eiffel Tower was constructed using Strand7 software. The model replicates the existing tower, with dimensions justified through the use of original design drawings. A static and dynamic analysis was conducted to determine the actions of the tower under permanent, imposed and wind loadings, as well as under blast pressure loads and earthquake loads due to an explosion. It was observed that the tower utilises the full axial capacity of individual members by acting as a 'truss of trusses'. As such, permanent and imposed loads are efficiently transferred to the primary columns through compression, while wind loads induce tensile forces in the windward legs and compressive forces in the leeward. Under blast loading, the tower experienced both ground vibrations and blast pressures. Ground vibrations induced a negligibly small earthquake loading into the structure which was ignored in subsequent analyses. The blast pressure was significant, and a dynamic analysis of this revealed that further research is required into the damping qualities of the structure due to soil and mechanical properties. In the worst case scenario, the blast was assumed to completely destroy several members in the adjacent leg. Despite this weakened condition, it was observed that the tower would still be able to sustain static loads, at least for enough time for occupant evacuation. Further, an optimised design revealed the structure was structurally sound under a 46% reduction of the metal tower's mass.



INTRODUCTION

The Eiffel Tower was constructed as the leading monument of the Universal Exposition to mark the centenary of the French Revolution of 1789. The large iron archways served as the gateway to Champ-de-Mars, with the Tower itself acting as the key attraction of the Universal Exposition. It was the first structure to reach the coveted 1000 feet, and maintained its status as the world's tallest structure until 1930. While today the Eiffel Tower is held in great revere, this was not always the case with calls for the Tower to be demolished in the early 20th century. The height of the Tower proved to be its saving grace with city officials recognising its significance as a radio tower, which proved instrumental in later years during WWI and WWII.

The Eiffel Tower is one of the world's most iconic monuments, with the architectural wonder attracting more visitors than any other paid tourist attraction in the world. In addition to its architectural value, the tower also represents significant improvements in engineering design with the four legs representing a roughly exponential curve to best resist wind loads (Weidman and Pinelis, 2004), allowing it to reach heights never before attained by any previous structure. Since the tower was initially constructed as a temporary structure, the focus of the following analysis is to both determine the adequacy of the structure to resist permanent loads, and the extent to which the tower was over designed with respect to its capacity to resist permanent and imposed loads. For the purpose of this analysis, loads will be based on Australian Standards to ensure rigour, rather than the original hand-calculated loads applied to the structure during its design. The European Standards were not established at the time of construction, and thus have not been included. An analysis has also been conducted to determine the capacity of the tower to resist blast loads resulting from a nearby explosion.

The Eiffel Tower is a large wrought iron lattice tower, comprising 7,300 tonnes of iron and 2.5 million rivets. The three observation decks, which are serviced by multiple stairways and elevators, attract an average of 25,000 visitors each day. This makes the observation decks of the tower some of the most highly foot trafficked areas in the world. The steel decking is required to resist significant imposed actions associated with this foot traffic. Additionally, the tower contains two restaurants that offer panoramic views of the surrounding city for diners.

TABLE 1. Tower Details

Location: Paris, France	Year Construction Complete: 1889
Architect: Stephen Sauvestre	Approximate Cost: 7,800,000 gold francs (equivalent current-day AU\$43 million)
Structural Engineers: Maurice Koechlin, Emile Nouguier	Overall Height: 324m
Function: Originally an entrance to the 1889 World's Fair. Then used for radio and television transmission. Now operates as a tourist attraction.	Floor Area: approximately 6200 m ²
The Structure of the Plan: Wrought iron lattice	
Number of Floors: 3 floors above ground	

STRUCTURAL MEMBERS

Floor system: Wrought iron deck supported underneath by a grid of large trusses that span between the legs.

Beams: Wrought iron trusses that span between the four legs, providing both load continuity and platform decking support. The lower and middle platforms are supported by a 16x16 and 6x6 roughly square grid with an area of 4200m² and 1650m² respectively. Beams in the upper half of the tower provide continuity between the four legs before they join to form a single leg. The spans of these beams vary from 1.8m to 15.7m.

Legs: The tower consists of four separate curved legs that meet to form a single point at the peak. Each of these legs are approximately 15m by 15m and consist of four columns that are connected by an iron lattice, allowing the columns to behave like a truss. The four columns contained in each of the legs is assembled from a series of angles and flat sections that form a roughly square hollow cross section (see Figure 1). The diagonal bracing connecting the four columns to form a single leg consists of trusses. The section properties of both the square column sections and the diagonal bracing members vary with height, reflecting the increase in permanent loads of the tower at lower heights. For the purpose of finite element modelling, the trusses and square hollow columns were represented as single beam elements with appropriate section properties given to match the section properties of the actual truss system / column section. An example calculation is provided below for a column section at ground level.

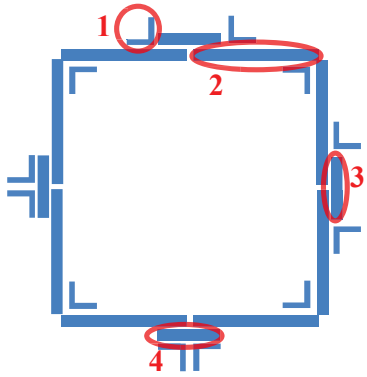


TABLE 2. Structural Properties for Section 1

Member	Dimensions	Area	$I_{x/y}$ ($\text{mm}^4 \times 10^3$)	J ($\text{mm}^4 \times 10^3$)
1	100 x 100 x 12	2256	2520.5	108.3
2	800 x 18.5	14800	422.1	1688.4
3	200 x 12	2400	28.8	115.2
4	205 x 12	2460	29.5	118.1

$$\text{Total area} = \Sigma \text{Area} = 95992 \text{ mm}^2 \quad (1)$$

$$\text{Total } I_x / I_y = \Sigma I_{\text{own axis}} + \Sigma A(y_o - \bar{y})^2 = 10.12 \times 10^9 \text{ mm}^4 \quad (2)$$

$$\text{Total } J = \Sigma J = 8.52 \times 10^6 \text{ mm}^4 \quad (3)$$

FIGURE 1. Section Properties for Section 1

Foundations: Each of the four legs rest on masonry blocks and are anchored into the foundation below the blocks by a total of sixteen anchors that have a diameter of 10cm and a length of 7.5m.

Ground Conditions: The soil conditions consist of both hard and soft soil. The soft soil is predominately located underneath the riverside legs, requiring deeper and larger foundations than the park side legs to reduce settlement of the tower.

TABLE 3. Structural Elements for Section 1 of the Tower

Details of the Structural Elements	Available Structural Element Sizes	Suggested Structural Element Sizes
Columns - Structural Systems	Uniform Box sections	Respective Second moment of areas inputted as detailed above
Beams - Structural Systems	T sections	T-sections varying from 60x120x6mm to 180x360x20mm
	Angle sections	Angle-section 60x60x6mm
Grated Floor System	Quad 4 Plates	20mm thick membrane

STRUCTURAL SYSTEM

The structural system of the Eiffel Tower grants the ability to withstand significant vertical loads from both the weight of the tower itself and imposed loading from the heavy foot traffic associated with visitors. The main components that resist vertical loads are each of the four columns located at the corners of all four support legs (16 in total). The size of these roughly square hollow sections varies according to height, with larger section dimensions located at the base of the tower. A series of diagonal truss elements join each of the four columns together to form a leg, while horizontal trusses also span between each of the columns at regular intervals. These members effectively brace the columns, reducing their effective lengths, which subsequently increases their resistance to global buckling.

Due to the heavy foot traffic associated with the large number of tourists packed onto the observation decks, imposed loads experienced by the platform decking are significant. The wrought iron decking on the lower platform is supported on the underside by large trusses that transfer the load to the four legs. Additionally, the arches serve to transfer some load from the platform supporting trusses to the legs of the tower. Due to the curvature of the tower, the second platform has a significantly smaller area. The platform requires fewer supporting trusses and is instead split into a sixteen metre, roughly square grid. The top platform only consists of an overhang around the perimeter of the lattice leg support. The overhang is supported by diagonal columns protruding from the tower a small distance below the platform such that it forms an approximately 30-degree angle with the tower. Overhangs of the lower two platforms are supported by diagonal columns which are connected to the legs where possible and are otherwise connected to the bottom chord of the truss supporting the platform.

Samples of the design used to model the Eiffel Tower are provided (see Figure 2, Figure 3 and Figure 4).

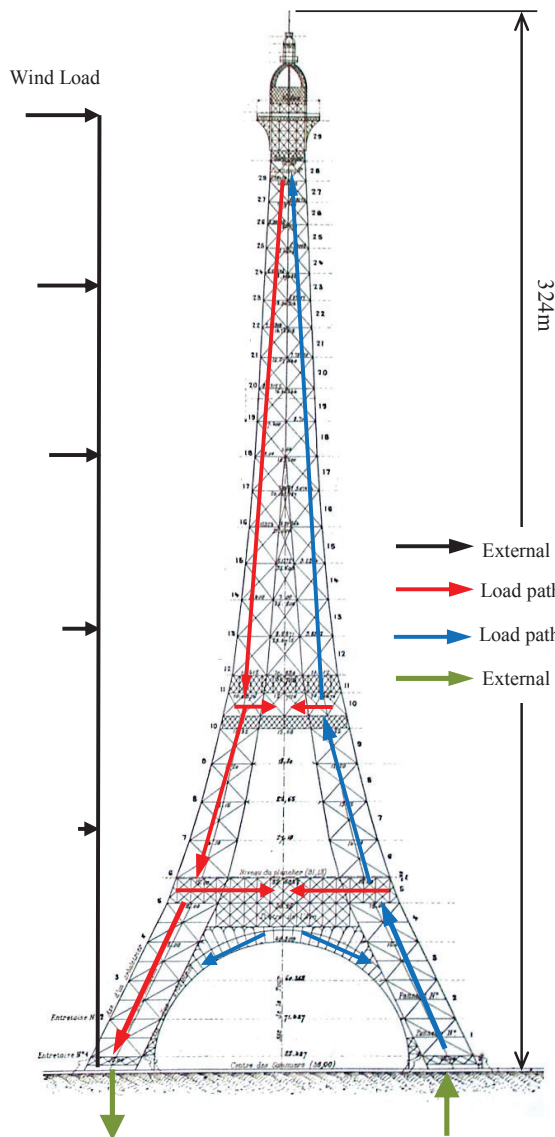


FIGURE 3. Elevation View Eiffel Tower (wind load paths)

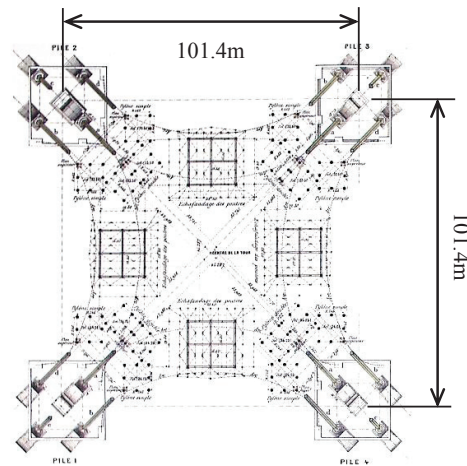


FIGURE 2. Plan View Eiffel Tower

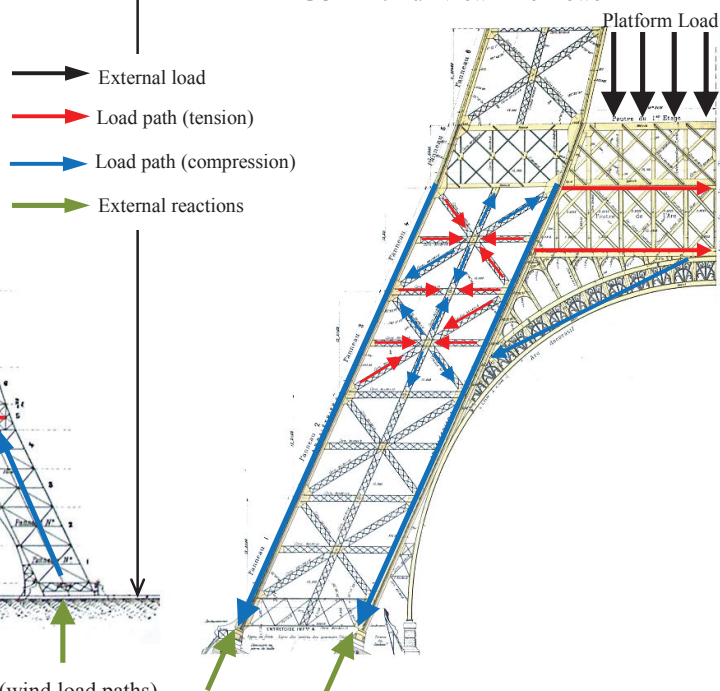


FIGURE 4. Permanent / imposed load paths

Lateral loads on the structure are predominately associated with wind loadings on the side of the tower. The curvature of the four supporting legs provides a base area that is significantly larger than the area at the top of the tower. This increases the tower's resistance to overturning moments caused by the wind, since the restoring force has an increased moment arm (see Figure 3). Similarly, by narrowing as the tower climbs in height the tower presents a reduced surface area for the wind to act on which proves significant because the wind pressure and overturning moment arm both increase with height. To ensure that lateral load is transferred and the four legs do not act independently from one another, continuity between the four legs is provided at the lower and intermediate platforms by large trusses that span between the legs. Concurrently, smaller horizontal trusses spanning between the legs provide continuity for the top half of the tower, prior to merging of the four legs into a single leg.

LOADS

Permanent Loads: The weight of the tower was applied to the structure through the use of a gravity load case. This resulted in a weight approximately equal to the quoted weight for the metal structure, 7,300 tonnes (Lemoine, 2008). While this accounted for the structural members of the Eiffel Tower, it failed to account for additional permanent loads from items such as internal stair wells and elevator shafts. This was accounted for by increasing

the density of the member components of the supporting legs. The density was increased in accordance with a sum of reaction forces at the base equal to the weight of the whole structure, 10,100 tonnes (Lemoine, 2008).

Imposed Loads: Areas of the tower that experience imposed loading are limited to the bottom, intermediate, and top platforms. Imposed loads result from the presence of restaurants and the heavy foot traffic of the observation decks. As a consequence, the imposed loading on these areas was conservatively assumed as 7.5kPa in accordance with AS1170.1 for areas susceptible to overcrowding.

Wind Loads: The wind loading varied as a function of height and was assumed to apply only to the exposed faces of the beam and plate members on one side of the tower. The width of the exposed area of the beams was taken conservatively as 800mm for all beams located below the middle platform, and 600mm for all beams located above it. Wind loading was calculated in accordance with AS1170.2 (equation 4), and verified against fluid mechanics derivations (equation 5). Wind speed varies for an external flow due to viscosity and drag effects.

$$p = 0.5 \rho_{air} [V_{des,\theta}]^2 C_{fig} C_{dyn} \quad (4)$$

$$\frac{U}{u^*} = 2.44 \cdot \ln \frac{\delta u^*}{\nu} + 5 \quad (5)$$

Where δ is the height of the boundary layer, U is the wind speed at a height δ , u^* is the wind speed variable, and ν is the viscosity. The wind speed, u^* and $V_{des,\theta}$ above, was observed to vary logarithmically with height. A cubic function was derived to approximate this logarithmic variation to enable it being entered into Strand7. This returned an equation for pressure, which was multiplied by the respective width, depending at what height the pressure was applied. The resulting equation was input as a linearly varying distributed load.

The four legs of the tower act as trusses themselves to resist permanent and imposed actions. Diagonal members experience tensile and compressive forces in an alternating fashion, while horizontal and vertical members are under tension and compression, respectively (see Figure 4). These members impart loads on the main columns of the structure, which take on the bulk of the compressive stress. The trusses supporting the first, second, and third platforms, act to not only distribute the imposed loading at these levels, but also to redistribute any overlying loading (permanent and imposed) to the members below. The aim of this is to more evenly distribute the load to underlying members. As observed in a static analysis of the Strand7 model under permanent and imposed loading (see figure 5), member stresses above the second platform truss are fairly uniform. Below the truss, stresses are reorganised such that alternating diagonal members experience tension and compression, similar to a truss. Increased permanent loading is experienced by members further down the tower, due to self-weight, so this reorganisation is lessened until the next platform truss redistributes the loading. The load paths associated with resistance to lateral loading can be thought of more simplistically due to the geometry of the tower. The splayed base provides a significant restoring moment, due to the increased lever arm, such that the windward legs experience tension and the leeward legs experience compression (see Figure 6).

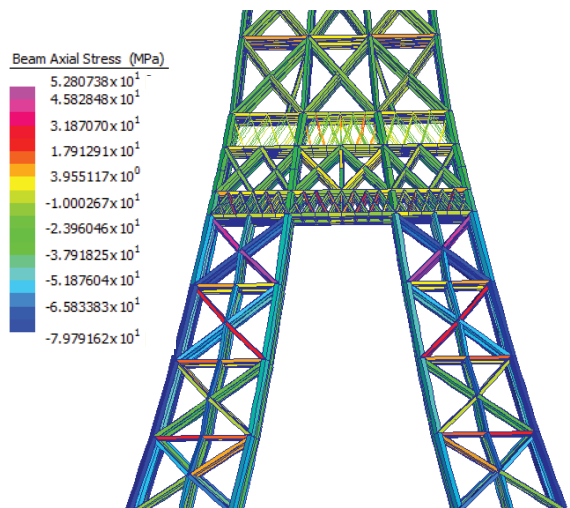


FIGURE 5. Load paths in model under 1.2G + 1.5Q

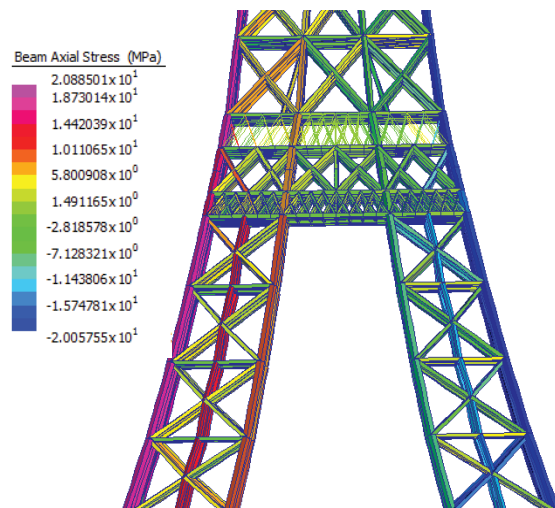


FIGURE 6. Load paths in model under wind loading

As shown in Figure 3 previously, a restoring couple is expected at the base of the structure. From the finite element model, it is observed that the maximum moment is at the fixed node on the base of the innermost primary column on the leeward side (-689kNm), while the minimum moment is similarly at the fixed node on the base of the innermost primary column on the windward side (639kNm). This indeed creates a significant restoring couple to resist lateral loading. Maximum bending stress is experienced by diagonal members directly beneath the redistribution trusses under the second platform, for both load combinations 1.2G + 1.5Q (52.8MPa) and 1.2G + W + ϕ_c Q (41.4MPa). Similarly, minimum bending stress is experienced by primary column members at the base for both load combinations, -162.2MPa and -132.8MPa respectively.

Blast Loads: As a result of the explosion, two different load components were analysed. The magnitude of the explosion was taken as the equivalent of 21kg of TNT, since reliable data was obtained from the 2013 fertilizer plant explosion in Texas, USA (Grinberg and Yan, 2016). The two load components resulting from the explosion comprised of air pressure waves and ground vibrations. The blast pressure varied based on its distance from the focal point of the explosion and was calculated using equations 6, 7, and 8 provided below (Lam, Mendis, & Ngo, 2004; Ngo, Mendis, Gupta, & Ramsay, 2007). The focal point was determined one metre from one of the tower's legs in an attempt to balance reasonability and worst case. The ground vibrations caused by the explosion were equivalent to a magnitude 2.1 earthquake on the Richter scale (Grinberg and Yan, 2016). Consequently, table 6.4 from the AS1170.4 standards was used to model the effect of this size earthquake on the soft soil conditions that the tower rests on. The relevant ground acceleration used for the model was defined according to a regression analysis by Wald et al. (1999) to give a value of 0.0017g. Since the explosion occurred on the surface, critical ground accelerations were assumed to occur only in the x and y axes.

$$Z = \frac{R}{W^{1/3}} \tag{6}$$

$$P_{so} = \frac{6.7}{Z^3} + 1 \text{ bar } (P_{so} > 10 \text{ bar}) \tag{7}$$

$$P_{so} = \frac{0.975}{Z} + \frac{1.455}{Z^2} + \frac{5.85}{Z^3} - 0.019 \text{ bar } (0.1 \text{ bar} < P_{so} < 10 \text{ bar}) \tag{8}$$

TABLE 4. Blast Loading with Distance

R: Distance from blast (m)	Z: Distance vs weight TNT Factor (m/kg ^{1/3})	P _{so} : Blast pressure (kPa)
1	0.36246	141.7
5	1.812301	1.944789
10	3.624601	0.483595
20	7.249202	0.158541
30	10.8738	0.087521
40	14.4984	0.05709
50	18.12301	0.040212

In addition to variation with radial distance from the focal point, the blast pressure also varied with time (see Figure 7). An amplification factor of 1.8 due to the blast pressure waves reflecting upwards off the ground was also included in the model. A peak blast loading was used for subsequent static loading, however a dynamic analysis was required to observe the reaction of the tower as the blast load decreased with time.

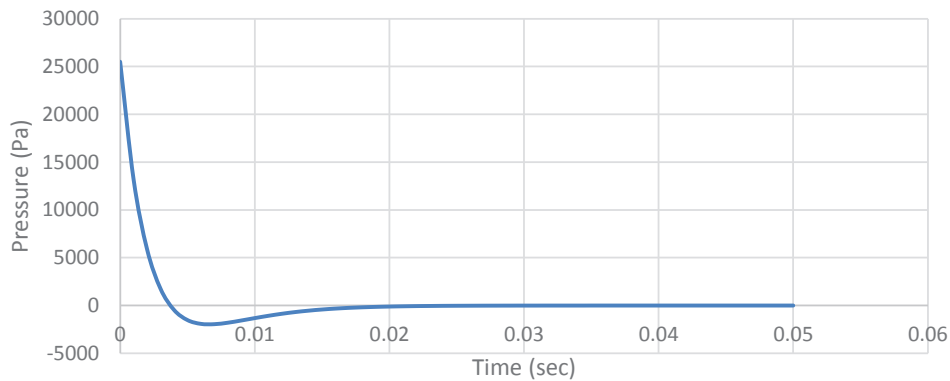


FIGURE 7. Blast pressure vs time

NUMERICAL ANALYSIS

The finite element model of the Eiffel Tower was constructed from beam2 and quad4 elements that matched the properties of the members used for construction of the tower. The Young's Modulus (E) and Poisson's Ratio (ν) of the wrought iron were modelled as 172 000 MPa and 0.28 respectively. Restraint was provided at the base of all four legs with fully fixed restraint applied to model the effect of bolting to the sizeable foundations. The entire lattice structure was created by first modelling a quarter of the structure, and mirroring this along the tower's two axes of symmetry. This quarter of the structure was manually created using dimensions from the original construction drawings found in Lemoine's *Gustave Eiffel: The Eiffel Tower* (2008). Once mirrored, quad4 elements were placed at the three platform heights primarily to facilitate the application of an imposed pressure. A lack of information regarding the current flooring within these platforms meant the plates have a thickness that approximates the expected permanent loads due to flooring. They also provide some structural support to surrounding beams.

Linear Static Analysis: The effect of permanent, imposed and wind loads on the structure, which are outlined in the previous section, were evaluated using a linear static analysis. The following load combination cases were applied in accordance with AS1170.0;

$$1.2G + 1.5Q \tag{9}$$

$$1.2G + W + \phi_c Q \tag{10}$$

Where G represents permanent loading, Q represents imposed loading, W represents wind loading and ϕ_c represents the worst-case distributed imposed load combination factor, equal to 0.6. The maximum vertical displacement and axial stress resulted from the 1.2G + 1.5Q load combination, the results of which are displayed in Figure 8 and Figure 9 respectively. As expected, the maximum vertical deflection of the tower was small, measuring 91 mm at the peak of the tower. Maximum axial compressive stress was experienced at the base of the innermost columns at 162MPa. Comparing this to the expected tensile strength of wrought iron in Europe towards the end of the 19th century, 358MPa (Kelton, Arwade & Lutenegeger, 2011), the tower has an estimated safety factor of 2.27 based on strength.

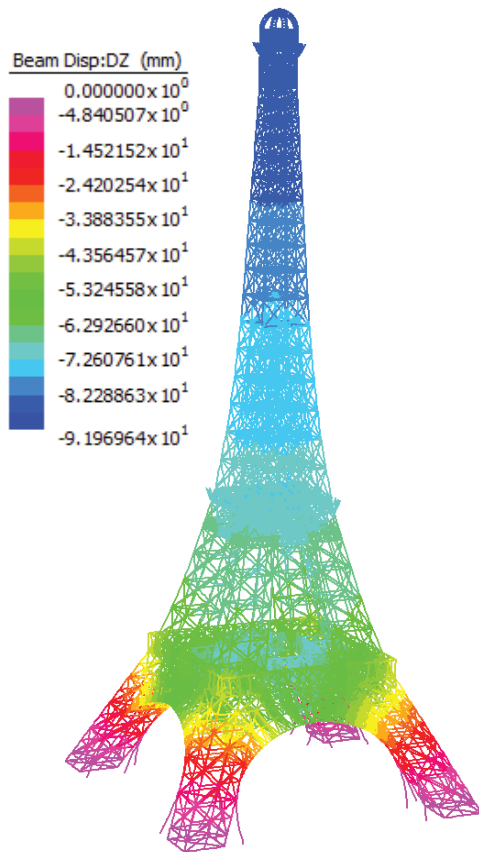


FIGURE 8. Vertical displacement under load combination 1.2G + 1.5Q

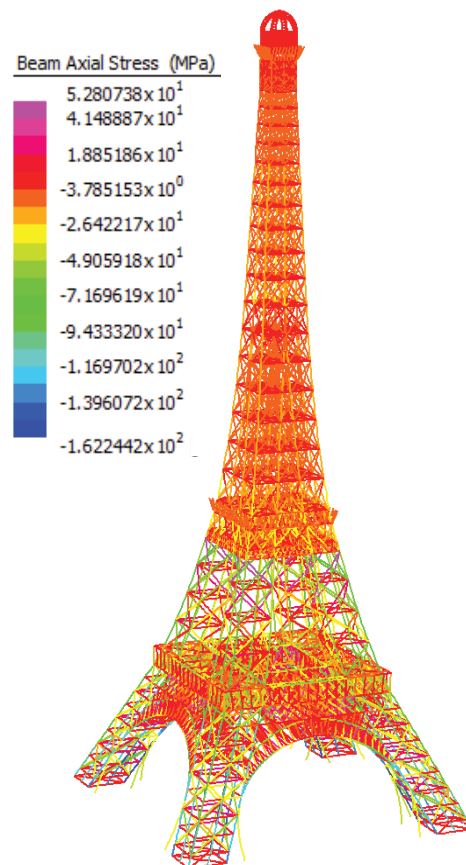


FIGURE 9. Axial stress under load combination 1.2G + 1.5Q

Conversely, maximum lateral displacement was present under the load combination of $1.2G+W+\phi_c Q$, the results of which are displayed in Figure 10. Maximal lateral displacement is observed to be 245mm at the peak of the tower. Serviceability limit state criteria from AS1170.0 suggests a maximum lateral displacement of height/500, or 565mm. Comparing the two, the tower has an estimated safety factor of 2.31 based on serviceability. Figure 11 displays the axial stress throughout the tower for the load combination of $1.2G+W+\phi_c Q$. Maximum tensile and compressive stresses are observed to be lower than the load combination of $1.2G + 1.5Q$.

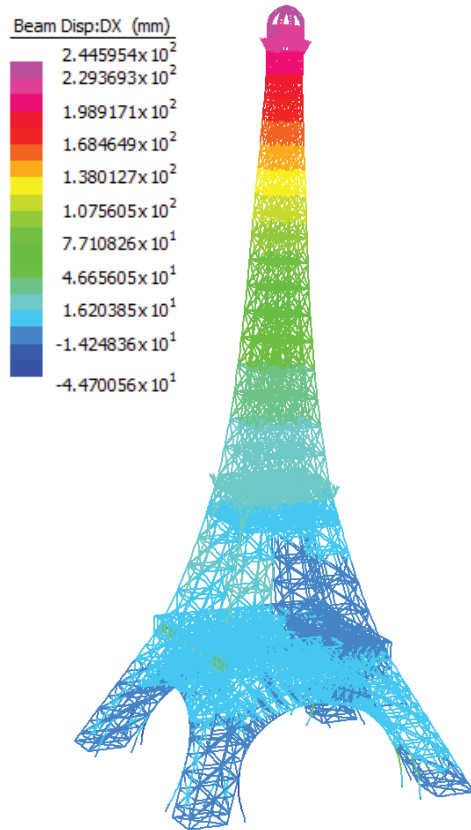


FIGURE 10. Lateral displacement under load combination $1.2G + W + \phi_c Q$

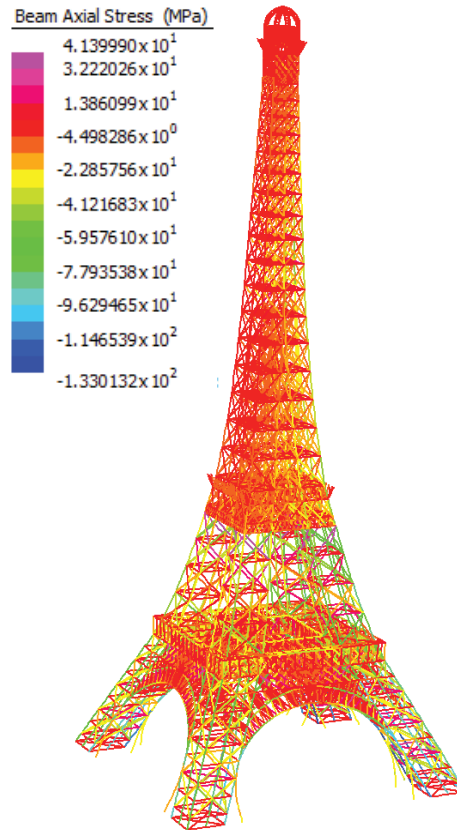


FIGURE 11. Axial stress under load combination $1.2G + W + \phi_c Q$

Blast Analysis: The effect of the ground vibrations due to the blast load were determined by first performing a natural frequency analysis of the tower. The first 6 modes that converged were then used, in conjunction with the period vs time graph (AS1170.4) to perform the spectral response analysis. Ground accelerations were based on historical data of earthquakes with similar magnitudes.

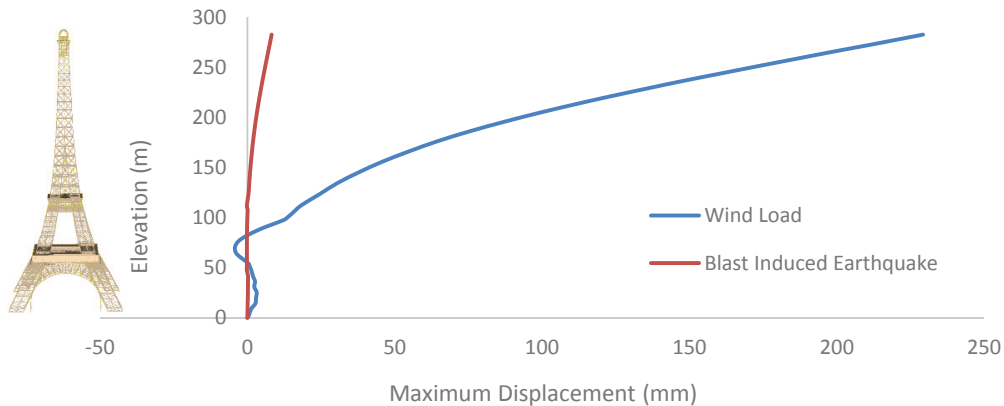


FIGURE 12. Maximum horizontal displacement with elevation

Figure 12 graphically represents the lateral displacement of the tower with its height due to wind and earthquake loading. The lateral displacement due to ground vibrations from the blast are seen to be insignificant in comparison to that experienced during wind loading. Instead, blast pressure is the critical load caused by the explosion. The effect of the blast pressure as a function of time was examined using a non-linear transient dynamic analysis, where factors with time were derived from Figure 7. A non-linear static analysis was conducted to determine the initial conditions for the dynamic analysis, which was imported into the solver. These results were compared with the linear static results, with no significant difference between the two.

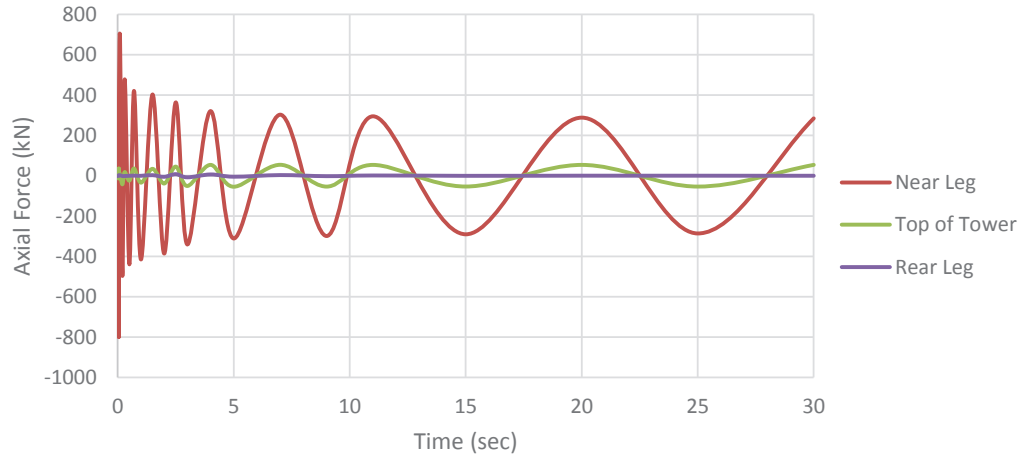


FIGURE 13. Blast induced axial force over time

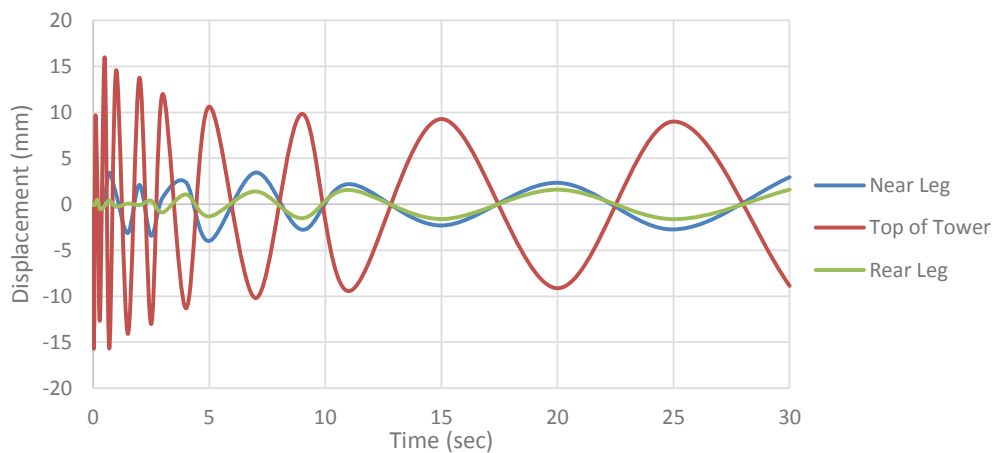


FIGURE 14. Blast induced displacement over time

The blast pressure induces large stresses in the leg closest to the blast, which propagates through the structure (see Figure 16) to cause oscillating positive and negative stresses in the members (see Figure 17). This reverberation is large within the time period analysed, however the effects of damping have not been taken into account and as such, beyond the first oscillations (within the first few seconds), the effects of inertia are observed to dominate. This is seen in Figure 13 and Figure 14, where over a longer period of time, the period of the oscillations increases while the amplitude remains constant. Inertial forces multiply the effects of the reverberation while in reality, damping due to soil and material properties is expected. The oscillation, provided all members remain intact, is estimated to reduce drastically with time as the stresses are distributed throughout the structure and into the soil underneath. Damping properties of the structure and soil have not been analysed within this finite element model, and should be subject to future analysis. There is, however, a substantial time lag between the first induced member stresses close to the blast, and those in members further from the blast (see Figure 15), which are also orders of magnitude smaller. It seems more likely that the members in the leg adjacent to the blast will exceed yield stress, and the stresses elsewhere in the structure will dissipate through damping. Thus the damping qualities are no longer of interest, but rather the structural capabilities of the weakened structure after the blast has caused damage to the structure.

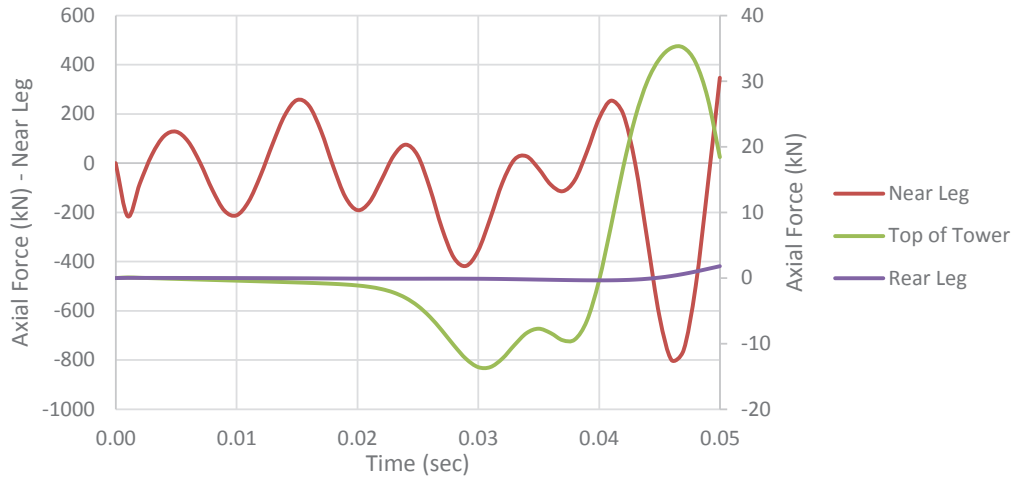


FIGURE 15. Time lag of force across tower

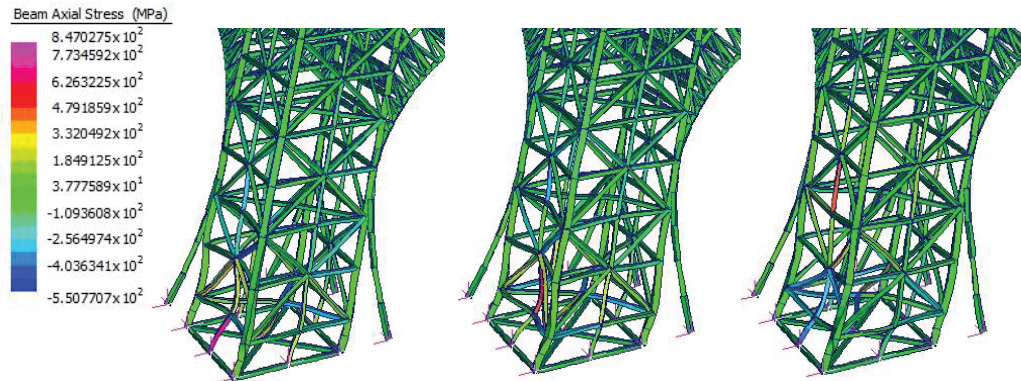


FIGURE 16. Time-phased propagation of axial stress close to blast at times 0.005, 0.007, and 0.013 s

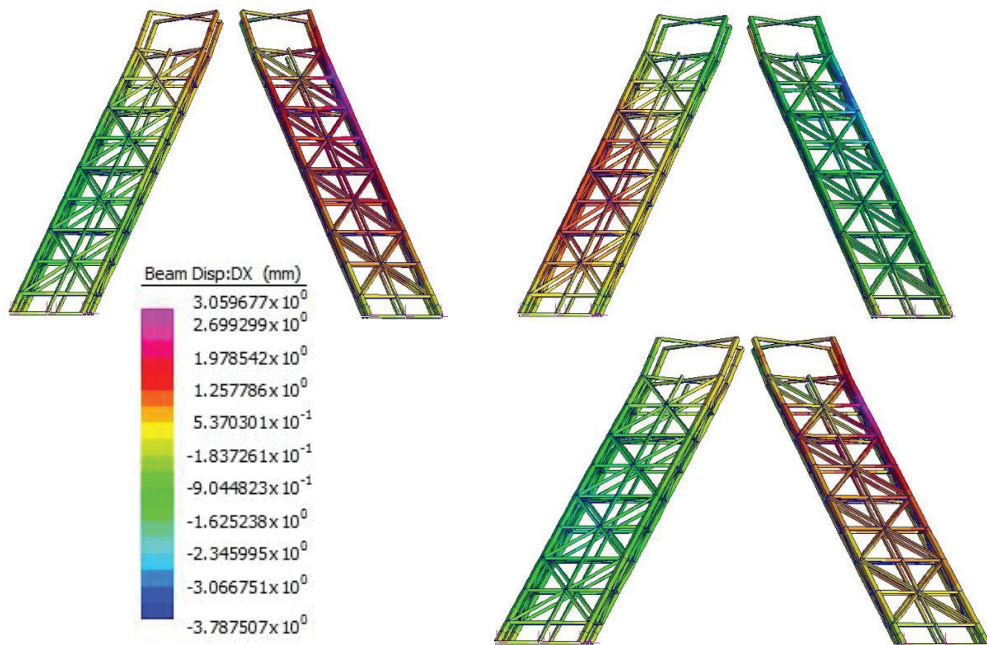


FIGURE 17. Oscillation in rear legs at 3 seconds (top-left), 4 seconds (top-right), and 5 seconds (bottom-right) from time of explosion

Elements with an axial stress that exceeds the ultimate stress of wrought iron, 358MPa (Kelton, Arwade & Lutenege, 2011), were removed from the model through an iterative process whereby members affected by the blast load were removed and again the structure reanalysed. The subsequent weakened structure was analysed under static loading. The recoil due to the blast pressure was not critical in comparison to static loading, and thus a static analysis sufficiently analysed the weakened structure to determine its structural integrity after the explosion.

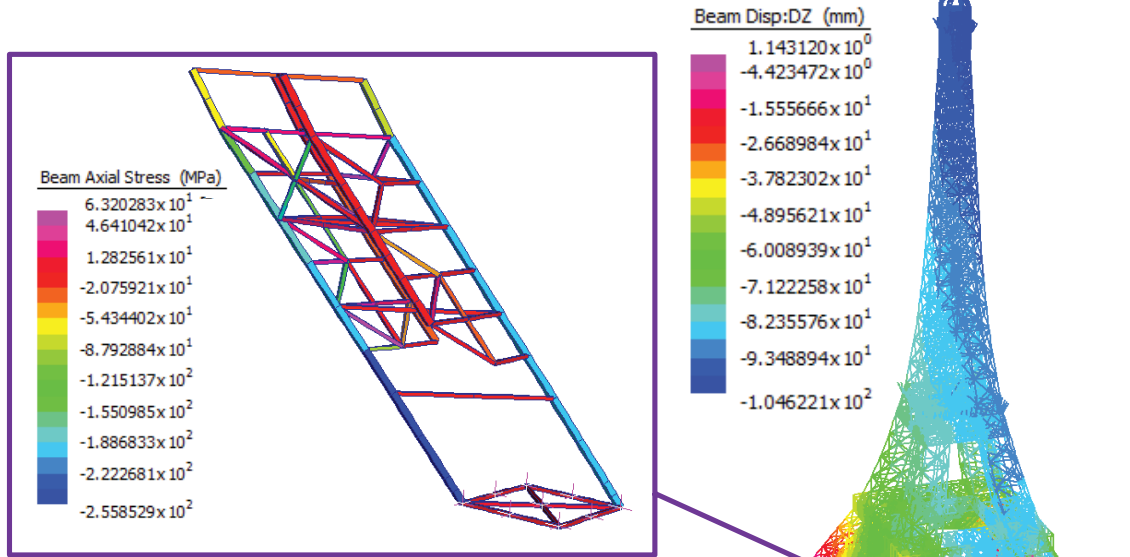


FIGURE 18. Axial stress in weakened leg due to blast loading

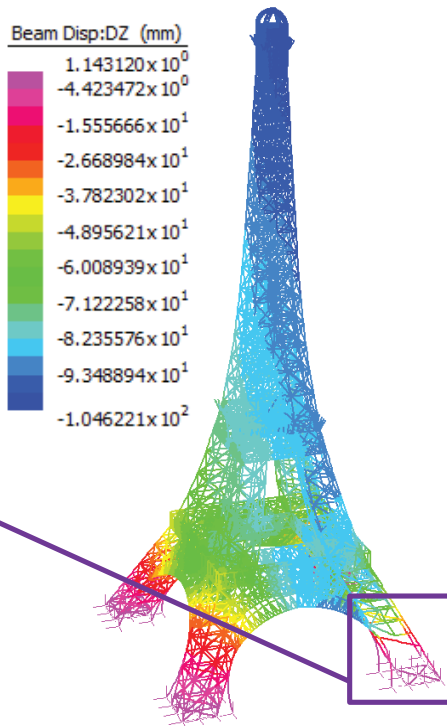


FIGURE 19. Static analysis of weakened structure

The maximum axial stress was experienced in the interior primary column within the affected leg. This is expected as the lean of the deformed structure places large compressive stresses on this member. It is possible that the remaining columns of the damaged leg could undergo buckling since the support provided from bracing is removed, increasing their effective lengths. It should be noted that despite these large stresses, the remaining three legs experience tension less than the tensile capacity of the member and thus the tower is expected to remain standing under static loading, at least for some period of time. It is also noteworthy that when completely removing this leg, the tower still remains structurally sound, indicating that regardless of whether buckling occurs or not the structure maintains its resistance to toppling. This is a result of the large footings, which allow the tower to hang off the leg furthest from the affected leg, placing this in tension.

STRUCTURAL DESIGN

The finite element model uses a variety of member types that aim to replicate existing beams used to construct the Eiffel Tower. Where possible, member properties have been calculated from these existing beams and substituted into the model. An example of this is seen in the Structural Members section of this report.

All beams are assumed to be purely under compression or tension due to the truss-like nature of the tower. Despite applying to steel members, AS4100-1998 has been used to determine sectional and member capacities for the wrought iron beams. The following analysis is for the primary column section at ground level, which approximates the cross-section of the beam as a square hollow section. The section and member capacities were determined for the members that contributed most to the weight of the tower (see table 5).

$$N^* \leq \phi N_s \tag{11}$$

$$\phi N_s = \phi k_f A_g f_y = 0.9 \times 1.0 \times 95992 \times 207 = 17883 \text{ kN} \tag{12}$$

$$\text{where } b_e = b \left(\frac{\lambda_{ey}}{\lambda_e} \right) = 850 \cdot \left(\frac{40}{27.4} \right) \leq b \quad (13)$$

$$N_c = \alpha_c N_s \leq N_s \quad (14)$$

$$\lambda_n = \left(\frac{l_e}{r} \right) \left(\sqrt{k_f} \right) \sqrt{\frac{f_y}{250}} = \left(\frac{7500}{324.7} \right) (\sqrt{1}) \sqrt{\frac{207}{250}} = 21.02 \quad (15)$$

$$\alpha_c = 0.979 \quad (16)$$

$$\phi N_c = 17650 \text{ kN} \quad (17)$$

$$\text{Maximum axial stress} = \frac{\phi N_c}{A_g} = \frac{17650}{95992} = 183.83 \text{ MPa} \quad (18)$$

TABLE 5. Existing member capacities

Member	Existing Members	Load Capacity (MPa)	Max Axial Stress (MPa)	Length of Section (m)
Bracing Section I	EA 100 x 100 x 11	186.30	141.67	6804.28
Columns Section I	SHS 850 x 850 x 28.3	183.87	162.24	1058.69
Bracing Section II	EA 80 x 80 x 9	182.05	76.43	4026.06
Columns Section II	SHS 800 x 800 x 21.2	176.84	81.94	978.96
Bracing Section III	EA 90 x 90 x 12	179.72	31.82	6909.34
Columns Section III	SHS 600 x 600 x 27.5	170.17	44.28	1187.06
Bracing Section IV	EA 90 x 90 x 11	182.20	31.59	4196.17
Columns Section IV	SHS 600 x 600 x 23.2	174.90	49.93	1336.29
Archway	SHS 400 x 400 x 7	145.61	138.91	9829.82
Truss Platform I	SHS 180 x 180 x 20	129.47	91.62	7636.20
Horizontal	SHS 800 x 800 x 24	186.23	42.67	1923.43

To determine more suitably sized members, the maximum axial stress experienced by each member type was recorded, and calculations using this stress value were carried out. The following analysis is for the primary column section at ground level, which approximates the cross-section of the beam as a square hollow section. Again, the following analysis is for the primary column section at ground level.

$$\text{Current load} = \phi N_s = 162.24 \times 95992 = 15574 \text{ kN} \quad (19)$$

$$\text{Suitable member area} = \frac{\phi N_s}{\phi f_y} = 83597 \text{ mm}^2 \quad (20)$$

To ensure the full area of the section is effective, i.e. the form factor k_f is equal to one, the following applies:

$$\frac{b}{t} \leq \frac{\lambda_{ey}}{\sqrt{\frac{f_y}{250}}} = 43.96 \quad (21)$$

For a square hollow section,

$$\text{member width} = \sqrt{\frac{b A_g}{4t}} = \sqrt{\frac{43.96 \times 83597}{4}} = 958.5 \text{ mm} \quad (22)$$

Checking section capacity,

$$N_c = \alpha_c N_s \leq N_s \quad (23)$$

$$\lambda_n = \left(\frac{l_e}{r} \right) \left(\sqrt{k_f} \right) \sqrt{\frac{f_y}{250}} = \left(\frac{7500}{382.5} \right) (\sqrt{1}) \sqrt{\frac{207}{250}} = 17.84 \quad (24)$$

$$\alpha_c = 0.989 \quad (25)$$

$$\phi N_c = 15109 \text{ kN} \quad (26)$$

$$\text{Maximum axial stress} = \frac{\phi N_c}{A_g} = \frac{15109}{83597} = 184.97 \text{ MPa} \quad (27)$$

Using this approach for all members, a static analysis was performed and the maximum axial stress for the optimised design was determined for all member types (see table 6).

TABLE 6. Proposed member sizes and capacities

Member	Suitable Members	Load Capacity (MPa)	Max Axial Stress (MPa)	Weight Savings (t)
Bracing Section I	EA 195.7 x 195.7 x 4.5	176.94	133.93	109.07
Columns Section I	SHS 958.5 x 958.5 x 21.8	184.97	155.73	110.30
Bracing Section II	EA 119.0 x 119.0 x 2.7	180.79	118.23	109.76
Columns Section II	SHS 573.0 x 573.0 x 13.0	163.93	119.29	276.64
Bracing Section III	EA 91.5 x 91.5 x 2.1	184.22	107.67	371.94
Columns Section III	SHS 415.3 x 415.3 x 9.4	158.68	108.66	437.30
Bracing Section IV	EA 87.9 x 87.9 x 2.9	185.53	121.69	210.65
Columns Section IV	SHS 405.3 x 405.3 x 9.2	165.60	125.47	400.72
Archway	SHS 300.3 x 300.3 x 6.8	183.59	146.43	216.17
Truss Platform I	SHS 150 x 150 x 15	115.10	109.73	215.25
Horizontal	SHS 433.0 x 433.0 x 9.9	184.20	82.32	808.53

All members satisfy the calculated axial load capacity. This has been carried out after only one iteration. Further iteration will reduce the size of members to their most optimum size for strength purposes, and is subject to further research. The size reductions thus far translate to a total weight saving of 3387 tonnes, which is 46% of the weight of the metal tower, or 34% of the weight of the entire structure including stairwells and elevator shafts. This can be further optimised after several iterations. It should be noted that the member capacities have been calculated using AS4100-1998, and thus are viewed as an approximation when calculating member capacities for wrought iron beams.

CONCLUSIONS

This finite element model of the Eiffel Tower has successfully enabled a thorough static and dynamic analysis of the structure under permanent, imposed, and wind loading, as well as under blast and earthquake loads due to an explosion. Dimensions have been justified through the use of original construction drawings, and are expected to largely replicate the existing tower. Nodes at the base are assumed to be fixed due to the rigid connection with the foundations, which themselves are very large and would require significant loading to affect. The tower utilises the full axial capacity of individual members by acting as a 'truss of trusses'. As such, permanent and imposed loads are efficiently transferred to the primary columns through compression, while wind loads induce tensile forces in the windward legs and compressive forces in the leeward. Under blast loading, the tower experienced both ground vibrations and blast pressures. Ground vibrations induced a very small earthquake loading into the structure which was ignored in subsequent analyses. The blast pressure was significant, and a dynamic analysis of this revealed that further research is required into the damping qualities of the structure due to soil and mechanical properties. However, in understanding the worst case scenario, the blast was assumed to completely destroy several members in the adjacent leg. Under this weakened structure, it was observed that the tower would still be able to sustain static loads, at least for enough time for occupant evacuation. In final, an analysis of the structural members allowed an optimisation in the design of the tower by reducing the member cross sections while maintaining structural integrity.

ACKNOWLEDGMENTS

Acknowledgements are made to the University of Sydney for providing software licences and supervisors to the project; Faham Tahmasebinia, Peter Ansourian and Fernando Alonso-Marroquin.

REFERENCES

1. P. Weidman and I. Pinelis, *C. R. Mecanique*, **332**(7), 571–584 (2004).
2. N. Lam, P. Mendis and T. Ngo, *Electronic Journal of Structural Engineering*, **4**(1), 28-44 (2004).
3. T. Ngo, P. Mendis, A. Gupta and J. Ramsay, *EJSE Special Issue: Loading On Structures*, **7**(1), 1-16 (2007).
4. E. Grinberg and H. Yan (2016). Town in shock over news that Texas fertilizer-plant explosion was deliberate. *CNN*. Retrieved from <http://edition.cnn.com/2016/05/11/us/texas-fertilizer-plant-blast/> [Accessed 5 Jun. 2016].
5. D. J. Wald, V. Quitoriano, T. H. Heaton and H. Kanamori, *Earthquake Spectra*, **15**(3), 557-564 (1999).
6. B. Lemoine, *Gustav Eiffel - The Eiffel Tower (Ed. 25)*. (Taschen, Cologne, 2008), pp. 1-160.
7. S. L. Kelton, S. R. Arwade and A. J. Lutenecker, *Journal of Materials in Civil Engineering*, **23**(5), 638-647 (2011).

Façade Greening: High-Rise Apartment Building in Milan Using Pre-Stressed Concrete Slab

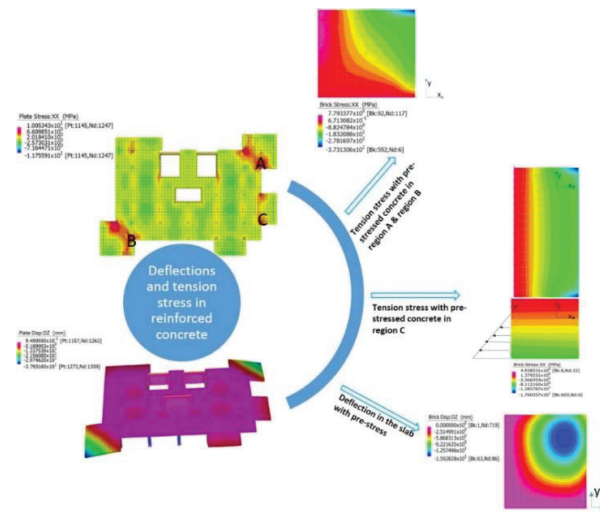
Wenning Sun, Mingxin Li, Yinong Han, Moqi Wang, and Peter Ansourian^{a)}

School of Civil Engineering, The University of Sydney, Sydney NSW 2006 Australia

a)corresponding author: peter.ansourian@uni.sydney.edu.au

Abstract. In this project, one single level of the Façade Greening was designed and modelled using finite element method in Strand7. A static analysis was performed in order to understand the deflection and the stress due to the extra loads imposed by the soil and plants. The results produced by the linear static solver are compared with the strength of the materials and the European limitations. The maximum tension stress which exceeds the tensile strength in concrete is found in the root of the cantilever balcony. An alternative design of the cantilevered balcony with pre-stressed concrete slab is modelled separately for the balcony. Decrease is found in the tension stress and the significant improvement of deflection of the balcony with pre-stressed concrete slab. The dynamic loads such as wind and earthquake did not suggest significant effect on the pre-stressed concrete slab.

Graphical abstract.



INTRODUCTION

Bosco Verticale (In Italian, “vertical forest”) was characterized as the sustainable residential building located in central Milan designed by the famous architect Stefano Boeri and it introduced the philosophy of the balance of nature in the polluted mega-cities (Flannery and Smith, 2015). The concept of sustainable building was gaining popularity in urban architectural designs. The façade greening in high rise residential buildings would effectively balance the limited land areas and the needs of green areas of urban people.

The Bosco Verticale consisted of two rectangular shaped high-rise residential towers of 117m (26 floors) and 76m (18 floors) height which covered a total surface area of 30501sqm (Giacomello, 2015). Both towers were featured by the dense vegetation on the outer edges as shown in Figure 1 (a). The vegetation was planted in the pre-fabricated boxes as shown in Figure 1(b) and located at the periphery of the balcony (ibid.). This building hosted more than 900 trees and over 2000 plants (shrubs and florals) on balconies in different façades. They added extra loads to the cantilevered balcony. The aim of this project was to model the overweighted balcony using both ordinary reinforced concrete slab and pre-stressed concrete slab and to compare the results of tensile stress and deflection.

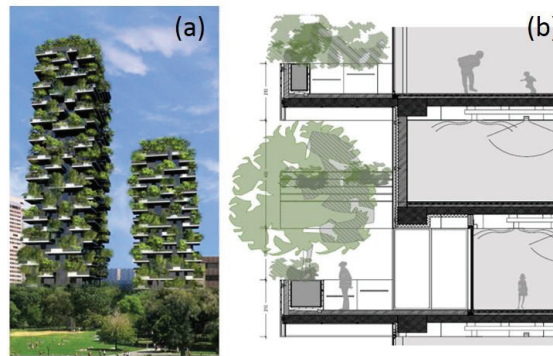


FIGURE 1, (a) the photograph of Bosco Verticale; (b) the pre-fabricated boxes for plants on the periphery (Giacomello, 2015).

TABLE 1. Building Details

Location: Milan	The Year of Built: 2014
Architects: Stefano Boeri	Approximate Cost: €2 billion
Structural Engineers: ZH Construction Company S.p.A.	Overall Height: 117m
Function: Residential building	Floor Area: approximately 30501 m ²
The Structure of the Plan: Two residential towers 85 meters (Tower D), 117 meters (Tower E)	
Number of Floors: 18 (Tower D) and 26 (Tower E)	

The highlight of this project is to model the pre-stressed concrete in cantilevered balconies and to investigate the effectiveness of using pre-stressed concrete to overcome the weakness of tension strength in over-weighted concrete slabs. The concrete would crack if the tensile stress reaches $f'_{ct,f}$ (characteristic flexural tensile strength) under flexural bending. A pre-introduced internal compressive stress at a designed magnitude is applied to the tension face of the slab (Hurst, 1998), therefore to create a counteracted force when the full service loads are loaded as shown in Figure 2(a). The pre-stressed concrete is usually achieved by applying tension to the steel tendons/cables (Hurst, 1998). Figure 2 (b)

shows the stress distribution of the cross-section without pre-stress and with pre-stress. The pre-stress can effectively decrease the tension stress and therefore prevent cracks in concrete.

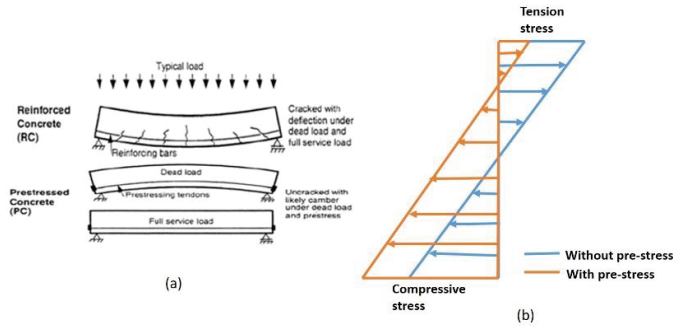


FIGURE 2, (a) the mechanism of pre-stress concrete (Frontdesk.co.in, 2016); (b) the stress distribution without and with pre-stress across a cross-section.

STRUCTURAL MEMBERS

Multistorey Buildings

Below is the description of the structure:

Floor system: Reinforced concrete two-way floor slab (150mm thickness of N12 bar at 280mm spacing) sits on the reinforced concrete beams as a composite system.

Beams: The reinforced concrete beams (350mm x 600mm 3*N20@top and 3*N28@bottom) spans 6.82m horizontally and spans 6.60m vertically, and the perimeter beam spans out 3.41m.

Columns: The reinforced columns at level one is 800mm x 800mm, the column spacing is 6.82m and 6.6m, the floor to floor height is 4m.

Core: Three rectangular shaped shear cores locates at the back of the structure.

TABLE 2. Structural Element for the Level 1 (Building – Projects)

Details of the Structural Elements	Suggested Structural Element Sizes(mm)	Suggested Standard Designs (AS3600)(mm)
Columns - Structural Systems	800 × 800	800 × 800
Beams - Structural Systems	350×600	350×600
Floor System	150	150
Pre-Stressed Concrete Slab	150	150
Reinforced Concrete Slab	150	150
Shear Walls	500	500

STRUCTURAL SYSTEM

Figure 3 shows the plan and elevations of the ground level of the structure. The vertical loads would apply to the internal floor slabs and then transfer to the beams and columns connecting to the ground. The vertical loads on the balcony slab would be transferred to the balcony beams and then connected to

the main structure. The 3 rectangular shaped concrete shear cores were the stiffest structure elements in the structure. The lateral loads are primarily resisted by the shear core and columns. The floor slabs and beams would resist bending from different types of loading. The columns would resist compression from the building weight, imposed loads and live loads. The shear core would resist compression and shear due to the loads.

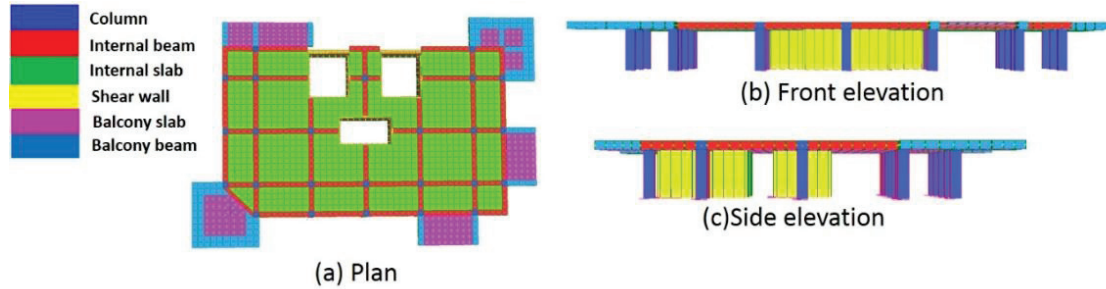


FIGURE 3, Structural system (a) Plan; (b) Front elevation and (c) Side elevation.

LOADS

The dead load of the internal floor and balcony slab is

$$W_{self\ weight,slab} = 0.15m \times 25kN/m^3 + 1.5kPa = 5.25\ kPa$$

The permanent imposed load on floor due to floor covering and ceiling is 1.5kPa (EN1991-1-1-2002, Table 6.2). The dead load of beams carrying loads from slabs is the calculation of dead weight of 7000mm-long beam at the central area of slab as below.

$$W_{dead,beam} = (7m \times 0.15m + 0.6m \times 0.35m) \times 25kN/m^3 = 31.5kN/m$$

The dead load of a single column carrying loads from slabs and beams is

$$W_{dead,column} = (0.8 \times 0.8 \times 4) \times 25 + (0.35 \times 0.6 \times (6.82 + 6.6)) \times 25 + (7.62 \times 7.4 \times 0.15) \times 25 = 345.9kN$$

The internal floor slab is subjected to a uniformly distributed live load of 2kPa and the balcony floor is subjected to a uniformly distributed live load of 3kPa (EN1991-1-1-2002, Table 6.2). The periphery of the balcony slab experienced a live load of 7kPa due to the tree and soil load. The serviceability load combination factor is used. The maximum design load on the internal floor is 7.25kPa. The maximum design load on the balcony slab is 8.25kPa and the design load on the periphery of the balcony slab is 10kPa.

According to Figure 3, the load would firstly apply on the floor as distributed load, then the load would transfer to the beam as line load and finally the load would transfer to the columns as axial compressive load.

NUMERICAL ANALYSIS

All the elements of the structure are subdivided into finer elements to ensure the accuracy of the analysis since mesh refinement is required where significant stress and strain gradients exist. There was no curve boundary in this structure, so T3 and Q4 elements were used to model the structure. The domain approximation error can be avoided using triangular and rectangular elements. Meanwhile the square shape of the elements also benefits for reducing the computational errors because the main source of computational errors is from the distortion of the elements. Each plate is divided into 8×8 elements and

the elements are all matched with each other to avoid mesh incompatibilities. The orders of them are relatively reasonable which is able to ensure that there is no significant approximation error.

The elements used in the structure are carefully chosen and the details of them are shown in the table below.

TABLE 3. The properties of elements on the building

Member	Element type	Element thickness (mm)	Material selection
Column	Beam2	800*800	$f_c = 40 \text{ Mpa}^*$
Internal slab	Plate(Quad4)	150	$f_c = 32 \text{ Mpa}^*$
Internal beam	Plate(Quad4)	600	$f_c = 40 \text{ Mpa}^*$
Shear wall	Plate(Quad4)	500	$f_c = 40 \text{ Mpa}^*$
Balcony slab	Plate(Quad4)	150	$f_c = 40 \text{ Mpa}^*$
Balcony beam	Plate(Quad4)	600	$f_c = 40 \text{ Mpa}^*$

The constraints are all forced on the basement which are the points on the bottom of the whole building. The restrains of them are all fixed (translation and rotation).

The solver used in the analysis is the linear static analysis and the input data required for this solver the geometry of the elements which are shown in table 3 and the loads applied on the different parts of the building which are shown in the part of LOADS.

Single level with beam and systems under ordinary reinforcement:

The Figure 4 (1) below shows the deflection of one level of the structure under ordinary reinforcement. The maximum deflection is located at the two tip points of the two-way cantilevered balcony under the serviceability load. The maximum deflection is 37.93mm. In Eurocode, the limit of serviceability deflection is calculated as $L/180$. Figure 4(2) shows the span of the two-way cantilevered balcony slab, the $L=7230\text{mm}$, therefore, $\delta_{limit} = 40.17\text{mm}$. The short term serviceability deflection satisfied the δ_{limit} according to the Eurocode.

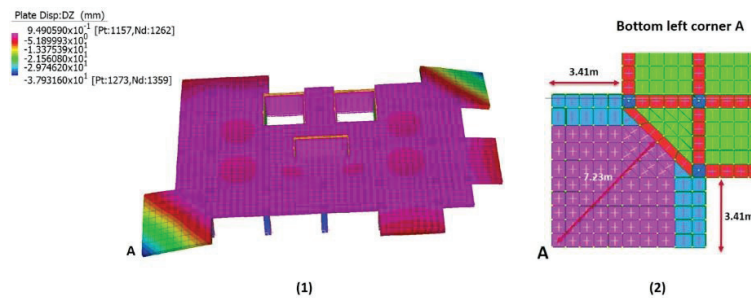


FIGURE 4, (1) the deflection of one level of the structure under normal reinforcement; (2) the maximum span of the cantilevered balcony.

The stress of one level of the structure under ordinary reinforcement is shown in the Figure 5. The maximum compressive stress σ_{xx} in plate is 11.76 Mpa and is less than the characteristic compressive strength of concrete. The characteristic flexural tensile strength of the concrete (with $f_c'=40\text{Mpa}$) is 3.79Mpa. The maximum tensile stress σ_{xx} in plate is 10.05Mpa which would cause the concrete to crack. The region A, region B and region C are the areas where cracks in concrete would highly likely

to occur. If the concrete is cracked, it will give rain water and water from the soil a pathway to penetrate into the slab, it may cause corrosion in the steel reinforcement and cause failure to the slab. Moreover, in the long-term stability of the structure, the cracks in concrete would increase the risk of failure in the cantilevered balcony.

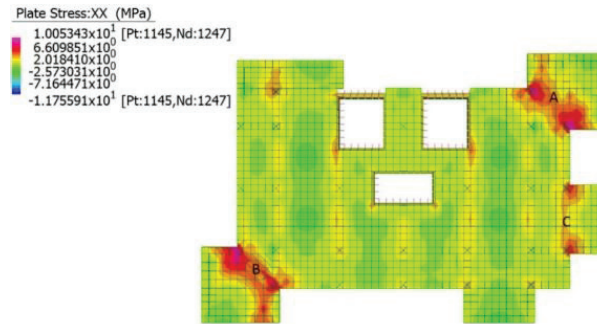


FIGURE 5, the σ_{XX} in one level of the structure.

In order to improve the design of the over-weighted cantilevered balcony, the pre-stressed concrete slab was used in the analysis, the approaches of how the pre-stressed concrete slab is model is explained as below.

One-way cantilever balcony slab:

A one-way cantilever balcony slab is modelled in Strand7 as shown in Figure 6(a). Brick elements are used in order to create the eccentricity for the pre-loaded forces as far from the neutral axis. Pre-stressed steel tendons were embedded into the top layer of the balcony slab shown as Figure 6(b). The steel tendons were 10mm diameter steel bars and the pre-load applied were 3Mpa. The pre-stressed steel tendons were design to induce a negative moment (hogging) according to the design loads which will be applied later. The boundary condition in this balcony slab model is fully fixed. The loads are applied according to LOADS.

Two-way cantilever balcony slab:

Similar as the one-way cantilever balcony, the structure also has two two-way cantilever balcony shown as Figure 6(c). Instead of one edge connecting to the main structure, the two-way cantilever balcony is assumed to have two edges connecting to the main structure. The steel tendons were embedded as shown in Figure 6(d).

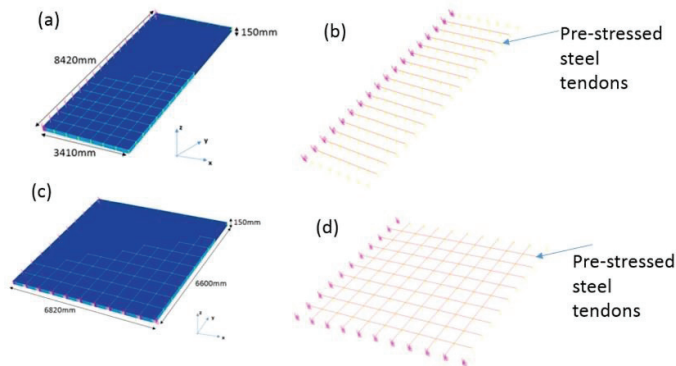


FIGURE 6, (a) one-way cantilever balcony model; (b) pre-stressed tendon layouts of one-way cantilever; (c) two-way cantilever balcony slab model; (d) pre-stressed tendon layouts of two-way cantilever.

Pre-stressed concrete cantilevered balcony:

Region A & Region B:

Alternative design with pre-stressed tendons is added to the two-way cantilever as explained above. Figure 7 shows the stress σ_{XX} with pre-stressed tendons under the design loads in table 1 for balcony. Although, the tension stress is still slightly higher than the $f'_{ct,f}$, the tension stress in the cantilever balcony decreased 23%. Without pre-stressing, the tensile stress was approximately 10Mpa. After applying the pre-stressing, the tensile strength dropped to 7.7Mpa. The material properties input into the cantilever balcony model is pure concrete. In reality, if the appropriate reinforcement is added to the balcony slab, the tension stress σ_{XX} in concrete would be smaller or very close to the $f'_{ct,f}$. Therefore, no crack or very minor crack would occur in the concrete slab and this would not affect the serviceability and stability of the balcony.

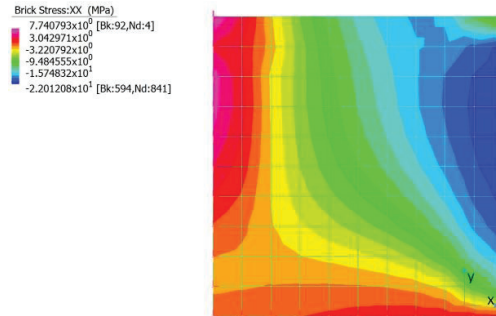


FIGURE 7, two-way cantilever balcony with pre-stress

Moreover, the pre-stress in concrete also significantly improves the deflection in the balcony. Figure 8 shows the deflection in the balcony. Compared to a deflection of 37.93mm with normal reinforcement, the deflection decreased approximately 50% at a value of 15.92mm with pre-stress concrete. This deflection would safely satisfy the limit of deflection required by the Eurocode.

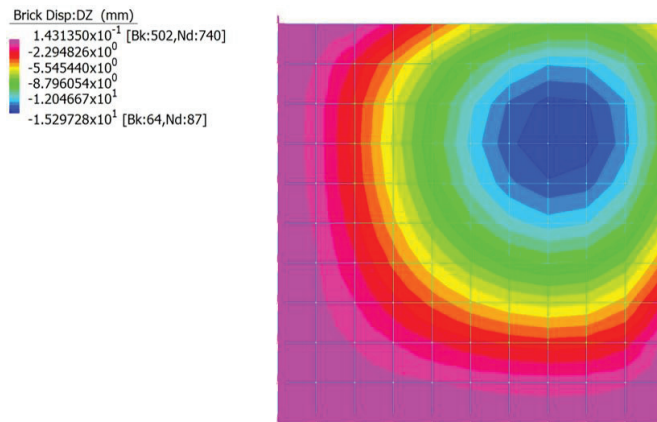


FIGURE 8, the deflection in the two-way balcony with pre-stress.

Region C:

Alternative balcony design model using pre-stressed concrete is also created for the balcony at region C. The comparison of tension stress σ_{XX} without and with pre-stress under same loading conditions is shown in Figure 9. Similar as region A & B, the tension stress σ_{XX} in pre-stress concrete decreases approximately 56% at a value of 5.96Mpa. This value is very close to $f'_{ct,f}$. If the appropriate

reinforcement is added to the slab, the balcony would be safe from the cracks. Viewing the model from ZX-plane, the shift of the stress distribution in the cross-section can be clearly identified. And this proves the theory explained in section 2.3.2. The validity of this method as a modelling pre-stressed concrete in numerical model is approved.

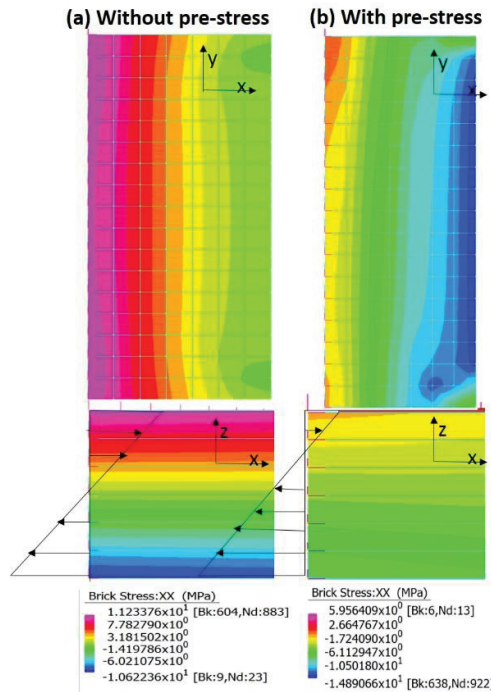


FIGURE 9, (a) the one-way balcony without pre-stress in xy-plane and in zx-plane;
 (b) The one-way balcony with pre-stress in xy-plane and in zx-plane.

Effect of Wind load and Seismic load on pre-stressed concrete structure.

The effects to pre-stressed balcony from the wind loads and earthquake loads have been analyzed. It turns out that the wind loads and earthquake loads are only affecting the lateral loads but pre-stresses are only used to resist vertical loads and deflections. The influences from wind and earthquake are not relevant to pre-stresses by using linear analysis.

According to the research of pre-stressed structure under earthquake load by W. Morley Southerland, the structural type of Green Façade with pre-stressed slab, reinforced column and shear core is a widely used type of resisting lateral and vertical load during earthquake. The pre-stressed members were designed for balancing vertical dead load and live loads for different load cases. As the earthquake load can be analyzed in lateral vibration and vertical direction caused by damping, the pre-stressing accomplished by adding post-tensioned tendons were investigated to be efficient in balancing seismic live load especially. (Southerland, n.d.)

STRUCTURAL DESIGN

According to the Australian Standard AS3600, the size of members of the project were redesigned by hand calculations. Since the load transfer was firstly from the distributed dead load and live load on slab, then transferred to beams and finally columns. Load case 1.2G+1.5Q was used for the member design as the worst case.

- a) Design calculation for beam A (as an example).

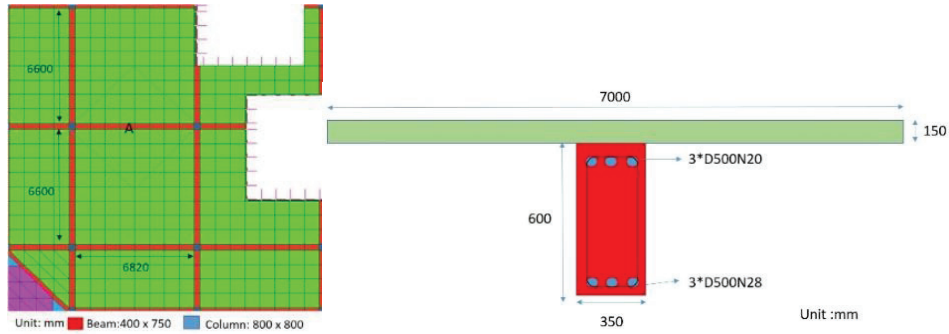


FIGURE 10. Plan and section view for a typical beam A.

$$\text{selfweight} = (7\text{m} \times 0.15\text{m} + 0.6\text{m} \times 0.35\text{m}) \times 25\text{kN/m}^3 = 31.5\text{kN/m}$$

$$\text{imposed load} = 1.5\text{kPa} \times 7\text{m} = 10.5\text{kN/m}, \text{ where } \text{live load} = 2\text{kPa} \times 7\text{m} = 14\text{kN/m}$$

Use load combination: $1.2G+1.5Q=71.4\text{kN/m}$

Since the slab is a two-way slab, the distributed load is a triangle shape shown as the diagram below. To simplify the calculation, transfer the triangular shape into a UDL by multiplying $2/3$.

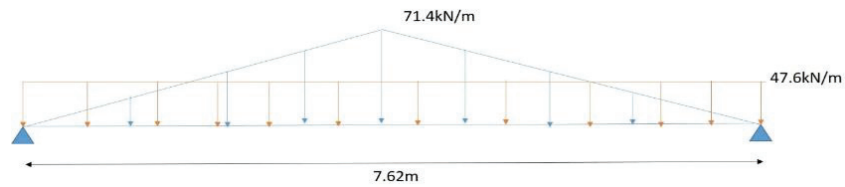


FIGURE 11. Load distribution on tributary area of beam A.

Hence the maximum bending moment $M^* = \frac{WL^2}{8} = \frac{47.6 \times 7.62^2}{8} = 345\text{kN} \cdot \text{m}$.

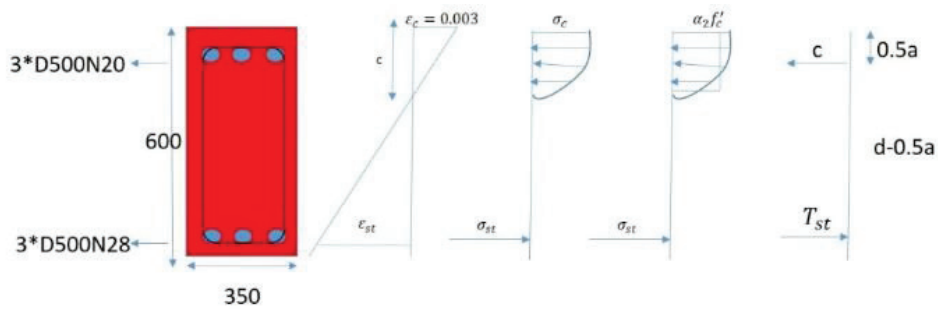


FIGURE 12. Design of reinforcement of beam A.

$$A_{st} = 3 \times (\pi 14^2) = 1847\text{mm}^2, \text{ and } A_{sc} = 3 \times (\pi 10^2) = 942\text{mm}^2.$$

Check for bending using AS3600 section 8.1.3

Assume tensile reinforcement has yield when the extreme compressive fibre reaches its maximum $\epsilon_c = 0.003$

$$\alpha_2 = 1 - 0.003f'_c = 0.85, \quad \gamma = 1.05 - 0.007f'_c = 0.77$$

$$\text{Hence } T_{st} = A_{st}f_y = 1847 \times 500 = 923500\text{N}$$

$$C_{st} = A_{sc}[\sigma_{st} - \alpha_2 f'_c] = 942[2 \times 10^5 \frac{c-30}{c} \times 0.003] \quad C_{st} = 565200[\frac{c-30}{c}]$$

$$C_{concrete} = \alpha_2 f'_c \gamma c b = 0.85 \times 40 \times 0.77 \times 350c = 9163c$$

$$\text{From } C_{concrete} + C_{st} - T_{st} = 0, \quad c = 66.8\text{mm} \text{ and } k_{uo} = \frac{c}{a} = \frac{66.8}{600} = 0.11 < 0.545$$

$$\epsilon_{sc} = \frac{66.8-30}{66.8} \times 0.003 = 0.0016 < 0.0025 \text{ not yield}$$

$$M_{uo} = C(d - 0.5\gamma c) + C_{sc}(d - d_{sc}) = 510.6\text{kN} \cdot \text{m}$$

$$\phi M_{uo} = 0.8 \times 510.6\text{kN} \cdot \text{m} = 408\text{kN} \cdot \text{m} > 345\text{kN} \cdot \text{m}$$

Check for shear using AS3600 section 8.2

$$V^* = \frac{wL}{2} = \frac{47.6 \times 7.62}{2} = 181.36\text{kN}$$

$$d_0 = 600 - 20 - 12 - 14 = 554$$

Section 8.2.6

$$V_{u,max} = 0.2f'_c b_v d_0 = 0.2 \times 40 \times 350 \times 554 \times 10^{-3} = 1551.2\text{kN}$$

$$V^* < \phi V_{u,max} = 0.7 \times 1551.2 = 1085.8\text{kN}$$

Section 8.2.7.1

$$V_{uc} = \beta_1 \beta_2 \beta_3 b_v d_0 f_{cv} \left[\frac{A_{st}}{b_v d_0} \right]^{\frac{1}{3}}$$

$$\beta_1 = 1.1 \left(1.6 - \frac{d_0}{1000} \right) \geq 1.1 = 1.15, \quad \beta_2 = 1 \text{ (pure bending)} \text{ and } \beta_3 = 1 \text{ (UDL)}$$

⇨

$$f_{cv} = f'_c{}^{\frac{1}{3}} = 3.42 \leq 4\text{MPa}$$

$$V_{uc} = 161.65\text{kN} \text{ and } 0.5\phi V_{uc} = 56.58\text{kN} \quad V^* < 0.5\phi V_{uc}$$

Section 8.2.9

$$V_{u,min} = V_{uc} + \max(0.1\sqrt{f'_c} b_v d_0, 0.6b_v d_0) = 284.3\text{kN}$$

$$\phi V_{u,min} = 0.7 \times 284.3 = 198.9\text{kN}. \text{ Hence } 0.5\phi V_{uc} < V^* < \phi V_{u,min}.$$

Section 8.2.8

$$A_{sv,min} = \max\left(\frac{0.06\sqrt{f'_c} b_v s}{f_{sy,f}}, \frac{0.35b_v s}{f_{sy,f}} \right) = 0.266s$$

Assume 2 legged stirrup diameter 12

$$A_{sv} = 226\text{mm}^2, \quad S \leq \frac{226}{0.266} = 849.6\text{mm}$$

Maximum spacing 8.2.12.2

$$S_{max} = \min(0.75D, 500) = 450\text{mm}$$

Therefore, the size of beam is shown as figure 12.

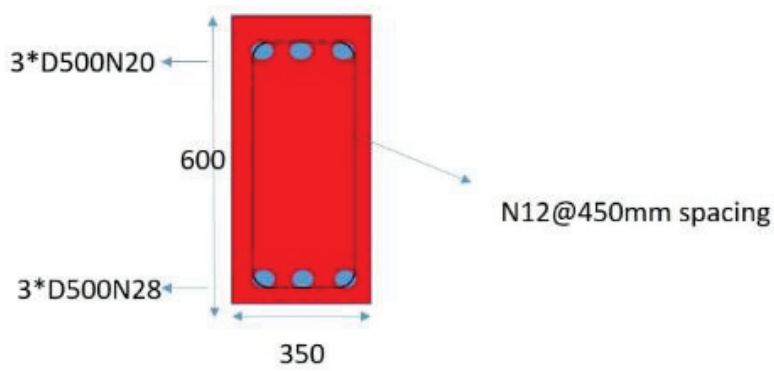


FIGURE 13. Section view of beam A.

b) Design calculation for column A (as an example).

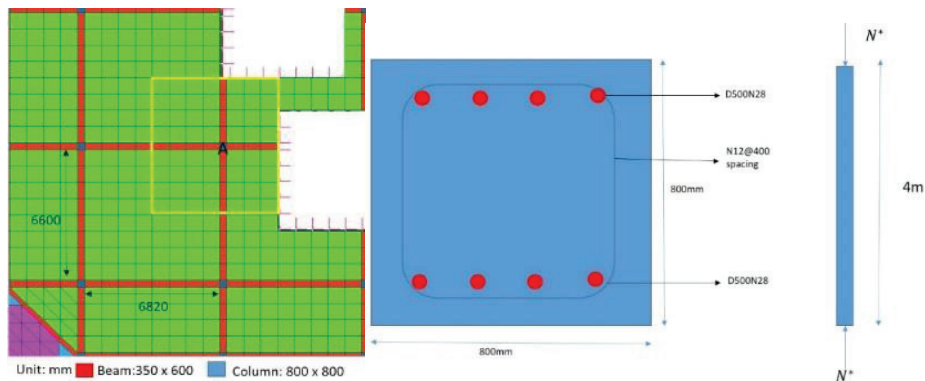


FIGURE 14. Plan, section and front view of column A.

$$\text{Self-weight of 1 floor} = (0.8 \times 0.8 \times 4) \times 25 + (0.35 \times 0.6 \times (6.82 + 6.6)) \times 25 + (7.62 \times 7.4 \times 0.15) \times 25 = 345.9 \text{ kN}$$

$$\text{Live load and imposed load} = 3.5 \text{ kPa} \times (7.62 \times 7.4) = 52.6 \text{ kN}$$

$$\text{Total of one floor} = 400 \text{ kN.}$$

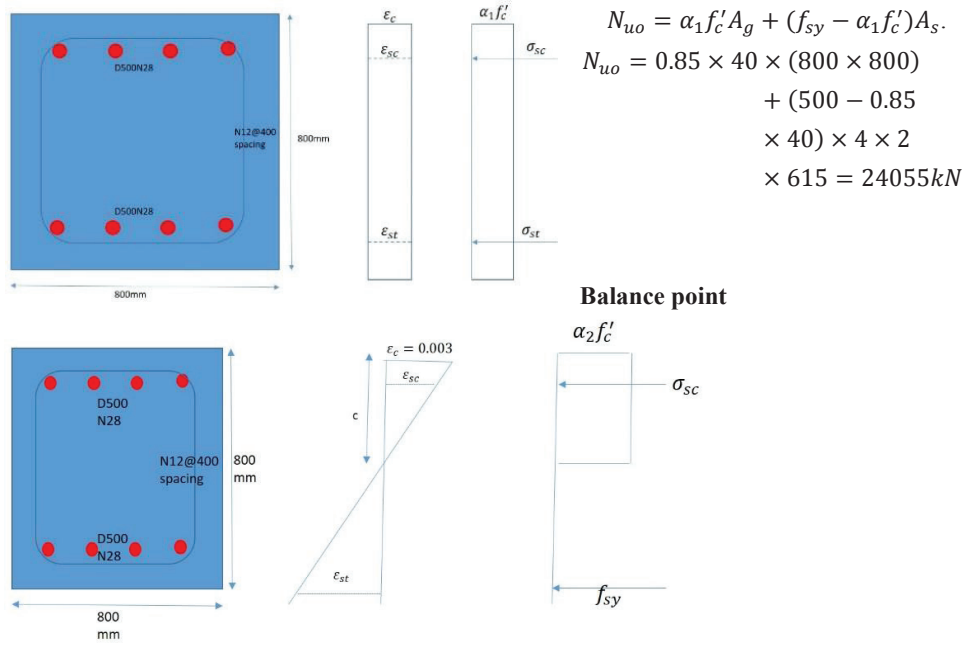
$$\text{For the column on the foundation } N^* = 27 \times 400 = 10758 \text{ kN}$$

Section 10.7.4 use N12 bae as fitments

$$S_{max} = \min(D_c, 15d_b) = 420 \text{ mm} \text{ therefore, use N12@400mm spacing is ok.}$$

Section 10.6.2.2: **Squash load**

The strain in reinforcement should be taken as 0.0025, which in case of D500 steel coincide with the yielding point.



$$c = 0.545 \times 766 = 417\text{mm}$$

$$\epsilon_{sc} = \frac{0.003}{417} \times (417 - 34) = 0.0027 \text{ (All bars are yielding).}$$

$$\alpha_2 = 0.85;$$

$$C_c = \alpha_2 f'_c \gamma c b = 0.85 \times 40 \times 0.77 \times 417 \times 800 = 8733648\text{N}$$

$$S_{st} = f_y A_{st} = 500 \times 4\pi 14^2 = 1231504\text{N}$$

$$S_{sc} = (f_{sy} - \alpha_2 f'_c) A_{sc} = (500 - 0.85 \times 40) \times (4\pi 14^2) = 1147762\text{N}$$

$$N_{ub} = C_c + S_{sc} - S_{st} = 8650kN$$

$$M_{ub} = C_c(400 - 0.5\gamma c) + S_{sc}(400 - 34) + S_{st}(400 - 34) = 3019kN \cdot m$$

Check the slenderness of the column:

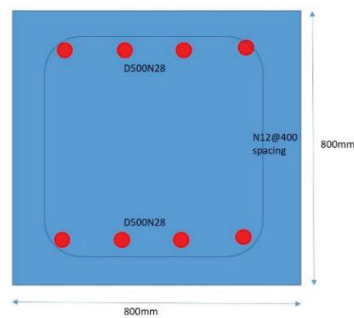
$$L_e = 4000 \times 0.7 = 2800\text{mm} \text{ (table 10.5.3 (A))}$$

$$r = 0.3D = 0.3 \times 800 = 240\text{mm}$$

$$\frac{L_e}{r} = 11.7 < 25 \text{ therefore, short column}$$

Buckling load $N_c = \left(\frac{\pi^2}{L_e^2}\right) [182d_0(\phi M_c)/(1 + \beta_d)]$ where $M_c = M_{ub}$ and $\phi = 0.6$

$$N_c = 317905kN > N^*$$



Therefore, the section for column is as shown on right.

CONCLUSIONS

In conclusion, the deflection and stresses in one single level of the structure is successfully model in Strand7. The deflection is close to the European limits but still satisfy the limits. There are no problems with the compressive stress in concrete. However, the significant high value of tension stress is identifying at the cantilever roots of the balcony. It will cause cracks in the concrete and in both long term and short term it will affect the serviceability and stability of the balcony. Therefore, a separate model of balcony with pre-stressed concrete is created. The results are compared with the balcony without pre-stress. A significant improvement has been observed with pre-stressed concrete in tension stress in concrete.

The model cannot fully simulate the pre-stressed concrete balcony with appropriate reinforcement. However, with reasonable assumptions, the effectiveness of pre-stressed concrete in dealing with large service load is justified. A better way to model prestress in the restricted model would be to place pre-stressing tendons (Truss elements) within the balcony slab. The slab itself would be in several layers of brick elements, one layer of which would house the tendons which would join the existing nodes of the brick elements. These tendons would have a pretension input as an ATTRIBUTE called "PRELOAD", defined by several thousand Newton's of force in each tendon. The level of preload can be easily assessed by varying preload until the maximum tensile stress under serviceability loads is in the order of 3MPa, an approximate cracking level.

REFERENCES

1. Flannery, J. and Smith, K. (2015). Eco-landscape design. pp.pp 52-61.
2. Frontdesk.co.in. (2016). Prestress Concrete| Front Desk Architects Jaipur. [online] Available at: <http://frontdesk.co.in/prestress.html#.V1DCrk3VyHs> [Accessed 2 Jun. 2016].
3. Giacomello, E. (2015). A new Urban Forest Rises in Milan. CTBUH JOURNAL, 2015(I), pp.12-18.
4. Hurst, M.K. (1998). Prestressed Concrete Design. 2nd ed. New York: CRC Press, pp.6-11.
5. Southerland, W. (n.d.). Prestressed concrete earthquake resistant structures - Development, performance and current research. [online] Available at: http://www.iitk.ac.in/nicee/wcee/article/vol3_IV-463.pdf [Accessed 8 Jun. 2016].

Full Dynamic Model of Golden Gate Bridge

Thomas Game, Cameron Vos, Rafid Morshedi, Rebecca Gratton, Fernando Alonso-Marroquin, and Faham

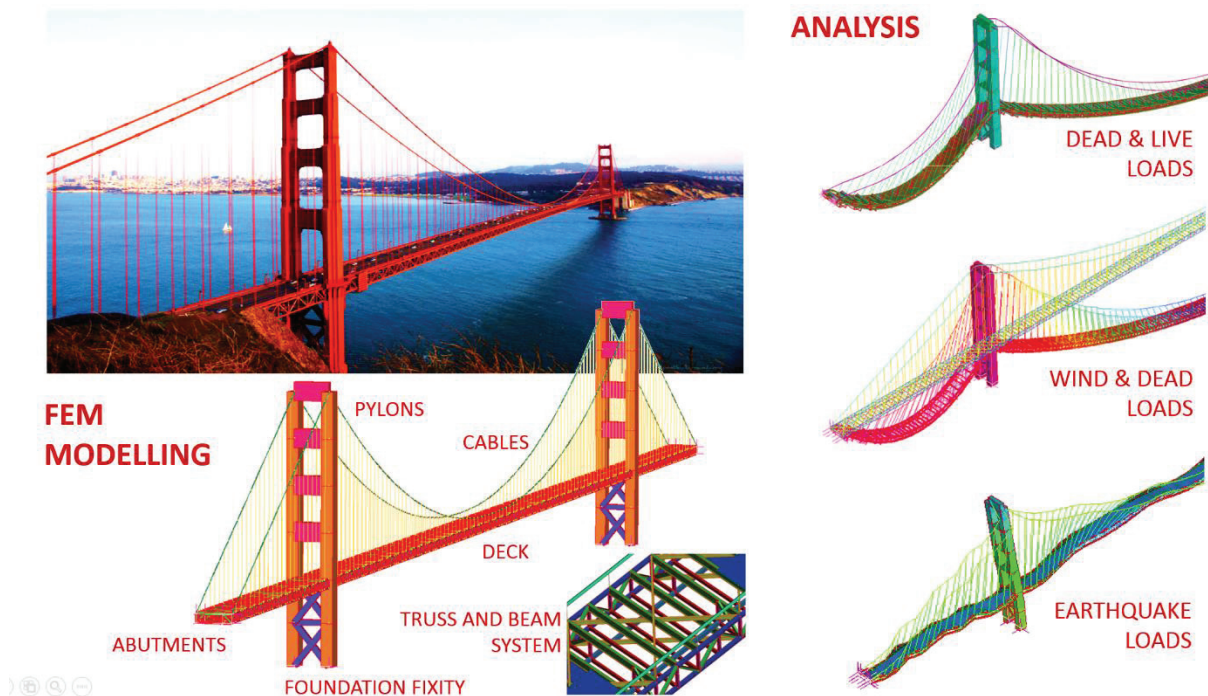
Tahmasebinia ^{a)}

School of Civil Engineering, the University of Sydney, Sydney NSW 2006 Australia

^{a)} Corresponding author: faham.tahmasebinia@sydney.edu.au

Abstract

An investigation into the structural systems of the Golden Gate Bridge when subject to dead, live, wind and earthquake loading was carried out using finite element modelling. This investigation was carried out using Strand7 and was verified through analytical calculations. This report begins with a study into the structural elements of the actual bridge which includes a summary of the member and section sizes and dimensions. From this study a finite element model was produced. This report outlines the modelling techniques, element types and analysis solvers used in modelling and analysing the structure. This report then considers the member sizes used in the model and outlines any variations in member sizes required for a successful analysis. Finally, this report discusses this results produces by the analysis and verifies the results through simple hand calculations.



INTRODUCTION

The Golden Gate Bridge is a 6 lane suspension bridge that crosses the Golden Gate Channel, connecting the San Francisco Peninsula to Marin County. After its conception in 1916, the bridge's construction was a controversial issue, and the final decision to proceed with construction was not passed until 1930. (Golden Gate Bridge Research Library, May 2012) The bridge was opened in 1937 and held the title for being the longest main span suspension bridge for 27 years. (Golden Gate Bridge Research Library, May 2012) The 2332m long catenary cables are the longest bridge cables ever made. These cables used an innovative process to bind thinner wires together to make one large cable which allowed for the construction of the record breaking main span. (Longworth, L., Loeterman, B., 2004) The bridge crosses the 1.6km wide channel which is well known for having high winds and it is situated adjacent to the San Andreas Fault line, a very active transverse fault. (Golden Gate Bridge Research Library, May 2012) The Golden Gate Bridge is one of the world's most spectacular and well known bridges. Having been declared one of the wonders of the modern world by the American society of Civil engineers, this bridge provided a very interesting case study for this investigation. (Golden Gate Bridge Research Library, May 2012) The analysis focused on the main span of the bridge as it was the most complex part of the bridge, and was a ground breaking structural engineering feat at the time of construction.

TABLE 1. Bridge Details (Highway and Transportation District, 2012)

Location: San Francisco	Year of Construction Completion: 1937
Architects: Leon Moisseiff & Irving Morrow	Approximate Cost: \$35 million
Structural Engineers: Joseph Strauss	Main Span: 1280.2m
Function: Motorway bridge / freeway bridge	Occupied Area: approximately 2,000 m ²
Structure: Suspension Bridge	
Number of Lanes: 6	

STRUCTURAL MEMBERS

The Golden Gate Bridge consists of a bridge deck, supported on a system of beams and trusses. This truss system spans between the bridge pylons and is hung from vertical cables at 15m intervals. These vertical cables are supported by two major catenary suspension cables which pass over the pylons and into anchors at either ends of the bridge. The loads applied to the bridge deck in service are transferred into the deck truss. Majority of this load in the truss is carried by the vertical cables, placing the vertical cables into tension. This tension load is then passed into the main cables which carries the load in tension into the abutment anchors at either end of the bridge. Some portion of the load in the truss is also carried by the pylons. The main function of the deck truss is to transfer loads applied at points not near a vertical cable intersection, into an adjacent cable. There is also a stiffening effect of the entire deck system against deflections. Below is the description of the main members of the structure:

Main Deck: Comprised of 4 major components;

- Concrete Bridge Deck.
- Permanent Corrugated Steel Formwork
- Cross Girders
- Deck Truss System

The deck truss shown in Figure 1 is a complicated system of members, most of which are made up of trusses themselves. The size for which were determined using drawings and scaled images, and recorded in Table 2. This truss system is attached to the Steel Cross Girders, which run perpendicular to the bridge's direction of travel, and sit on top of the truss. These cross girders are Deep UB sections, designed to carry flexure, and transfer load into the truss below. Sitting on top of this is the permanent steel formwork, which works both to distribute the load of the deck onto the cross girders, as well as act as tensile reinforcement for the slab on top.

Catenary Cables: There are two "main" cables which are 2332m in length, each. These are made up of 27572 galvanised steel wires, with a total diameter of 0.92m. These cables have a yield stress of 1100MPa, and a suspended length between the two pylons of 1280m.

Vertical Cables: There are 250 pairs of vertical cables with a diameter of 68.3mm and a yield strength of 1100 MPa.

Pylons: 227m tall and constructed from structural steel, 300 MPa yield stress. Base dimensions at footing are 10m x 16m. These are rigidly connected to the deck truss via a riveted plate.

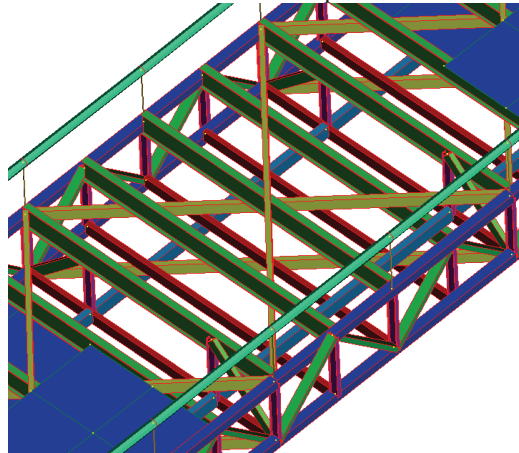


Figure 1. Internal View of Deck Truss

TABLE 2. Structural Element for the Section 1 (Bridge – Projects)

Details of the Structural Elements	Available Structural Element Sizes	Revised Member sizes for Modelling
Green Cross Girder	2500UB3650	2500UB3650
Red Cross Girder	1200x500x50 RHS	2000x2000x200 SHS
Blue Top and Bottom Chords	1400x700x75 RHS	2000x2000x200 SHS
Yellow Cross Bracing	1200x500x50 RHS	1200x500x50 RHS
Green Cross Bracing	500x250x50 RHS	1000x500x50 RHS
Blue Main Girders	1000x1000x100 SHS	1400x700x75SHS
Pink Vertical Members	500UB667	1500UB1590
Vertical Cables	0.126m Diameter	0.3m Diameter
Catenary Cables	0.92m Diameter	1.2m Diameter
Pylons	16000x10000	16000x10000
Pylon Diagonal Bracing	2500x2500	5000x5000
Pylon Cross Bracing	8000x4000	16000x8000
Bridge Deck Slab	0.5m Thick	0.5m Thick

STRUCTURAL SYSTEM

The Structural System Used to Resist Vertical Load

The system used to resist vertical load consists of the following elements:

- The reinforced concrete bridge deck which is loaded directly by traffic
- Cross girder I-beams which directly support the bridge deck
- A truss system which supports both the cross girder beams and bridge deck
- Vertical cables connecting the truss system to the catenary cables
- Two primary catenary cables which pass over the pylons and are anchored at the abutments
- Anchor abutments at either end of the main span which anchor the catenary cables and transfer load to the ground
- Two pylons which support the catenary cables and allow the cables to maintain a catenary shape. The pylons also locally support the bridge truss system at their intersection.
- 4 Cross beams above the deck and 4 diagonal members below the deck connect the pylons and stabilise the vertical structures
- Very deep pile foundations resting on bedrock which support the pylons

Vertical loads applied to the bridge deck are carried by the deck through bending. The deck is a reinforced concrete deck and employs the same design principles as a reinforced concrete slab in a building, i.e. under vertical downward load, the concrete mass in the top of the slab is in compression while the reinforcing steel at the bottom of the slab is in tension. The deck is supported every 5m by cross girders. Thus the deck acts as a continuous slab with one-way action.

The cross girders supporting the deck span across the deck and are deep I-beams with multiple web stiffeners along their length. These cross girders carry load from the deck to the truss system below the deck through bending. The I-beam experiences tension in the bottom flange and compression in the top flange. This beam could be designed using standards such as AS4100. The web stiffeners act to increase the deep beams shear capacity and decrease the chance of shear buckling in the web.

The system of trusses below the deck support the cross girders and the bridge deck at the deck edges. This system of trusses is actually made up of smaller trusses. Therefore, in modelling the bridge, the trusses were modelled as rectangular hollow sections to simplify the design. Figure 2 shows the complex truss system below the bridge deck and the simplified truss system used in modelling the bridge. These trusses carry the load from the cross girders and bridge deck and spread it along the main longitudinal truss. This main longitudinal truss spans between the vertical cable supports and carries the load through bending. This bending is carried within the truss by compression in the top chord, tension in the bottom chord and axial forces in the diagonal members.

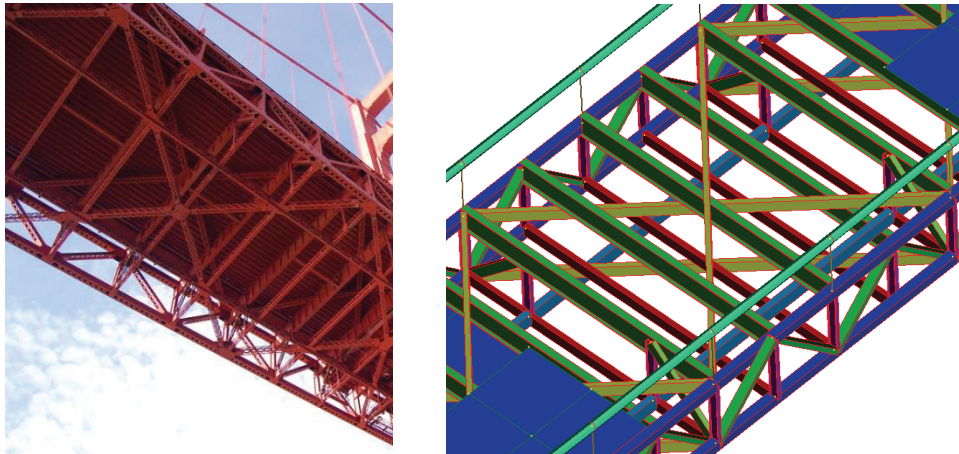


Figure 2: Truss system below bridge deck in reality and simplified for Strand7 model.

The vertical cables connected to the bridge truss every 15m pick up the load carried through the longitudinal truss. These cables carry this load from the bridge deck up to the catenary cable through tension. These vertical cables are able to carry load according to the cable cross sectional area and the tensile strength of the steel.

The catenary cables pick up the tensile forces in the vertical cables and carry the force up over the pylons and down to the anchors at either end of the bridge. The catenary cable acts in pure tension due to its catenary shape and is able to carry tensile load according to the cable cross sectional area and the tensile strength of the steel. The catenary cable is in fact made up of 27,572 galvanised steel cables which are grouped into 61 cable groups which are then bunched together to form the 0.92m diameter cable. These main cables are anchored at the abutments to keep them in tension and to pass the tensile load into the ground through the abutments.

The anchors at the abutments receive the load from the catenary cables and transfer the tensile force into the ground. The numerous cable bunches which make up the main cable are set into the concrete anchor blocks in a splayed out pattern to distribute the load throughout the anchor. The anchors resist the pulling tension in the anchors through their own self weight and through friction as they are embedded into the ground. The anchor blocks weigh approximately 54,400,000kg and contain approximately 4,400 tons of steel reinforcement (Golden Gate Bridge Research Library, May 2012).

The pylons support the catenary cables and locally support the bridge deck. The pylons are loaded in compression by the catenary cables as they keep the cables' catenary shape and carry part of the vertical component of the tensile force in the cable. The pylon is further placed into compression as it carries load from the deck itself at the pylon deck

intersection. Figure 3 shows this intersection and an estimation of the transfer of load from the deck and truss to the pylon.



Figure 3: Connection of deck and truss system to pylon

The pylons rest upon deep foundations which lie on bedrock below. The northern pylon rests on solid diabase or basalt rock which has a high bearing strength and is able to easily dissipate the load down into the ground. This northern foundation uses wall friction around the foundation periphery as well as end bearing of the foundation on the bedrock to dissipate load into the ground. (Sedgwick, A. E., 1931, February). The southern pylon rests on serpentine rock which consists of sedimentary formations of sandstone and clay. This southern foundation has a reduced bearing strength and is designed to dissipate load to the sounding ground through wall friction alone. (Sedgwick, A. E., 1931, February). As a result, this southern tower is embedded 34m deep. (Golden Gate Bridge Research Library, May 2012).

The Structural System Used to Resist Lateral Load

The major lateral loads acting on the bridge are wind and earthquake loads, although the action of earthquake loads are significantly more pertinent due to the bridge's proximity to the San Andreas Fault. Therefore, this section of the report will focus on the bridges capacity to resist lateral loads from earthquakes. After a 7.1 magnitude earthquake in 1989 the bridge has undergone a series of retrofitting for seismic activity. (Overview of Golden Gate Bridge Seismic Retrofit Construction Project, 2013, February) this process began with the retrofitting of the northern and southern approach spans, while the retrofitting of the main span remains incomplete. Therefore, in analysing the bridges capacity to resist earthquake loads, we will consider the bridge as it was at the time of the 1989 earthquake which the bridge withstood successfully.

Earthquakes act on the bridge through the foundations of the two pylons and the anchorages. (Ichiro Konishi & Yoshikazu Yamada, 1960) According to Ichiro Konishi & Yoshikazu Yamada (1960), the connection between the towers and bridge deck and the towers and cables are not a significant concern when considering the movement of the bridge under earthquake loads. It is suggested that the movement and subsequent forces acting in the bridge towers or pylons are of primary concern. These loads are primarily dependent on the dimensions and configuration of the pylons and the foundations on which they rest. This response of the bridge is dependent on the inertia and stiffness of the pylon system as well as the conditions and stiffness of the foundation system. (Ichiro Konishi & Yoshikazu Yamada, 1960). Therefore the primary system used to resist lateral load consists of the following:

- The two pylons which support the bridge deck and rest on the bedrock below. These towers are braced with 4 Cross beams above the deck and 4 diagonal members below the deck. These cross members connect the pylons and provide lateral stability. These cross members will act in tension and compression as the earthquake pushes and pulls the pylons on either side of the bridge deck
- The deep foundations resting on bedrock below the river, supporting the pylons acts of resist lateral load as they dissipate the lateral movement of the pylons back into the ground after earthquake has stopped.

LOADS

Dead Load

The dead loads acting on the structure were based entirely on self-weight as there are no significant loads that act on the structure in addition to its self-weight. The Strand7 model included the members' sizes and the material densities and thus the combination of the two allowed the mass of the structure to be determined. The input of gravitational acceleration allowed Strand7 to work out the dead loads on the structure and they were included in the analysis by specifying the acceleration due to gravity.

Live Loads

The live load applied to the structure was in accordance with AS5100.2 SM1600 Loading. An extract of the loading has been included in Figure 4.

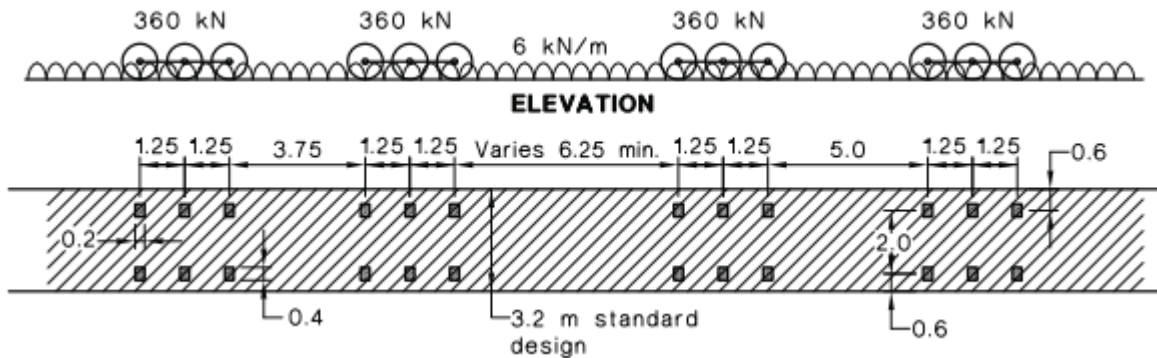


Figure 4: M1600 Traffic Loading AS5100.2

To simplify the computation, the live load was applied as a pressure load. The total load specified by AS5100.2 was added together and averaged as a pressure load over the road deck. Since there are 6 lanes of traffic this load was multiplied by six. Live loading is applied for the worst case. In light of this the bridge was assumed to be fully loaded with the worst case truck as specified in the above standard. On a global level this simplification provides almost no significant change in the results determined. Had there been more time allocated to the task and more computing power available the live loading would be calculated using the load path tool. The load path tool uses the loading taken from AS5110.2 and applies it over a lane. The load influencer solver is then used to work out the critical position for this loading case. This is performed by selecting primary members within the structure and calculating the worst case position for the traffic loading with respect to these elements. Once the load path and load influence tool have been used a position is determined with translates into a static load applied to the structure.

Static Wind Loads

The design wind speeds were determined by analysing wind speed data from the National Oceanic and Atmospheric Administration's National Climatic Data Centre (NCDC). The data gathered from the bridge as it exist today as well as the data gathered from a buoy just west of the bridge in the middle of the Golden Gate were analysed. The design wind speeds for the structure were also determined in accordance with the American Society of Civil Engineers, Minimum Design Loads for Buildings and Other Structures (ASCE 7-10) standard for a risk category IV structure. The two design wind speeds were compared and it was found that the ASCE 7-10 design wind speed matched well with the 500 year design wind speed derived from NCDC data. The ASCE 7-10 design wind speed was 115 mph (51.4 m/s). The design wind speed was multiplied by the width of the members and applied as a UDL to plate and beam members. For truss members the tributary lengths of the beams were found and an equivalent point load was applied to the nodes at the end of each truss member. Only lateral wind loads were considered from the westerly direction since it is the most critical. The westerly direction is the most exposed to winds coming in from the Pacific Ocean.

Dynamic Earthquake Loads

The bridge is located in a very active seismic region and thus it is important to use location specific earthquake spectra. The design spectrum of the applied earthquake was derived from the 2009 AASHTO Guide Specifications for LRFD Seismic Bridge Design for 37.815°N, 122.48°W. The soil of the site was identified as Site Class B – “Rock” and the highest importance category, IV was assigned to the structure. The spectrum for the site was derived from United States Geological Survey (USGS) data, the USGS design report may be found in the Appendices. The seismic load spectrum was applied to the structure as a base acceleration from the X-direction. That is, it was assumed that the earthquake ground accelerations would arrive from the East which is accurate given that the San Andreas runs North-South and is east of the bridge.

Dynamic Wind Loads

Wind loads present a significant risk to the structure given its long span and its exposure to relatively strong winds. Dynamic wind loads are a function of the aerodynamic interaction between the structure and the flow of air past the various structural elements. However, whilst an analysis of sufficiently detailed wind data (not available for the Golden Gate Bridge) can be used to determine the turbulence buffeting loads on the structure, the dynamic wind effects caused by the interaction between wind flow and the structure such as flutter, wake excitation etc. cannot be determined without wind tunnel testing or computational fluid dynamic modelling. Such loads are also beyond the scope of bridge and wind design codes which recommend “specialist advice” be sought. As a result of the lack of information in this regard, dynamic wind loads were not modelled in this analysis. The authors acknowledge that the wind loads are significant, but have chosen not to model these loads due to a lack of sufficient data

NUMERICAL ANALYSIS

Mesh and Mesh Quality

Plate elements were used to model the bridge deck while truss and beam elements were used to model the remainder of the bridge. Only the plate elements within the model required meshing as truss and beam elements do not require meshing. The mesh refinement of the bridge deck was governed by the node positions of the truss below the bridge deck as nodes of the deck had to align with the nodes of the truss supporting the deck. This resulted in relatively coarse mesh, however this did not impact on the analysis as the deck was not a critical component to be analysed in the model.

Element Types

Bridge Deck

The bridge deck was be modelled as a plate elements which had the properties of concrete. It was deemed that these plate elements would provide a suitable approximation of the actual reinforced concrete bridge deck system. The cross girders supporting the deck were modelled as beam elements. In reality these cross girders are I-beams with numerous web stiffeners along their length and as such may have be more accurately modelled using plate elements. However, it was determined that this modelling would not provide any additional helpful information on the bridge and would only serve to overcomplicate model. Therefore, modelling the cross girders as beam elements provided a sufficient level of accuracy.

Cross Girders

The cross girders are supported by a system of primary trusses, which in turn are made from smaller secondary trusses. The primary truss system was modelled using B2 beam elements with beam properties, while the secondary trusses which made up this primary truss were simplified to be square hollow sections (SHS) in the model. The dimensions of the rectangular hollow sections (RHS) used in the model were determined by finding a RHS section which had a similar second moment of area to the estimated second moment of area value of the truss members. It was assumed that this approximation would provide a sufficient representation of the real structure.

Pylons

The pylons and cross beams connecting the pylons were modelled using B2 beam elements.

Catenary and Vertical Cables

The Catenary cable was modelled using truss elements which spanned between nodes with coordinates that mimicked the catenary shape of the cable. These node coordinates were determined via both a theoretical analysis using catenary curve equations and through Strand7 modelling. Strand7 contains a function to determine the deflected shape of cables using B2 cable elements. The catenary cable was modelled separate to the main structure and by assigning the appropriate Cable Free Length the deflected shape of the cable was easily found. The node locations of the deflected cable was exported to a spreadsheet and the points were compared to the theoretical values. It was found that the theoretical values derived from the theoretical equations underestimated the amount of sag by a small amount. This was to be expected given that material strain is not taken into consideration by the catenary equations. The nodes were then imported into the final Strand7 model for the entire bridge. The nodes were then joined by B2 Truss elements.

The catenary was modelled with truss elements as this allowed for a string groups to be used at the point where the cables pass over the pylons. It should be noted that string groups can only be used with truss elements. This use of a string group was an important feature of the model as the string group allowed the cable to act as if it could slide over the top of the pylon. The sting group forces the tension to stay constant over the truss elements. This effect emulated the realistic cable attachment as found on the Golden Gate Bridge and ensured that the pylons where not excessively loaded by the catenary cables. The string group and trusses elements on either side of the pylon achieved this sliding effect by allowing the truss elements to lengthen and shorten concurrently on either side of the pylon. Truss elements were also used since Strand7 concentrates the mass of cable elements at the nodes when running an analysis whilst truss elements allow the mass to be distributed along the length of the cable.

The vertical cables were similarly modelled using truss elements, under static load cases in which they were under no compressive loads. However, under the earthquake loading scenario, cut-off bars with no compressive capacity were used since these elements may come under compressive loads under the dynamic action.

Material Properties

Concrete components were given the properties of AS3600 32MPa concrete. All steel elements were given the properties of structural steel. Young's moduli were not altered, however the yield strengths were. The yield strength of all cable elements were made to be 1100MPa, as previously mentioned. All other steel members were taken to have a yield strength of 300MPa, typical of the era.

Geometric

The geometric properties of all of the sections and members were measured from scaled photographs of the bridge. These geometric properties were then used to model the members themselves. The actual section dimensions were either replicated in the model, or, where the member configuration was very complex, the actual dimensions were used to find the dimensions of an equivalent member which was then used in the model to provide a simplification.

Nodal Constraints

The fixity at the base of the pylons was completely fixed in all directions of translation and rotation that is DX, DY, DZ as well as MX, MY, MZ were all fixed. This is similar to the real structure which has very deep foundations that do not allow any movement.

The fixity at the end of the bridge span, i.e. at the anchors, was the same as at the base of the pylons - DX, DY, DZ as well as MX, MY, MZ were all fixed. Again given that these are giant anchor blocks designed to prevent any movement it was sensibly assumed that these nodes would be fixed.

Solvers Used in the Analysis

Different solvers were used to analyse the bridge under differing load conditions. The stresses in the members of the bridge and deflections of the bridge under dead, live and wind loads were all found using a **Non-linear Static Solver with the non-linear geometry option**. This solver was used as it allows for the cables of the bridge to lengthen/move and increase in stiffness progressively as the tensile forces in the cables develop as the load is applied. A linear static solver was not used because it would produce skewed results as the linear static solver would not allow the cables to become fully loaded as they are in reality. This would result in incorrect member stresses and the deflections of the

bridge would greatly amplified. Non-linear materials were not used. Member sizes were adjusted to ensure that the stresses in the members were below the yield stress of steel and thus the need for non-linear materials were eliminated.

To determine the natural frequencies of the bridge a **Natural Frequency Solver** was used. In order to run this natural frequency solver the model was input with the mass of the structural elements and the acceleration due to gravity. This solver was required to solve up to 250 natural modes of the structure in order to get sufficient mass participation of the bridge. This large number of modes was required because the structure is so large and heavy.

Once the natural frequency modes of the structure were found, a **Spectral Response Solver** was run to determine the mass participation of the bridge and the deflection of the bridge when subject to an earthquake spectra. This analysis required the input of the earthquake spectra and scaling factors which were established using the American Association of State Highway and Transportation Officials (AASHTO) seismic code.

STRUCTURAL DESIGN

In Designing Structural Members for the Golden Gate bridge, the capacity of the members used to model the bridge have been checked against the loadings found to be acting on each respective member, given from the results file outputted by Strand7. The most critical area for each member has been identified as the area experiencing the most stress, moment or deflection (depending on what is being considered), and all members have been designed for this case. Prior to comparing a section's capacity to the max loading experienced, the sections yield stress has been factored by 90%, and the reduced strength has been used for redesign.

Cable Design

Design of Cable Members has been carried out by finding the maximum stress in each element type, and looking at the response of the selected member under these stresses. Members were then redesigned if they were found to be insufficient to carry the applied loading. The maximum stresses were considered by looking at the highest stress values for an element under all loading conditions, and then considering the max of these.

TABLE 3. Redesigned Cable Sizes

Member Type	Member Dimensions	Maximum Stress.	Redesigned Dimensions
Vertical Cables	0.3m Diameter	3.28×10^5 kPa.	0.172m Diameter
Main Cables	1.2m Diameter	1.14×10^6 kPa.	1.288m Diameter

Since the Cable elements are in Tension, the design of these is simply based on their tension yield capacity. As aforementioned the grade of steel used in the cables is 1100MPa. The maximum stress was divided by the area used in the model to find the maximum tensile loading on the element. This load was then used in conjunction with the yield stress to determine the required cross sectional area of the Cable.

Vertical Cables;

$$3.28 \times 10^5 \times \left(\pi \times \frac{0.3^2}{4} \right) = 23184.96 \text{ kN}$$

$$N^* = \phi \times f_y \times A$$

$$A = 23184.96 \div (0.9 \times 1100000)$$

$$A = 0.0234 \text{ m}^2 = \pi \times \frac{D^2}{4}$$

$$D = \sqrt{4 \times \frac{0.0234}{\pi}} = 0.172 \text{ m}$$

Main Cables;

$$1.14 \times 10^6 \times \left(\pi \times \frac{1.2^2}{4} \right) = 1289309.6 \text{ kN}$$

$$N^* = \phi \times f_y \times A$$

$$A = 1289309.6 \div (0.9 \times 1100000)$$

$$A = 1.302 \text{ m}^2 = \pi \times \frac{D^2}{4}$$

$$D = \sqrt{4 \times \frac{1.302}{\pi}} = 1.288m$$

After redesign of the members, the new dimensions indicate failure of the modelled main cable, but sufficient strength in the modelled vertical cables. It should be noted however that both of these dimensions are larger than that calculated to be on the structure in reality. The main cable has a diameter of 0.9m, and the verticals have a diameter of 0.126m, both of which prove to be insufficient in the loading applied by this model.

For elements governed by their flexural strength, the maximum bending moment was considered instead of the axial stress. These were the Pylons and part of the deck system. For the deck system, all members were considered separately and the maximum moment was considered in the members deemed to be experiencing flexural loading. Given the system is a truss, each member was also considered on the axial force acting through it. Similar calculations to above were carried out in the below spreadsheet.

Flexure was considered by looking at the maximum bending moment, and comparing that to a design bending moment based on a sections yield stress and section modulus. A sample hand calculation has been performed for the pylons, but was encoded into the spreadsheet below.

TABLE 4. Redesign of Truss Members based on Capacity

Truss Members										
Geometry				Loading	Capacity				% Cap	
Member	h	b	t	A	Max Load	F _y	φ	Factored Strength	A _{yield}	
Bot Cross Girder	2	2	0.2	1.44	24000	300000	0.9	270000	0.0889	6%
Top/ Bot Chords	2	2	0.2	1.44	288000	300000	0.9	270000	1.0667	74%
Diag Top/Bot Cross Bracing	1.2	0.5	0.05	0.16	15200	300000	0.9	270000	0.0563	35%
Side Cross Bracing	1	0.5	0.05	0.14	57000	300000	0.9	270000	0.2111	151%
Blue longitudinal	1.4	0.7	0.075	0.293	36400	300000	0.9	270000	0.1348	46%
Vert Side Bracing	1500UB1590			0.203	114000	300000	0.9	270000	0.4222	209%
Flexural Members										
Geometry				Loading	Capacity					
Member	I	y	A	Z	Max BM	F _y	φ	Factored Strength	Z _{yield}	
Top Cross Girder	0.3277	1.25	0.465	0.2621	19000	300000	0.9	270000	0.0704	27%
Top/ Bot Chords	0.7872	1	1.44	0.7872	738800	300000	0.9	270000	2.7363	348%
Bot Cross Girder	0.0276	0.6	0.16	0.0460	1422	300000	0.9	270000	0.0053	11%

Table 4 shows the geometric properties, as entered into the model, as well as the calculated required capacity of the section to withstand yield under maximum loading. Looking at the required capacity returns a new value for the geometric property considered. This property is then compared with that inputted into the model. In the value for the % Capacity column, it can be seen which members have sufficient capacity and which do not. For Values <100%, the

proportion given describes the proportion of the area used in modelling, actually required to resist the applied loading. For sections with % cap >100%, the section has yielded and so an increase in section size is required. For the Truss members, this means scaling the area by the proportion given. For the Flexural Members a new member should be selected such that the section modulus is sufficient to withstand applied moments.

Pylon Design

The pylons were initially modelled as solid beams 16m by 10m. It is assumed that the bridge pylons are actually hollow steel members, but due to a lack of technical drawings of the structure the above solid dimensions have been used in the model. To check the validity of this assumption the following simple calculations have been conducted to quantify the area necessary to withstand loading.

The first case that was considered was bending. An I value for the section was determined at the stress at the outermost fibre determined.

Bending

$$I = \frac{bh^3}{12}$$

$$I = \frac{10000 * 16000^3}{12} = 3.4133 * 10^{15} \text{ mm}^4$$

$$M_{Max} = 6.22 * 10^6 \text{ kNm} = 6.22 * 10^{12} \text{ Nmm}$$

$$f = \frac{My}{I} = \frac{6.22 * 10^{12} * 8000}{3.413 * 10^{15}} = 14.6 \text{ MPa}$$

Compression

Following the flexural calculation axial compression was considered in the member. The maximum design stress was determined from the Strand7 model.

$$N^* = 5.08 * 10^6 \text{ kN}$$

$$f_y = 300 \text{ MPa}$$

It is assumed that given the sheer size of the pylon that it does buckle and therefore has complete section capacity.

$$\phi N_c = 0.9 * 300 * 16000 * 10000 = 43.2 * 10^6 \text{ kN}$$

∴ Sufficient Axial Capacity

Redesign

$$A_{new} = \frac{5.08 * 10^6}{0.9 * 300} = 18814814 \text{ mm}^2$$

Proposed Dimensions 7000mm x 2687mm

$$f = \frac{6.22 * 10^{12} * 3500}{\frac{2687 * 7000^3}{12}} = 283 \text{ MPa}$$

∴ The new proposed dimension has sufficient capacity

Considering both axial compression and flexure it was found that axial compression induced the most critical stress in the pylon. It was also determined that the area of the pylon could be reduced by approximately 88% and still satisfy a stress lower than the yield stress of 300MPa. This confirms the assumption that the pylon is in fact hollow.

RESULTS

Vertical Deflection along bridge Centreline

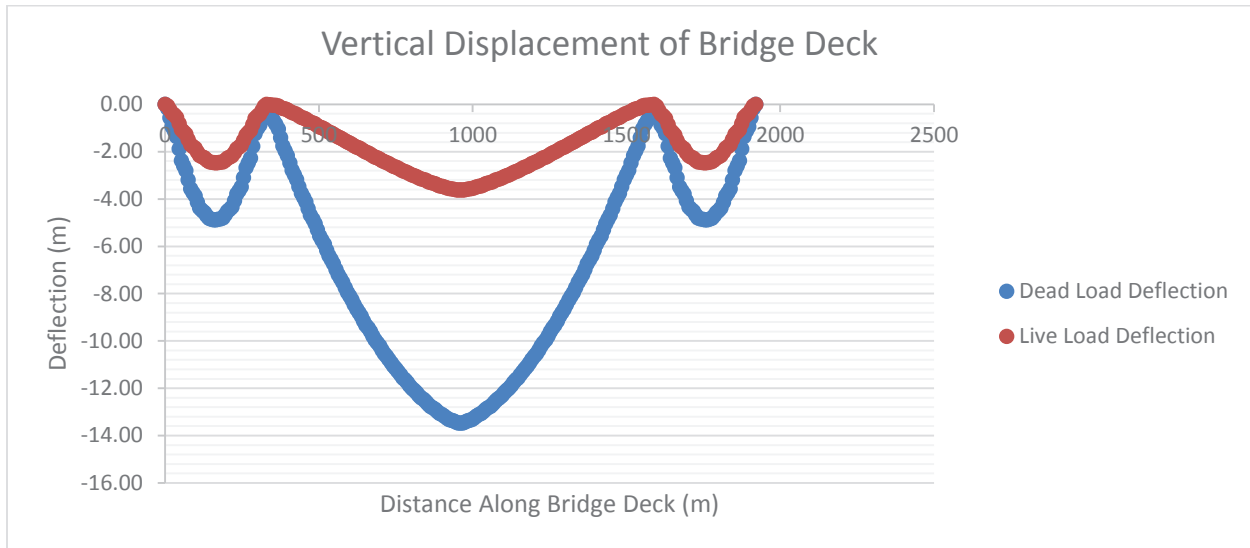


Figure 5: Vertical Deflection along bridge centreline

The bridge was initially constructed with a negative concavity or camber. This upward camber was built into the bridge such that the deflection of the deck under its own dead load would bring the bridge to a relatively 'level' or 'horizontal' position. The bridge camber during construction is shown in the photograph in Figure 6. The model was not able to account for this pre cambering of the bridge deck because the complex nature of the cambered construction meant that modelling it would have been unrealistic. Therefore, it has been assumed that the deflections due to dead load, as shown in figure 5, will have been taken up in the pre camber of the bridge and would act to return the bridge to a neutral flat position. Therefore the dead loads need not be considered when looking at the serviceability deflections of the bridge under serviceability loads.

Having accounted for the dead load by assuming it will return the cambered bridge to a neutral horizontal position, only the live load and wind load need to be considered when looking at the serviceability deflections. The serviceability load case for live load applied to the bridge was 1.0 time live load. Under this serviceability live loading the largest vertical deflections were 3.6m at the midspan of the bridge. This deflection under the live serviceability load corresponds to the maximum deflections expected for the actual golden gate bridge structure which is estimated to be 3.3m (Golden Gate Bridge Research Library, May 2012). We conclude from this that the deflection under live load falls within the serviceable limits.

The vertical deflection under wind load has not been included in the graph because the vertical deflection due to wind is comparable to the deflection under live and dead load alone. This is because of the large restoring or inertial action of the bridge dead load itself which acts against the wind load and the deflections due to wind. Therefore, it is concluded that the deflection due to wind do not governing the serviceability requirements of the bridge.



Figure 6: Golden Gate Bridge under construction showing

Lateral Deflection along bridge Centreline

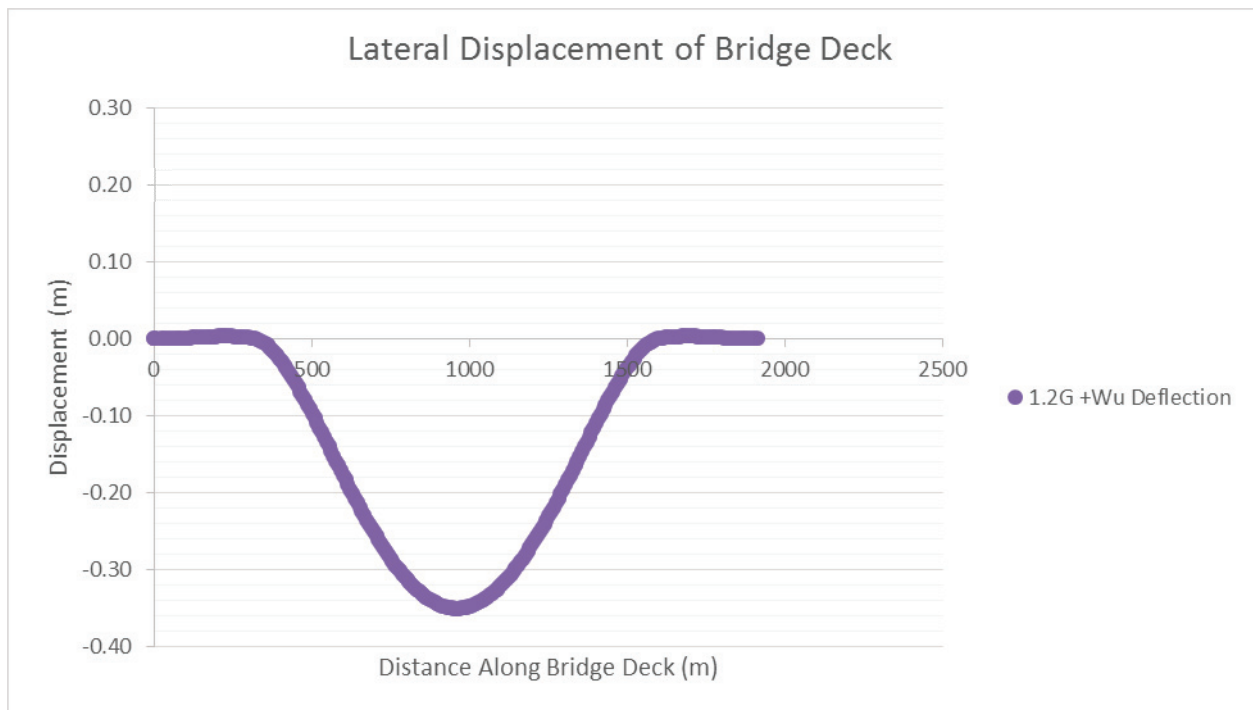


Figure 7: Lateral Displacement of Bridge Deck

Limited deflections were observed laterally in the bridge deck. A maximum displacement of 0.35m was observed under the load combination including wind actions. This deflection may be small due to the solver used. The load combination including wind action was run with the non-linear static solver, and this doesn't enable loadings to be run excluding the gravity load. As such, the wind was not able to be considered independently. As a result of this, the bridge's own weight applies a restorative moment to that felt by the wind in the lateral loading. The bridge's inertia stops the bridge from deflecting as much as would have been observed if this load had been considered independently. Since the bridge's weight is obviously effective in reality, the situation emulated is in nature, more accurate than considering wind alone, with the downside being wind's effects not being able to be accurately quantified as its own entity.

Vertical Deflection and Longitudinal Stresses at the Bridge Midspan

As expected when compared to the main span the differential deflection transversely across the bridge deck is minimal. Most notably the deflection graph for wind load involves a twisting of the bridge deck as seen in Figure 8. As restraint from the cables is only applied one way in the vertical direction the bridge twists under the load. This twist is further accentuated given that the graph is taken at the bridge midspan far away from the support provided from the pylons. Twisting is observed to occur about the centre node of the bridge deck given that this node undergoes minimal displacement between the dead and wind load case.

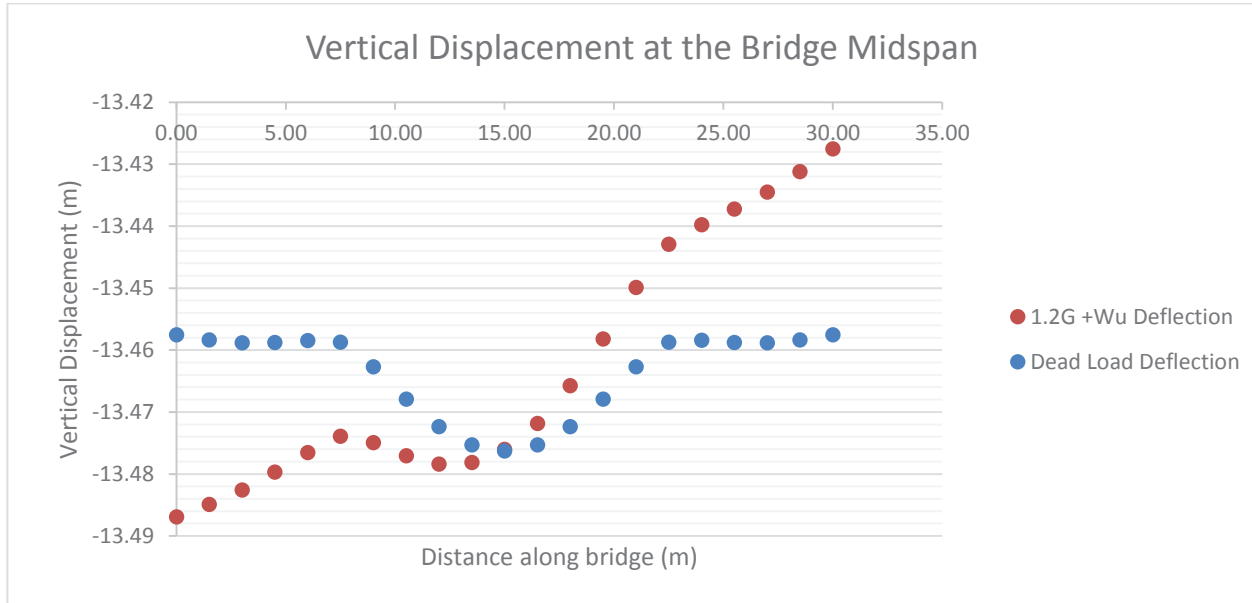


Figure 8: Vertical Displacement at the Bridge Midspan under Dead and Wind Load

Longitudinal Stresses along the Bridge Centreline

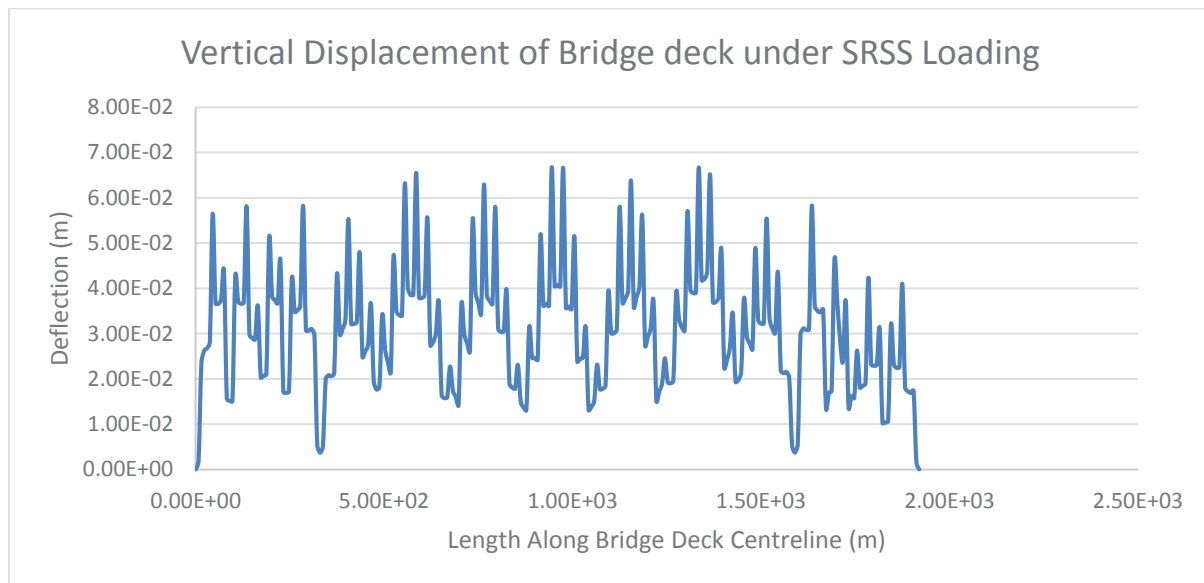


Figure 9: Vertical Displacement of Bridge deck under SRSS Loading

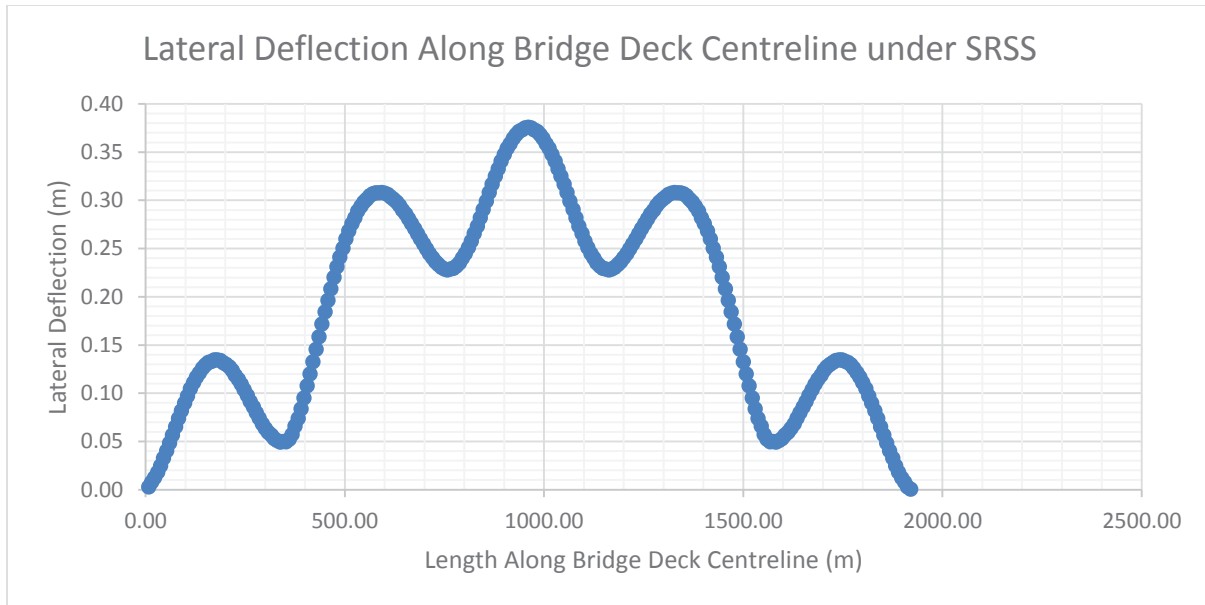


Figure 10: Lateral Deflection along Bridge Deck Centreline under SRSS

Only a small amount of deflections were observed under the earthquake case, both vertically and laterally which can be seen in Figures 9 & 10. Due to the very low natural frequency of the structure (given its substantial size and weight), compared with the very high natural frequency of the applied earthquake, very minimal engagement is observed. Many modes had to be considered to get any meaningful mass participation, to support this phenomenon. Observing the graphs above it can be seen that the deflection laterally in the bridge deck under earthquake loading are of a higher magnitude than the vertical deflections.

Validation of stresses in elements found using Strand7 through hand calculations

With the aim to rationalise the results produced by Strand7 and to verify the validity of the model a series of hand calculations have been provided as below. The various members considered in this section will be considered under the 1.2G+1.8Q load combination as this was the governing load combination.

Cross Girders

Forces acting in a cross girder due to the load combination 1.2G+1.8Q

The cross girders are assumed to be simply supported by the truss system and spanning 30m

$$G = \text{Selfweight of concrete deck} = 1.1 \times 0.5m \times 25kN/m^3 = 15kPa$$

$$Q = \text{Traffic load according to SM1600} = 1.8 \times 10.16kPa = 18.3$$

$$\text{Tributary width of cross girder} = 7.5m$$

$$\text{UDL acting on cross girder} = 7.5 \times (15 + 18.3) = 249.75 \frac{kN}{m}$$

$$M^* = \text{design bending moment} = \frac{249.75 \times 30^2}{8} = 28,097 \text{ kNm}$$

This design bending moment found through simple hand calculation is of a similar magnitude to that which was determined from Strand7, 19000kNm. The difference observed is likely due to the differing support condition used in the model and in the hand calculations. The hand calculations assume that the cross girder is simply supported and thus there is not moment at the connections. In comparison in the model moment is carried through the connections to the vertical members. The transfer of moment through the connection lowers the maximum moment in the section.

Vertical Cables

Load acting on Vertical Cable due to Load combination 1.2G+1.8Q

$N^* = 1.2 \times \text{Concrete Deck Self Weight}$

$$\text{selfweight of concrete deck} = 0.5m \times 25kN/m^3 \times 1.2 = 15kPa$$

TABLE 5. Self-weight of Structural Members

Element	Cross Sectional Area (mm ²)	Length (mm)	Volume (mm ³)	Unit Weight (kg/m)	No.	Weight (kN)
Green Cross Girder		30000		3650	3	3222.585
Red Cross Girder	760000	30000	22800000000		3	1755.7938
Blue Top and Bottom Chords	760000	15000	11400000000		4	877.8969
Yellow Cross Bracing	82500	42426	3500145000		1	269.5409162
Green Cross Bracing	27500	10607	291692500		2	22.46280189
Blue Main Girders	151875	15000	2278125000		2	175.4349891
Pink Vertical Members		7500		1590	2	23.85
					Weight	6347.564407

Pressure load is equal to:

$$\frac{6347.56}{30 * 30} = 7.05kPa$$

$$\text{Tributary width of vertical cables} = 15m$$

As calculated traffic load is equal to:

$$Q = 10.416kPa$$

$$N * (\text{self weight of concrete deck} + 1.1 * \text{Selfweight of Truss system}) \times 30 * 15 + 1.8 * Q * 15 * 30$$

$$N = (15 + 1.1 * 7.06) \times 30 * 15 + 1.8 * 10.416 * 30 * 15 = 18682kN$$

This is then divided by two as there is one cable on each side of the bridge.

$$N^* = 5131.72 * 0.9 = 8407kN \text{ per cable}$$

The actual load felt by the vertical cables modelled in Strand7 is around 23000kN. The difference is likely to be caused by the distribution of load into each of the cables. Under a non- linear analysis the deflected shape changes the stresses felt by each element.

CONCLUSIONS

In summary, the Golden Gate Bridge has been modelled to emulate the various loading conditions imposed on it in reality. The bridge's weight is evidently extremely substantial, given its large size and span. For a bridge of this magnitude to span the distance it does, massive structural members need to be utilised, which then add to the structures weight. Even when compared with scaled up, worst case traffic loads, design wind loads and dynamic earthquake loading, the self-weight of the structure alone was the biggest contributing factor to stresses and deflections observed in the bridge.

The initial model using the structures real dimensions was insufficient to carry the loadings applied. Therefore, every member was increased in size to allow the model to run. Ultimately, this led to the review of structural member sizing, by checking them against the maximum stresses and moment applied, and suggesting their geometrical properties for efficient and sufficient capacity against yield. Some members were found to be loaded at 3.5 times their yield stress, while others as little as 5%. This suggests some inconsistencies in the way loads are transferred through our model – either in the modelling phase (and member sizes) or the way the bridge has been loaded.

Due to simplifications made, as well as assumptions about the process of construction, some of the data for stress and deflection does not accurately represent the magnitude of that felt by the structure in reality. However, the trends observed, and critical sections identified do appropriately match what is to be expected in reality. In future, a dynamic analysis of the wind loading would greatly improve the confidence had in the results, given that gusts are a large issue in the geographic location, however due to the complex nature of this analysis they have been neglected by this modelling exercise.

REFERENCES

Golden Gate Bridge Research Library, (May 2012), Date Retrieved: 1 June 2016, Retrieved from: <http://goldengatebridge.org/research/>

Longworth, L., Loeterman, B., (2004) General Article: Spinning the Cables, Date Retrieved: 1 June 2016, Retrieved from: <http://www.pbs.org/wgbh/americanexperience/features/general-article/goldengate-spinning/>

Ichiro Konishi & Yoshikazu Yamada, (1960), Studies on the earthquake resistant design of suspension bridge tower and pier systems, II WCEE, Vol.2, pp. 107-118

Overview of Golden Gate Bridge Seismic Retrofit Construction Project, (2013, February) date retrieved 24.05.2016, retrieved from: <http://goldengatebridge.org/projects/retrofit.php>

Sedgwick, A. E., (1931, February), Foundations of the Golden Gate Bridge, date retrieved 24.05.2016, retrieved from: http://goldengatebridge.org/research/documents/Foundations_of_the_GGB_AESedgwick_1931Feb.pdf

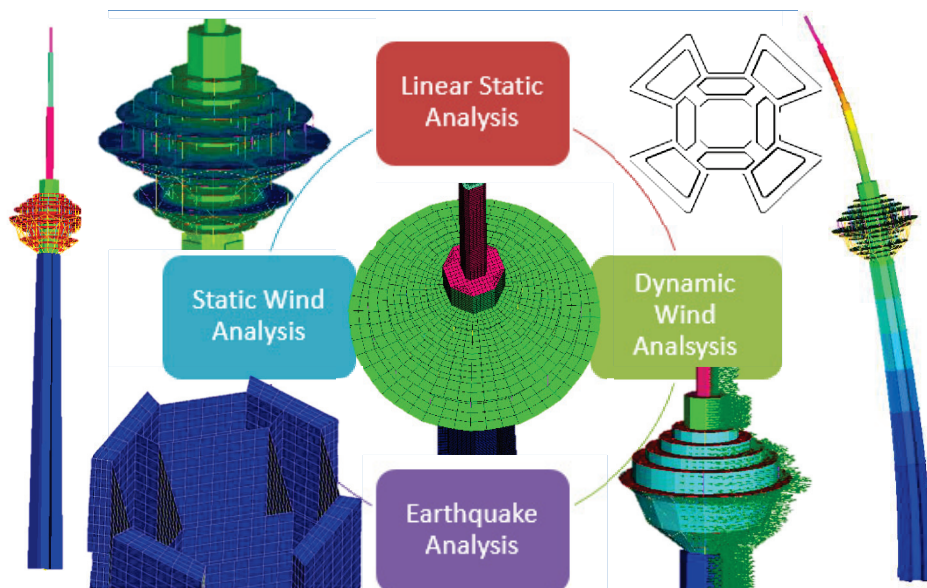
Dynamic Analysis Of The Milad Tower

Edwin Wilhelm, Mitchell Ford, Darren Coelho, Lachlan Lawler, Peter Ansourian, Fernando Alonso-Marroquin, and Faham Tahmasebinia^{a)}

School of Civil Engineering, The University of Sydney, Sydney NSW 2006, Australia

^{a)}*Corresponding email: faham.tahmasebinia@sydney.edu.au*

Abstract. This report involves the modelling of the Milad Tower using the finite element analysis program Strand7. A dynamic analysis was performed on the structure in order to understand the deflections and stresses as a result of earthquake and wind loading. In particular, Linear Static as well as Natural Frequency and Spectral Response solvers were used to determine the behaviour of the structure under loading. The findings of the report highlight that the structure was modelled accurately with the outputs representing realistic values. The report suggests that the design of the beams, columns, slabs and all structural members was sufficient enough to support the tower during maximum loading cases. The governing load case was earthquake loading.



INTRODUCTION

The Milad tower is a multipurpose tower located in Tehran, Iran. Since Tehran is located close to two tectonic plate fault lines, seismic behaviour is of particular interest. The Milad Tower is the 6th tallest tower in the world, at 436 metres high and is also the 4th tallest telecommunications tower. The tower includes many stories of shops and restaurants as well as being used for telecommunications, with highly sensitive equipment.

The tower, as shown by the photo of the tower in Fig 1, is made up of five main components; the antenna mast, the head structure, the concrete tower shaft, the lobby and the foundation. The antenna mast is a slender concrete section that stretches over 100m, composed of four different sections. The head structure sits around the main concrete shaft and makes up a 12 storey structure. This structure is a space basket and consists of radial and peripheral beams and columns. The radial and peripheral beams transfers the loads directly to the columns. The loads from the columns are transferred directly to the steel basket and then to the concrete shaft.

The concrete shaft carries most of the gravitational and lateral loads of the structure. It is 315 metres high and consists of four main tapered trapezoidal walls and two octagonal shapes connected by several walls. The octagons are post tensioned in order to increase the bending capacity and stiffness of the structure to reduce the deflections. The foundation and lobby area consists of a circular foundation which is a transition structure (Yahyai et al. 2009). The circular mat foundation is approximately 66 metres in diameter and sits directly beneath the transition structure. The transition structure is a pyramid shape and is made up of a central core, inclined walls and triangular-shaped walls. The structure is also post-tensioned in order resist the high stresses and punching shear that the foundation will experience.

The Milad Tower was proposed as part of the ‘Shahestan Pahlavi’ project, which was planned to encompass five million square metres, accommodating 50,000 residents, government ministries, commercial offices and a variety of cultural centers (libraries and museums). However this project was cancelled following the 1979 Revolution. The tower was brought back and construction began in 1997, taking 11 years to complete (2008). The structure is multipurpose, consisting of 63 trade units, many food courts, observation decks, telecommunication services and a carpark of 27,000 m².

TABLE 1. Structure Details



FIGURE 1. The Milad Tower in Tehran

Location: Tehran, Iran
Architects: Mohammad Reza Hafezi
Structural Engineers: Mohammad Reza Hafezi
Function: Shops, Restaurants, Hotel and Conferences, telecommunications tower
The Year of Built: 2009
Approximate Cost: \$5 billion
Overall Height: 436m
Floor Area: approximately 154,000m ²
The Structure of the Plan: Space structure around the concrete core.
Number of Floors: 145 floors above ground, a 6 storey lobby and 12 levels in the head structure

STRUCTURAL MEMBERS

Below is the description of the members of the structure:

- Floor system: Concrete slab (220mm deep with N16 bars at 300mm centres) sitting on steel beams, acting compositely (the slab provides lateral restraint to the top flanges of the beams).
- Beams: Steel beams (460UB82.1) are in the space truss and extended radially from the core, the beam span is 10m at the perimeter and 5m at the core.
- Columns: Steel columns (350WC158) are in the space truss and the largest column spacing is 10m at the perimeter. The column spacing closer to the core is 5m. Floor to floor height is 4m.
- Core: The core is 40MPa concrete and consists of four main tapered trapezoidal walls and two octagonal shapes connected by several walls, as shown by Fig. 1. The octagons are post tensioned in order to increase the bending capacity and stiffness of the structure to reduce the deflections, in particular for the wind loading.
- Foundation: The foundation design was outside the scope of this project and the boundary conditions. For this reason, the substructure and associated structure at the base of the tower have not been analyzed. The bottom of the tower is fully fixed to prevent translational and rotational movement. This aims to provide a similar representation of the foundation in real life.

Table 2 shows the Structural elements of the tower and the comparison between the suggested members from the Australian Design Codes and the members chosen for the design.

TABLE 2. Structural Elements for the Head Structure

Details of the Structural Elements	Suggested Structural Element Sizes	Suggested Standard Designs (e.g. AS3600, AS4100)
Head structure columns	350WC230	310UC158
Head structure beams	460UB82.1	460UB82.1
Slabs	40MPa 220mm deep	210mm
Foundation	40MPa 1.5m thick	1.25m
Core Shaft	40MPa 1.5m thick	1.25m
Spire	40MPa 0.5m thick tapered	1.25m
Steel Basket	400WC270	500WC440

STRUCTURAL SYSTEM

Figure 2 shows the key plan of the core of the structure at ground level. The central concrete core extends through the entire structure. The hollow concrete structure has a large amount of area away from the centroid and thus has a large second moment of area, which contributes greatly to increasing the stiffness for lateral loading. The core has varying degrees of post-tensioning, depending on the height, which increases the bending capacity of the structure as well as the stiffness. By increasing the stiffness of the structure, the mast will also deflect less.

The lateral loads from wind that act on the concrete core will place one side of the structure in tension and the other in compression. The post-tensioning within the structure will aid in resisting the tensile forces in the concrete and reduce potential cracking. The tower can be treated as a cantilevered beam structure, where lateral loading will induce a bending moment through the system. This bending moment will travel through the structure and into the foundation. The design of the foundation is outside the scope of this analysis and it is assumed that the base of the structures acts as a fixed support.

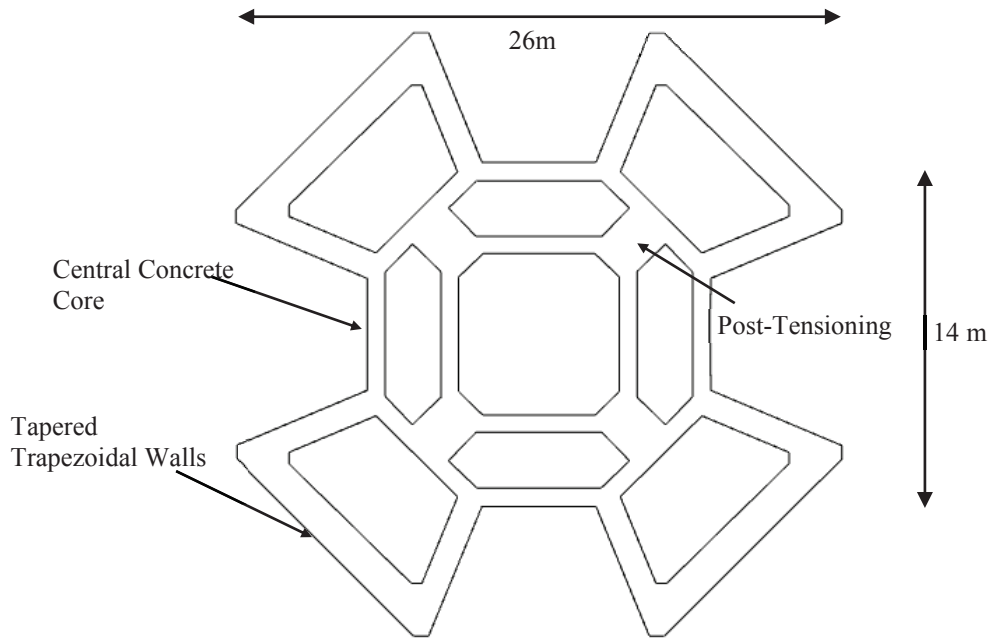


FIGURE 2. Plan section of the concrete core of the tower at ground level

The main components of the head structure are the radial and peripheral beams, columns, space basket and concrete shaft, this can be seen in Fig. 3. Figure 3a shows an isometric view of the head structure, which includes the 12 floors of restaurants and shops. Figure 3b shows a cross section of the head structure and the critical structural members, namely the slabs, steel space basket, radial beams and the peripheral beams and the core shaft. The structure firstly transfers loads to both the radial and peripheral beams. The radial beams are between columns or between the columns and the concrete shaft, working to transfer the loads from the slab to the columns or to the shaft. The peripheral beams are on the perimeter of the structure and work to transfer the loads to the columns. The columns will transfer the loads through columns or to the space basket, which is finally transmitted to the concrete shaft. Figure 4 shows a plan view of level 7 of the head structure, which is the biggest floor. As shown by the layout, the I-beam columns are orientated outwards to ensure the major axis bending is in the radial direction. This is done to increase the stiffness and reduce deflections in the radial direction. However, the members for the columns are steel welded columns, which are also quite stiff in minor axis bending, meaning that the capacity is also quite high in the minor direction. The layout for each of the other floors is very similar to the level 7 layout shown in Fig. 4.

The beams and columns were designed in accordance with Australian Design Codes to be 460UB82.1 and 310UC158 respectively and the concrete slabs were initially designed to be at a depth of 210 mm. The members had been designed in accordance with strength and the members were put into the Strand7 model and the linear static analyses were performed. It was found that the deflections of the members were too great as they were exceeding design deflection limits hence the members were changed to 460UB82.1 and 350WC230 for beams and columns respectively and 220 mm slab depth. This member choice is shown in Table 1 and discussed further in the results section. Figure 5a. shows an elevation of the structure, with a total height of 436m, which highlights the slenderness of the tower and hence the sensitivity to lateral loading. Figure 5b. shows a typical detail of the slab to beam connection for the floors of the head structure. It should be noted that full lateral restraint is provided to the top flange of the beam, which reduces the tendency of the beam to flexurally torsionally buckle, when the top flange is in compression. This is the case for most of the beams on the floors. However, at the same time, when the beams are cantilevered (such as at the outer edge of each floor), the bottom flange will be in compression. Therefore, the slab will provide no restraint to prevent the torsional buckling mode. Therefore, a deep UB section was chosen to provide sufficient bending capacity.

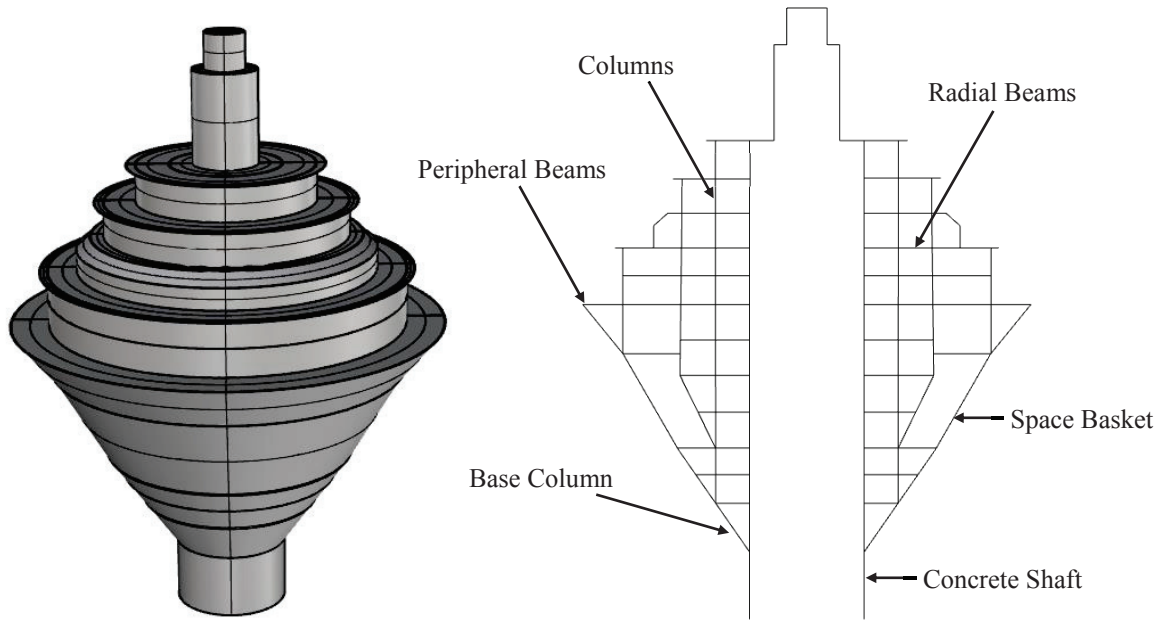


FIGURE 3. a) Isometric view of head structure b) Head structure elevation

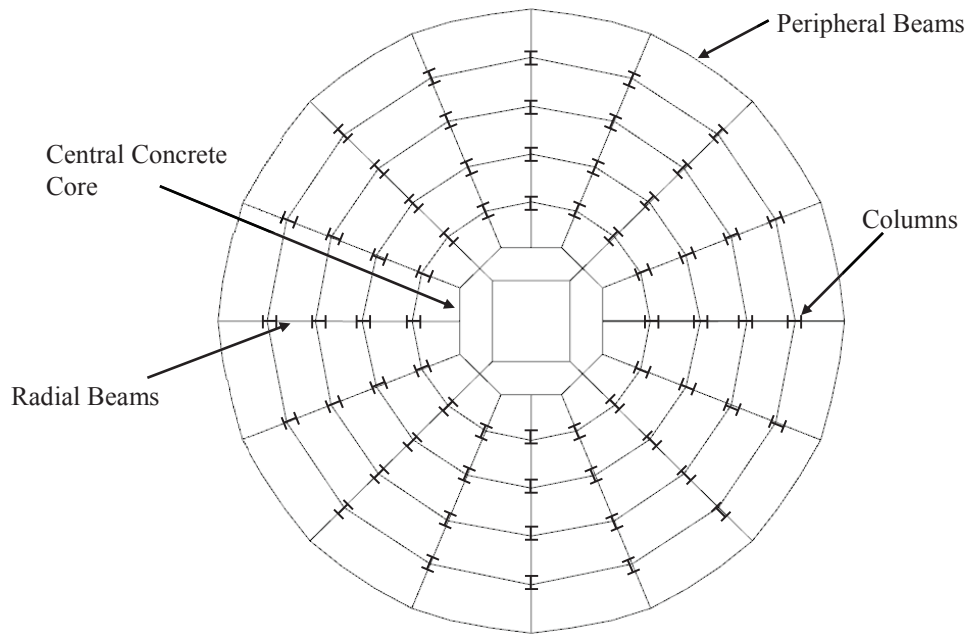


FIGURE 4. Typical plan view of the head structure

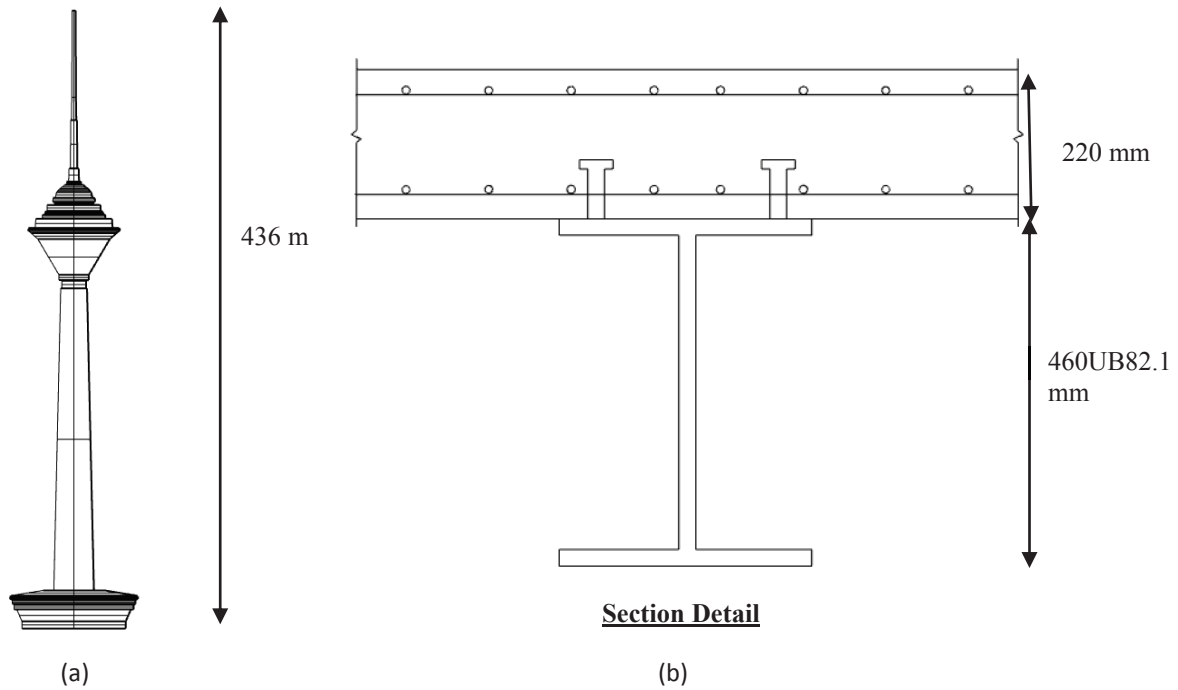


FIGURE 5. (a) Elevation of the structure, (b) Typical beam and slab section connection detail

LOADS

The following describes the methodologies involved to determine the different loads which would be imposed on the structure to run in Strand7.

The Dead Load of the Floor

The dead weight of the floor was calculated over the 12 floors of the head structure. The slab depth was 220mm thick. And an additional dead load of 1kPa to account for services and furnishing was also added. Thus, the dead load of the floor is:

$$P = 0.22 \times 25 + 1 = 6.5 \text{ kPa} \quad (1)$$

The Dead Weight of the Beams and Columns

The dead weight for the beams were calculated by finding the mass per metre of both the columns and beams (provided by the One Steel Manufacturing Catalogue). The weight was found multiplying the mass per length by gravity. The beam chosen was a 460UB82.1 which has a mass per metre as 82.1kg/m:

$$W_{\text{beams}} = \frac{\text{mass}}{\text{length}} \times g = 82.1 \times 9.81 = 0.81 \text{ kN/m} \quad (2)$$

Similarly, the columns are calculated using a 350WC230 section, which has a mass per metre of 158kg/m.

$$W_{columns} = \frac{mass}{length} \times g = 230 \times 9.81 = 2.26kN/m \quad (3)$$

The Live Load on the Floor

The live load was found from AS1170.1 (2007) to be 2kPa for restaurants. Therefore,

$$Q = 2kPa \quad (4)$$

The Maximum Design Load on the Floor

The maximum design load for the floor can be found using the load combinations in AS/NZS1170.0. The worst case was given by a combination of the pressure from the floor and live load as well as the dead load from the beams and columns.

$$Pressure = 1.2G + 1.5Q = 1.2(6.5) + 1.5(2) = 10.8kPa \quad (5)$$

$$Line.Load = 1.2(0.81 + 2.26) = 3.68kN/m \quad (6)$$

Wind Loading on the Tower

The wind load was applied as a pressure to the plates on one side of the building. The velocity profile, varying with height was found in accordance with AS/NZS1170.2 (2011). The terrain category was taken to be 2 as Tehran's skyline is similar to the profile described by TC2. The velocity of the wind flow was established from the mathematical expressions developed from the Deaves and Harris model (D&H Model, 1978). This model is based on full scale data and the mean velocity flow profile in strong winds and is derived using the logarithmic law. Equation 7 below can be found in the supplementary document for AS/NZS1170.2

$$V_z \approx \frac{u^*}{0.4} \left[\log_e \left(\frac{z}{z_0} \right) + 5.75 \left(\frac{z}{z_g} \right) - 1.88 \left(\frac{z}{z_g} \right)^2 - 1.33 \left(\frac{z}{z_g} \right)^3 + 0.25 \left(\frac{z}{z_g} \right)^4 \right] \quad (7)$$

Where the mean velocity is based on a mean gradient wind speed of 50 m/s. \bar{V}_z is the design hourly wind speed at height z , u^* is the friction velocity which is a non-dimensional measure of the surface shear stress, z_0 is the roughness length and z_g is the gradient height which are experimentally found parameters which vary with the terrain category. Once the mean velocity has been found, it is used to find the gust wind speed which is given by Eq. 8.

$$V = \bar{V}_z \left[1 + 3.7 \left(\frac{\sigma_v}{\bar{V}_z} \right) \right] \quad (8)$$

Where σ_v is the fluctuating wind speed (standard deviation) of the flow and is given by Eq. 9.

$$\sigma_v = 2.63\eta u^* \left[0.538 + 0.09 \log_e \left(\frac{z}{z_0} \right) \right]^{\eta^{16}} \quad (9)$$

Where η is defined by Eq. 10 below.

$$\eta = 1.0 - \left(\frac{z}{z_g} \right) \quad (10)$$

The velocity profile was then converted to a pressure using Eq. 11 found in AS/NZS1170.2.

$$P = \frac{1}{2} V_{des}^2 C_{fig} C_{dyn} \quad (11)$$

C_{fig} was taken as 0.7 (for a cylindrical cross section) and C_{dyn} was taken as 1. The velocity and pressure profiles are shown below in Fig. 6a and 6b.

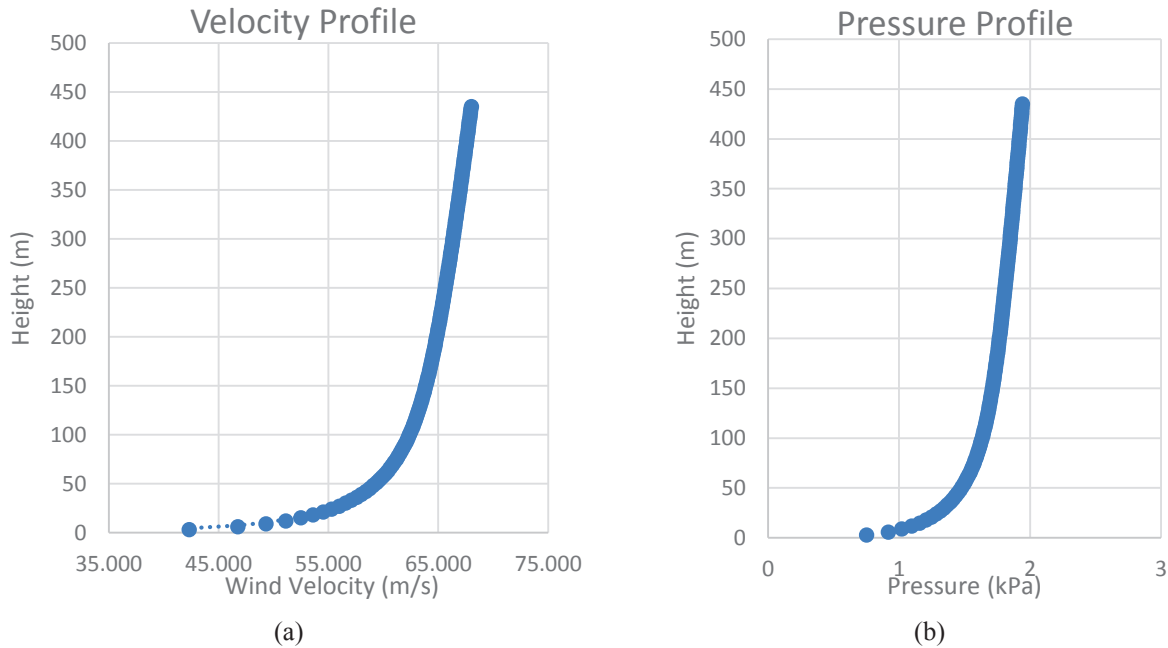


FIGURE 6. (a) Wind velocity profile (b) Pressure profiles acting on the structure

It can be seen in Fig. 6b that the pressure profile cannot be accurately modelled by a single straight line equation. Therefore, the curve was separated into four separate approximate linear sections. The pressure equations were applied to the model in Strand7 as plate loads in the global horizontal direction varying with height z . To increase accuracy, the head structure was modelled with 30mm glass panels which the load was applied to.

Earthquake loads on the fixities of the building

The earthquake loads were applied by first conducting the natural frequency analysis to determine the natural vibrations of the building. The natural frequency analysis was run for 20 modes, 17 of which were converged. From this, a load factor vs. period table taken from AS/NZS1170.4 for soil class C, as discussed in the earthquake analysis section.

Load Paths

The floor loading is transmitted through the slab to the beams, which is then transferred to the columns. The load then moves down to either the space basket, or the columns below which is transferred to the concrete core shaft, which is finally taken to the foundation. This can be seen in red in Fig. 7. The wind loading acting on the structure will act on the glass panels which will be transmitted to the beams and columns. The loads will then move through the beams, columns and space basket until it reaches the concrete core, which transmits the loads to the foundation. The wind acting on one panel can be seen in Fig. 7 in blue, this shows how the load moves through the structure when acting at that particular level.

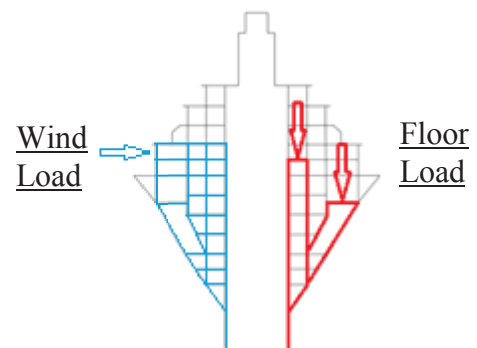


FIGURE 7. Wind and gravity load paths through the structure

NUMERICAL ANALYSIS

The model was created by modelling one quarter of the tower and then mirroring it about the vertical axis to create the full model. The first section was to model the concrete core, shown by the yellow plates in Fig. 8a. Using the cylindrical coordinate system, the nodes of the concrete shaft were input and connected with beam2 elements. The beams were extruded up a height of 250m, the height at which the head structure begins, creating plates members (plate members will be subdivided later to create square mesh).

The core shaft for the head structure, shown as the green plates below in Fig. 8a was modelled. The nodes for the coordinates of the first floor were drawn. These nodes were linked with beam2 elements, shown in red in Fig. 8a. Quad4 plate elements were drawn between the beams. The plates and beams for the first floor were subdivided to create squarish elements which can be seen in Fig. 8b. It is to be noted to ensure that the nodes for the beams and the plates line up, to guarantee that the mesh is compatible. The columns are modelled by extruding the according nodes upwards by a height of 4m. Lastly, the nodes on the outermost part of the floor were adjusted to an absolute radial value. Therefore, a curvilinear approach to the mesh was utilized. The final mesh for the first floor is shown by Fig. 8b for one quarter of the building.

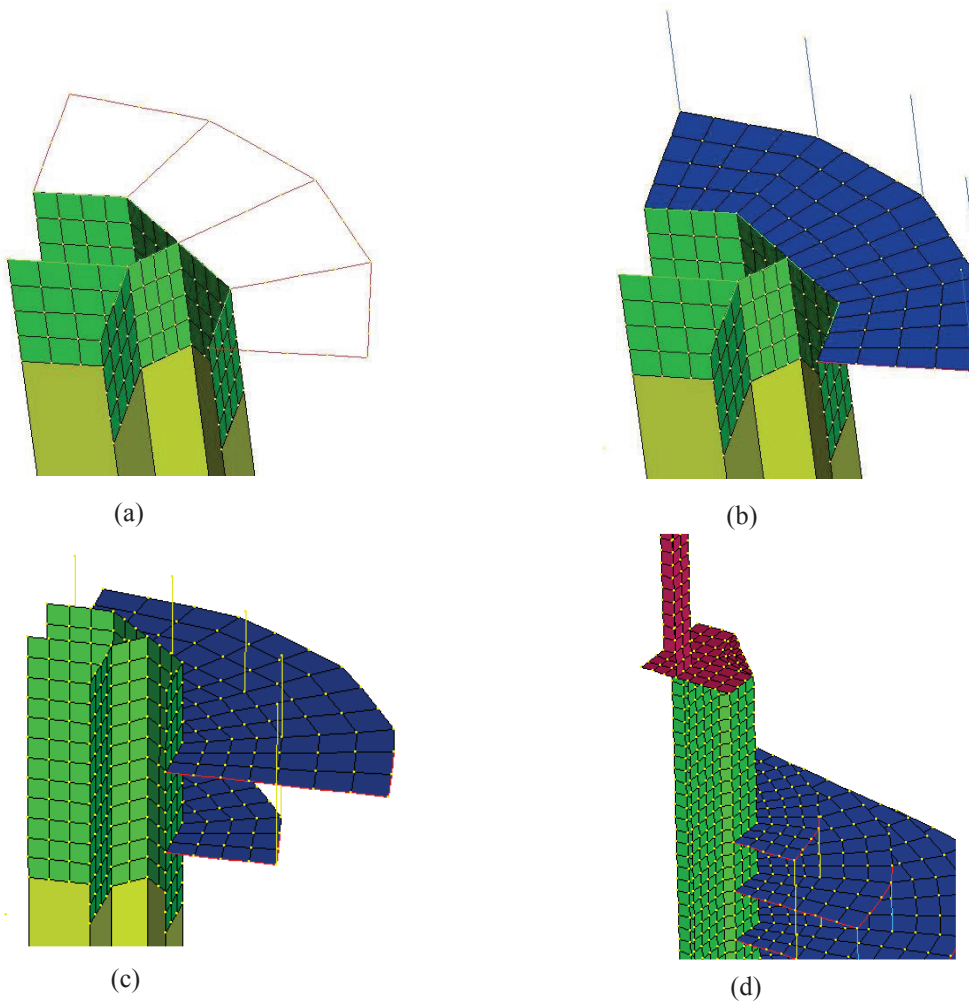


FIGURE 8. (a) Beam layout for first floor, (b) First floor mesh, (c) Second floor mesh, (d) Spire mesh

The second floor was generated by copying all plates and beams for the first floor to a height of 4m above the first floor. From this, the extra nodes, beams and plates were input in the radial direction, shown by Fig. 8c. Again, this process was repeated, adding the necessary plates and beams as the floor number increased, in order to match the structural design of the head structure. Once all twelve floors were completed, the spire was added to the top of the building. This involved drawing elements similar to how the core was modelled. From this, these beams were extruded upwards to create plates and subdivided accordingly, as shown by Fig. 8d. This was then done again at a smaller diameter, to represent the spire getting narrower as the height increases.

Lastly, the yellow plates shown in Fig. 8a were subdivided to match the mesh for the green plates. The quarter section of the model is now ready to be copied and mirrored about the vertical axis in order to create the full model. The total model involved roughly 50000 plates and 4000 beams, with the mesh size equating to roughly 1m x 1m squares. Although this mesh will lead to a substantial computational time for the different solvers in Strand7, it assists in providing a more realistic stress distribution, especially in high gradient stress zones.

With regards to the restraints for the model, the only restraints provided were fully fixed restraints to the bottom nodes. All other nodes in the model were left as free. It should be noted that the vast majority of the modelling was performed using the cylindrical coordinate system, to allow the use of radial measurements. This assisted in ensuring an appropriate mesh for the model, to increase the accuracy of the tower design.

Once the model was created with the associated boundary conditions, the properties were allocated for each member type. This involved using the Structural Steel library available in Strand7 to allocate all steel sections for beams and columns. The concrete members including the slabs and the core shaft were then chosen as the appropriate sizings and characteristic strengths.

Figure 9a shows an elevation view of the full mesh, along with close-up views of the meshing at the connections of the slab and the core shaft and a view of the full head structure. Figure 9b shows an isometric view of the concrete core shaft and the mesh used. As mentioned earlier, it is critical that the mesh used has no incompatibilities, as this will lead to inaccurate results for the stress distributions.

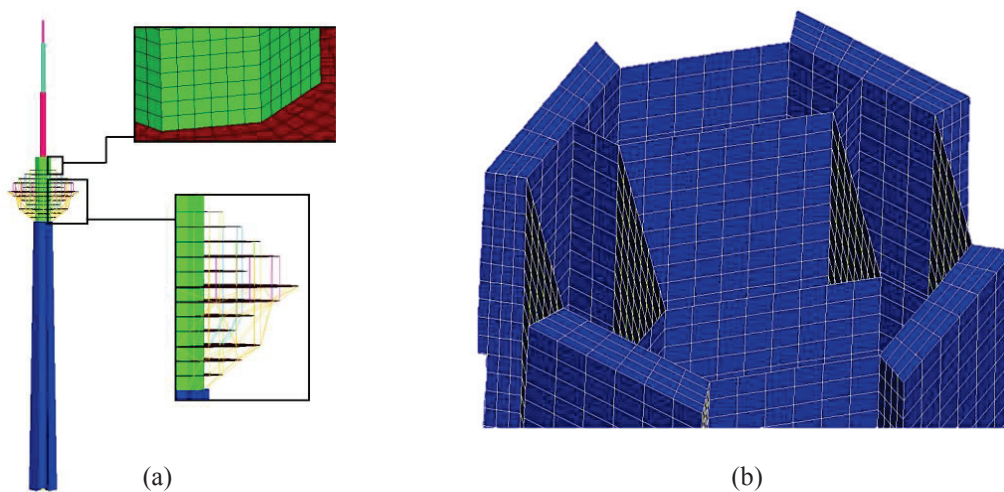


FIGURE 9. (a) Modelling the structure in Strand7, (b) Meshing of the concrete core

member sizes of the main elements of the structure are displayed below in Table 3.

TABLE 3. Member sizes and modelling technique for the elements used in the model

Structural Element	Material/Size	Strand7 Modelling Technique
Head structure columns	Steel – 350WC230	Beam 2
Head structure beams	Steel – 460UB82.1	Beam 2
Slabs	40MPa 220mm deep	Quad 4 plate
Foundation	40MPa 1.5mm thick	Quad 4 plate
Core Shaft	40MPa 1.5mm thick	Quad 4 plate
Spire	40MPa 0.5m thick tapered	Quad 4 plate
Steel basket	500WC440	Beam 2

Linear Static Analysis

The linear static analysis involved two loading cases; dead load and live load. The dead load was performed by applying gravity to the structure as well as the additional 1kPa imposed load. The live load involved applying a 2kPa face pressure to the slab plates in the head structure (which is the live loading for restaurants according to AS1170.1, 2002). A loading combination of 1.2G + 1.5Q was then applied. The deflection contours are shown by Fig. 10.

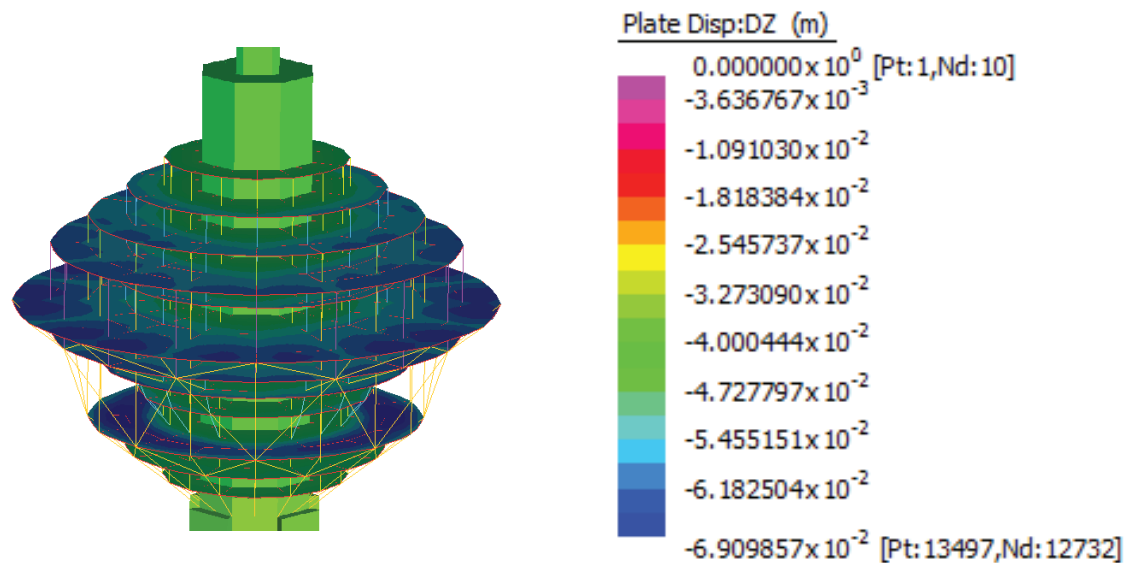


FIGURE 10. Linear Static Analysis contour for load case 1.2G+1.5Q

TABLE 4. The maximum deflection, stress and bending moment from Linear Static Analysis

Load Case (plate analysis)	Maximum Deflection (mm)	Maximum Stress (MPa)	Maximum Bending Moment (kNm)
G	52	5.8	76
Q	8.8	2.0	29
1.2G+1.5Q	75	9.9	141

As shown by Table 4, the maximum deflection is 75mm at the cantilevered sections of the slabs. It should be noted that this is a global deflection of 75mm. That is, the deflection of the core section is 45mm. The local deflection of the slab was found to be 30mm, which is within the deflection limits stated by AS1170.1. The stresses in the concrete slab, particularly for the combined case are significant. This could cause cracking of the section, meaning that slab depth could arguably be increased to gain a higher capacity. However, this does create issues with having excessive masses high up in the building and thus increases the moment effects in an earthquake.

Static Wind Analysis

The static wind analysis involved applying the global pressure that was discussed previously. The load was applied to the plates as pressures, in the global x direction, varying with height z (m). These results are shown by Fig. 11a and 11b. As shown by the results, the largest deflection for the plates is 873mm.

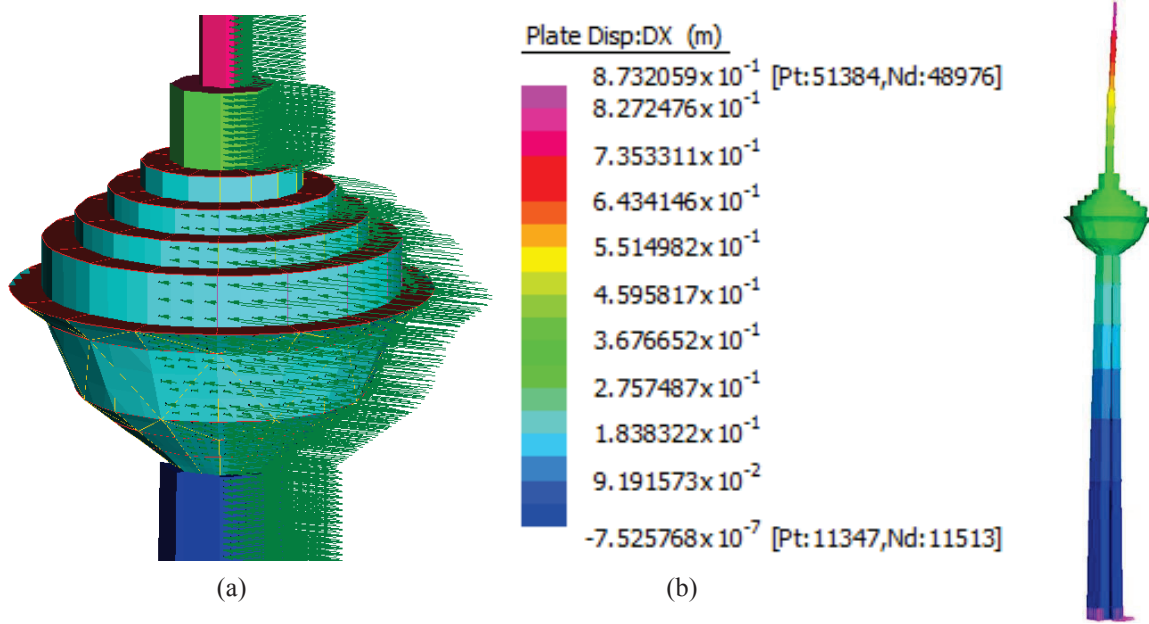


FIGURE 11. (a) Wind Loading applied to head structure, (b) Deflection results

Natural Frequency Solver

In real situations, structures are subject to random fluctuations in wind speed that will interact with the vibrational modes. This results in a dynamic wind load which varies in time acting on the structure. Therefore, it is not realistic to solely base a tall building design on a static analysis. In particular for high-rise buildings, the wind loads and earthquake loads activate the structures natural frequencies which in turn produce oscillations which must be damped. Instead, the use of a dynamic analysis provides a closer representation to how wind acts on structures, particularly for those outside the scope of the Australian Design Codes.

For any multistory structure the matrix element equation becomes (Alonso-Marroquin, 2016).

$$M\ddot{U} + KU = F(t) \quad (12)$$

Where M is the matrix equation, \ddot{U} is the acceleration vector, K is the stiffness matrix, U is the displacement vector and F(t) is the time dependent force acting on the structure. Normally, a transient solver will provide a solution to Eq. 12. However, due to the enormity of the Milad Tower an alternate method can be used which is known as the Spectral Response Solver. The theory and methodology for this is explained in detail below.

A Natural Frequency solver is first used to determine frequencies, modes and mode shapes which can later be utilized in a Dynamic Wind and Earthquake Analysis. To do so, an oscillatory function with a frequency ω is substituted into Eq 12. This takes the form of:

$$U(t) = U_0 e^{j\omega t} \quad (13)$$

In terms of the mathematical process of finding the natural frequencies, Eq. 12 is used and the external forces and damping forces acting on the structure are taken as 0:

$$\det(K - \omega^2 M) = 0 \quad (14)$$

Solving this equation yields a polynomial function of ω^2 , which is the natural frequency of a mode. The order of this equation is equal to the number of degrees of freedom for mass displacements in the structure. This will then provide the natural frequencies in the structure. The natural frequencies of the structure as calculated in Strand7 can be seen in Table 5.

TABLE 5. The converged modes from natural frequency of the structure

Mode	Frequency (Hz)	Period (s)
1	0.151	6.617
2	0.151	6.617
3	0.383	2.612
4	0.383	2.612
5	0.807	1.240
6	0.807	1.240
7	1.238	0.808
8	1.242	0.805
9	1.242	0.805
10	2.054	0.487
11	2.054	0.487
12	2.601	0.385
13	2.601	0.385
14	3.070	0.326
15	3.554	0.281
16	4.053	0.247
17	4.201	0.238

By finding the natural frequencies ω , the different mode shapes can be found. By replacing Eq. 13 above into Eq. 12, we obtain Eq. 15 below. This equation is solved for U_i for each mode of the structure.

$$(K - \omega^2 M)U_i = 0 \quad (15)$$

$$U_i M U_i = 1 \quad (16)$$

U_i is solved utilizing the relationship shown in Eq. 16: This is the simplified process for how Strand7 solves natural frequencies of the structure.

Dynamic Wind Analysis

The second step of the analysis involves generating a Power Spectral Density (PSD) curve for the wind force. A PSD curve gives a measure of the winds intensity within the frequency domain. Utilising the Strand7 webnotes, it was possible to develop an equation for the curve based off a number of variables specific to the Milad Tower, as shown by Eq. 17.

$$S_p(n) = 4(C_d \rho)^2 \bar{V}^4 k \frac{x^2}{n(1+x^2)^{\frac{4}{3}}} \quad (17)$$

Where; $S_p(n)$ =wind pressure factor, C_d =drag coefficient, ρ =air density, V =wind velocity, k =surrounding surface roughness parameter, $x=\frac{1200n}{v}$ and n =frequency. The resulting equation yields the Wind Force PSD as shown in Fig. 12.

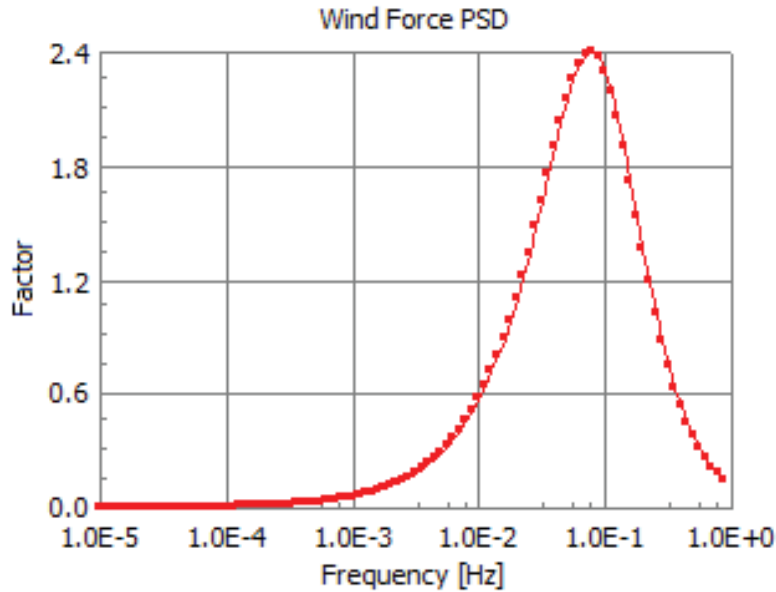


FIGURE 12. Factor vs. Frequency graph for dynamic wind analysis

This graph is then included in the Strand7 spectral response analysis as a factor vs frequency table. The Wind Force PSD has the effect of factoring the wind effects at certain frequencies. Therefore, when the building's natural frequencies coincide with the frequencies that are heavily factored, the effect of the wind loading will be significantly greater. The peak shown by the graph occurs at approximately 0.1Hz, which coincides with the Fundamental Mode of frequency of the tower, as shown by the natural frequency solver. Therefore, the response of the building to dynamic wind will be more intense. It is important to note that a number of different factor vs frequency graphs exist, and they are greatly dependent on the location of the wind. Therefore, there is a degree of uncertainty in this calculation, however it provides a platform for further research into the area of wind dynamics. Other effects of wind that should be considered is the crosswind excitation which occurs due to a process called vortex shedding along the height of the building.

Utilising the Strand7 spectral response solver with the included natural frequencies, factor vs frequency graph, and the applied wind pressures (as opposed to base acceleration for earthquake) we are able to calculate the displacements and stresses of the various modes of vibration. Utilising the combined SRSS case it is then possible to determine the peak displacements, stresses and their locations within the structure as shown in Fig. 13. As shown by the results, the largest deflection for the plates is 2.74m.

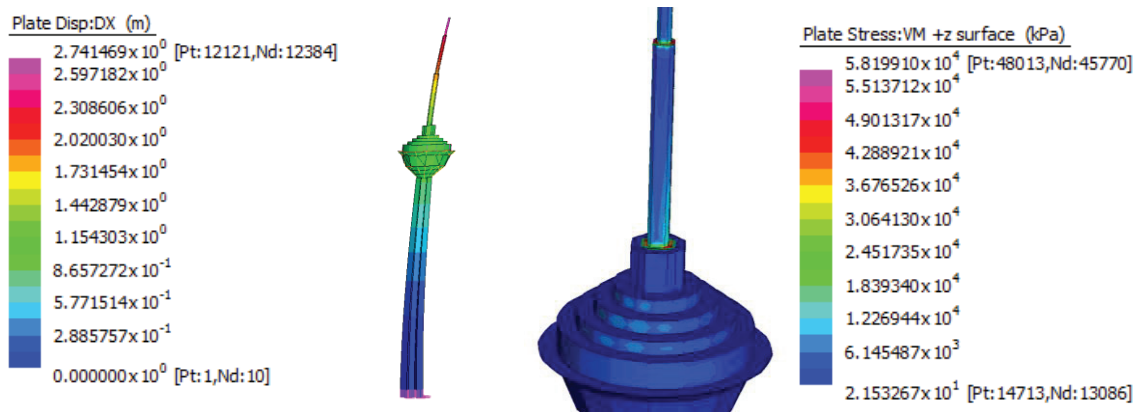


FIGURE 13. Deflection and peak stress locations of spectral Analysis case SRSS

Earthquake Analysis

The earthquake design involved using the previously determined natural frequency vibrational modes. From this, a spectral analysis was performed. The spectral analysis solves ordinary differential equations by utilizing harmonic oscillator with the natural frequency and damping ratio to an imposed acceleration. Both SRSS and Modal analysis were used for the earthquake analysis. Spectral analysis involved inputting a relationship between spectral ordinates $C_h(T)$ and period (T) (factor vs. frequency). The soil category was chosen to be Class C as this is the most similar geological conditions, in accordance with AS1170.4 (2007). This is shown by Fig. 14.

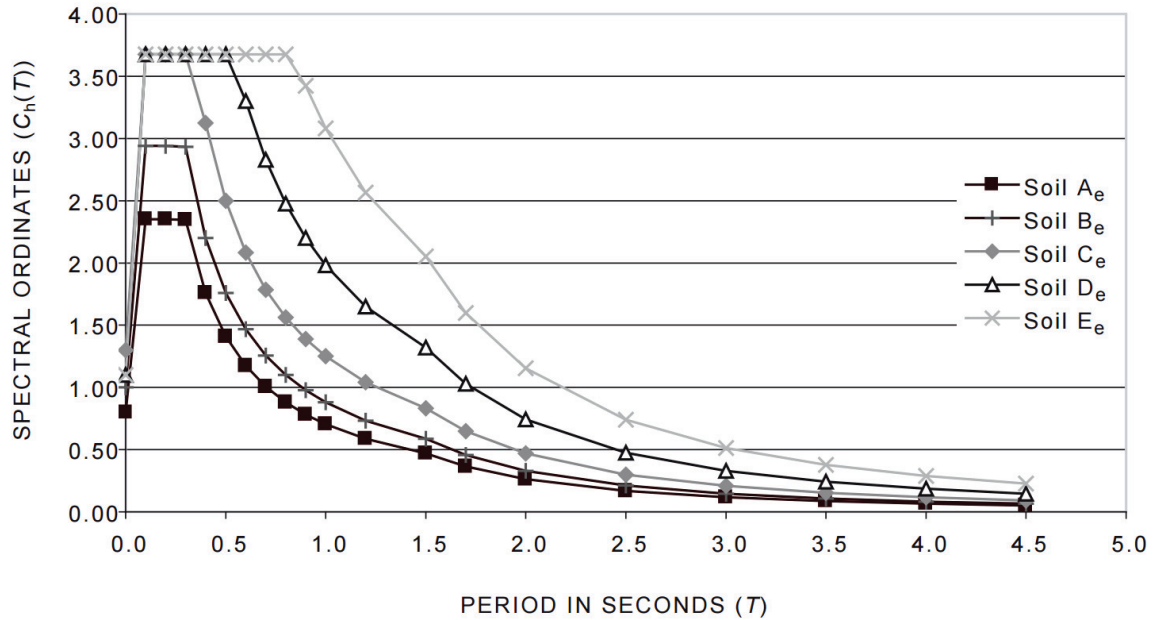


FIGURE 14. Spectral Response curve (AS1170.4, 2007)

The $C_h(T)$ factor is the spectral shape factor for the period of T seconds. This varies with the type of soil class that the structure sit on. The earthquake was then factored by 0.22 of the value of gravity and applied in the x direction to simulate an applied earthquake along a single axis. Since the model is axisymmetric, the effect would be the same from the y direction. The earthquake was applied as a base acceleration, to represent the ground moving. The results for the plate deflection in the x direction are shown by Fig 15.

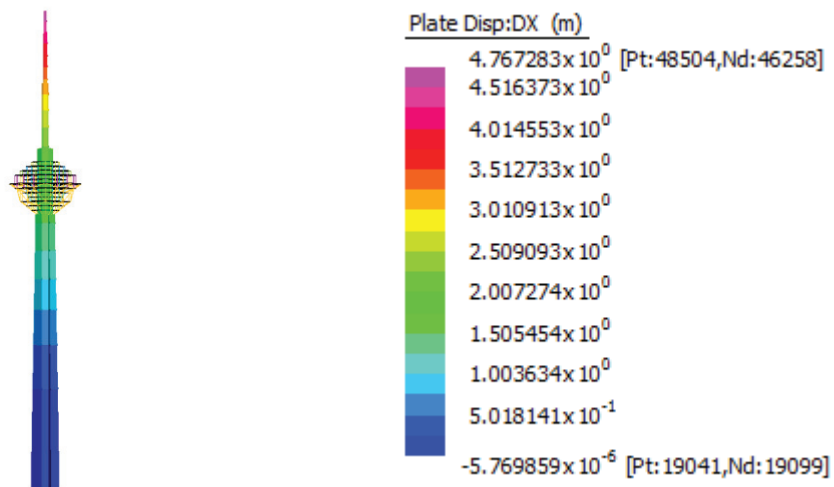


FIGURE 15. Earthquake Deflection Contour Plot

Figure 16 shows the deflected shape for a number of different natural frequencies. Due to the height of the tower, there are many different failure modes, all of which need to be considered during the design process.



FIGURE 16- Deflected shape of different vibrational modes and their frequencies.

The modal analysis finds the natural frequencies of the structure and the shape of each mode at that frequency. As the mode shapes are orthogonal, they can be expressed as a linear combination of these eigenvectors. Using Eq. 13 and 14, the mode shapes U_i can be found and the mass participation factor for each node subsequently calculated.

$$\Gamma = \frac{U_i^T M r}{U_i^T M U_i} \quad (18)$$

Where r is taken as an arbitrary vector in the number of degrees of freedoms dimensional space. At every mode, mass participation will take place and will be associated with a frequency. The mass participation is the amount of mass which has contributed in that mode. All modes with a low mass participation can be ignored. The accumulated mass participation is expected to be greater than 90%. A value of 84.31% was obtained through the calculations on Strand7 which for the design of a tall structure is relatively close to the expected outcome. The results of mass participation can be seen below in Table 6.

TABLE 6. Mass participation of the structure following earthquake analysis

Mode	Participation (%)	Mode	Participation (%)
1	54.854	10	7.221
2	0.012	11	0.001
3	2.317	12	0.27
4	0	13	0
5	18.321	14	0
6	0.004	15	0.001
7	0	18	0
8	1.302	19	0.003
9	0	20	0.003
TOTAL MASS PARTICIPATION		84.31%	

STRUCTURAL DESIGN

Maximum distributed load

Dead Load and Live Load:

The dead load is calculated from the self-weight of the concrete slab. An additional 1 kPa is conservatively added for services and furnishing.

$$q_D = 25 \times 0.22 + 1 = 6.5 \text{ kPa} \quad (19)$$

$$q_L = 2 \text{ kPa} \quad (20)$$

Since it is a 2 way slab, tributary areas are chosen appropriately equating to one quarter of the span. The tributary area is therefore equal to 2.25 metres. This is multiplied with the loading factors to convert the pressure into a distributed load.

$$UDL_D = 6.5 \times 2.25 = 14.6 \text{ kN/m} \quad (21)$$

$$UDL_L = 2 \times 2.25 = 4.5 \text{ kN/m} \quad (22)$$

The maximum loading combination for the distributed load was found in accordance with AS1170.0. This was considered as 1.2G + 1.5Q.

$$Q_{1.2G+1.5Q} = 1.2 \times 14.6 + 1.5 \times 4.5 = 24.27 \text{ kN/m} \quad (23)$$

Maximum Axial Load

The maximum axial load found to be acting on a member is the column situated at the bottom of the steel basket. The tower head is 12 stories tall and therefore there are 11 stories acting on the column. The slab, beam and predicted column size are to be accounted for when considering the axial load.

Column:

Assuming column is a 310UC158 and the storey height is 4 metres:

$$AF_{column} = 158 \times 4 = 6.32 \text{ kN} \quad (24)$$

$$AF_{C11} = 11 \times 6.32 = 69.52 \text{ kN} \quad (25)$$

Beam:

As calculated below, the chosen beam is a 610UB125, and is located twice along a 9 metre span.

$$AF_B = 125 \times 9 = 11.25 \text{ kN} \quad (26)$$

$$AF_{B11} = 11 \times 11.25 \times 2 = 247.5 \text{ kN} \quad (27)$$

Slab:

For the slab calculated below, the depth corresponded to 220 mm for an area of 91 m².

$$AF_S = 0.22 \times 91 \times 25 = 400 \text{ kN} \quad (28)$$

$$AF_{S11} = 11 \times 400 = 4400 \text{ kN} \quad (29)$$

Therefore, the maximum total axial force acting on a column is given by:

$$AF_{max} = 69.5 + 247.5 + 4400 = 4717 \text{ kN} \quad (30)$$

Beam Design

Using the maximum distributed load calculated previously, the formula for the maximum bending moment for a continuous support over the span of 3 columns is:

$$M^* = 0.2wl^2 = 0.2 \times 24.3 \times 9^2 = 393.66 \text{ kNm} \quad (31)$$

As the top flange of the beam is fully restrained by the concrete slab, M_b shall be taken as M_s . This is in accordance with clause 5.3 of AS4100. The formula for section capacity is given by:

$$M_s = f_y Z_e \quad (32)$$

Rearranging this for the section modulus

$$Z_e = \frac{M_s}{f_y} = \frac{393660000}{300} = 1312.2 \times 10^3 \text{ mm}^4 \quad (33)$$

Therefore, a member with a greater section modulus than 1312.2 must be chosen. The most economic beam to be chosen in accordance with section modulus would be 460UB82.1.

Column Design

The maximum axial force acting on any member was calculated to be 4717 kN. For strength design, this must be less than the nominal section capacity as well as be less than the nominal member capacity. All values and equations were extracted from AS4100.

Nominal section capacity:

$$N^* \leq \phi N_s \quad (34)$$

$$N_s = k_f A_g f_y = 1.0 \times 20100 \times 300 = 6030 \text{ kN} \quad (35)$$

These factors were obtained from onesteel for a 310UC158, as an initial estimate.

Nominal Member Capacity:

$$N_c = \alpha_c N_s \quad (36)$$

$$\lambda_n = \left(\frac{l_e}{r} \right) \left(\sqrt{k_f} \right) \left(\sqrt{\frac{f_y}{250}} \right) = 40.33 \quad (37)$$

The effective length was taken as the 4 metre height multiplied by a k value of 1. The radius and yield strength was obtained from onesteel.

$$\alpha_b = 0 \quad (38)$$

Taken as 0 for a hot rolled UC.

Therefore, from table 6.3.3(3):

$$\alpha_c = 0.905 \quad (39)$$

$$N_c = 0.905 \times 6030 = 5457.15 \text{ kN} \quad (40)$$

$$\phi = 0.9 \quad (41)$$

Hence,

$$\phi N_s = 5427 \text{ kN} \quad (42)$$

$$\phi N_c = 4911.435 \text{ kN} \quad (43)$$

Since the maximum axial force is less than both the section and member capacity, the chosen structural member for the column is 310UC158. However, although the column was designed for strength, the suggested column caused large deflections in STRAND7. For a high profile tower an extra safety factor was considered and the selected column which led to a reduction in the total deflections was a 350WC230.

Slab Design

The deemed to comply approach for the design of a slab designs for both serviceability and for strength in accordance with clause 9.3.4.1, if the below equation is satisfied.

Initially, a slab depth of 210 mm was selected to determine the loading combinations to apply to the slab. The dead load had an additional 1 kPa added to it for services and furnishing.

$$q_g = 0.21 \times 25 + 1 = 6.25 \text{ kPa} \quad (44)$$

$$q_l = 2 \text{ kPa} \quad (45)$$

The 2 kPa was chosen in accordance with AS1170.1, table 3.1, for a typical restaurant loading.

The actual slab area is a complicated shape, however for simplicity, the tributary area for the slab was assumed to be a 9 by 9 metre square.

The method used was a deemed-to-comply approach:

$$\frac{L_{ef}}{d} \leq k_3 k_4 \left[\frac{\left(\frac{\Delta}{L_{ef}}\right) 1000 E_c}{F_{d,ef}} \right]^{\frac{1}{3}} \quad (46)$$

$\frac{\Delta}{L_{ef}}$ is limited to 1/500 where provisions are made to minimise the effect of movement.

k_3 is taken as 1 given by 9.3.4.2(a)

k_4 is taken as 3.6 for all four edges of the slab being continuous (Table 9.3.4.2)

E_c is taken as 32,800 MPa given by Table 3.1.2

$F_{d,ef} = (1.0 + k_{cs})g + (\psi_s + k_{cs}\psi_l)q$

And, $k_{cs} = [2 - 1.2(A_{sc}/A_{st})] \geq 0.8$

For a conservative approach, k_{cs} is assumed to be 2.0 (i.e. no tensile reinforcement).

ψ_s is taken as 0.7 and ψ_l is taken as 0.4 for retail and office space (AS/NZS1170.0 Table 4.1)

Therefore,

$F_{d,ef} = (1.0 + 2.0)6.25 + (0.7 + 2.0 * 0.4)2 = 21.75$

$L_{ef} = 9000mm$

Therefore,

$$d \geq \frac{9000}{1 \times 3.6 \times \left[\frac{\left(\frac{1}{500}\right) 1000 \times 32800}{21.75} \right]^{\frac{1}{3}}} = 173mm \quad (47)$$

Assuming N16 bars will be used, with a 30 mm cover for a conservative approach:

$$D \geq 173 + \frac{16}{2} + 30 = 211mm \quad (48)$$

The final depth of the slab will therefore be taken as 220 mm.

Shrinkage effects govern the design, and for moderate crack control, $p_{min} = 0.0035$. (AS/NZS3600 9.4.3.4). Therefore the minimum reinforcement spacing required is:

$$p_{min} = \frac{\left(\frac{A_{st}}{s}\right)}{d} \quad (49)$$

$$s \leq \frac{\pi \times 8^2}{0.0035 \times 173} = 332mm \quad (50)$$

Taking N16 bars as reinforcement, spaced at 300mm centres, this corresponds to

$$\frac{\pi \times 8^2 mm^2}{0.3m} = 670mm^2 / m \quad (51)$$

Therefore, the final design of the slab is 220 mm depth with N16 bars at 300 mm spacing's.

CONCLUSIONS

The results from the wind analysis and linear static analysis of the tower were as hypothesized, however the excitation due to earthquake loading was the governing loading case. The structural systems found in the structure are tapered shear walls and a steel basket head structure. These systems had realistic results in terms of stress, deflection and bending moments. The mesh size and quality that was generated allowed for a more accurate stress distribution for each loading case. The selected members that were designed such as beams, columns and slabs were done with a degree of accuracy and minimized deflections in the tower.

The beam and column members in the head structure were derived by hand calculations to be 310UC158 and 460UB82.1 respectively (in accordance with AS/NZS 4100). However due to excessive deflections encountered in the analysis of the structure, the column members were slightly modified to be 350WC230. The slab depth was initially designed to be 220mm and this depth was found to be sufficient after running the analysis.

The wind loads were derived in accordance with AS/NZS1170.2. The velocity at each storey were found employing the Deaves & Harris model that was based on full scale data. These velocities were then converted to a corresponding pressure utilizing the quasi-static assumption

The greatest local slab deflection was found to be 69mm in the largest span. The deflection at the top of the tower from the static wind analysis was found to be 1m. The deflection at the top of the tower due to the dynamic wind analysis was found to be 2.75m. And the total deflection found from the greatest mass participation mode in earthquake analysis was found to be 5m. The governing loading case is therefore the earthquake loading as this yields the greatest deflection of the structure.

Further analysis could be undertaken to refine the accuracy of this analysis and yield more accurate results by using a denser mesh and higher order elements. However due to the scope of this analysis, the model has been simplified.

REFERENCES

- Alonso-Marroquin, F, 2016. Finite Element Modelling for Civil Engineering, Quantumfi Publishers, Sydney, ISBN 978-0-9944287-0-7
- AS/NZS1170.0-4 – Australian/New Zealand Standards for Structural Design Actions, Part 2: Wind Actions, 2011
- AS/NZS1170.2 – Australian/New Zealand Standards for Structural Design Actions Commentary (Supplement to AS/NZS 1170.2), Part 2: Wind Actions, 2002
- Deaves, D.M. and Harris, R.I., 1978. A mathematical model of the structure of strong winds. na.
- Ghorbani-Tanha, A.K., Noorzad, A. and Rahimian, M., 2009. Mitigation of wind-induced motion of Milad Tower by tuned mass damper. *The structural design of tall and special buildings*, 18(4), pp.371-385.
- Holmes JD. Wind loading of structures. CRC Press; 2015 Jan 27.
- Mendis, P., Ngo, T., Haritos, N., Hira, A., Samali, B. and Cheung, J., 2007. Wind loading on tall buildings. *EJSE Special Issue: Loading on Structures*, 3, pp.41-54.
- Oruj Travel,. Milad Tower. 2016. Web. 1 June 2016.
- Strand7, 2015. PSD Analysis of a Wind Load. Strand7 Webnotes - Linear/Dynamics, 1.10.20.3, pp.1-11.
- Yahyai, M., Daryan, A.S., Ziaei, M. and Mirtaheri, S.M., 2011. Wind effect on milad tower using computational fluid dynamics. *The Structural Design of Tall and Special Buildings*, 20(2), pp.177-189.
- Yahyai, M., Rezayibana, B. and Daryan, A.S., 2009. Nonlinear seismic response of Milad Tower using finite element model. *The Structural Design of Tall and Special Buildings*, 18(8), pp.877-890.

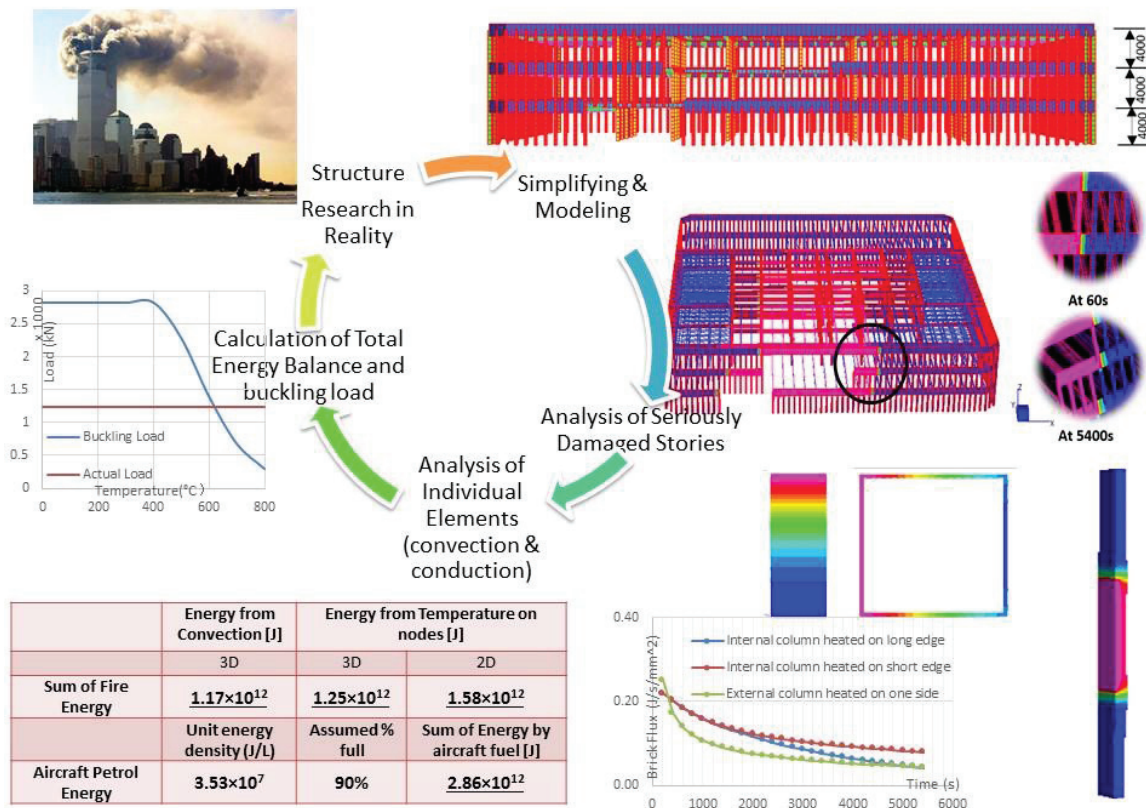
Energy Balance In The WTC Collapse

Kaiqi Zhu, Kang Xu, Peter Ansurian, Faham Tahmasebinia, and Fernando Alonso-Marroquin^{a)}

School of Civil Engineering, The University of Sydney, Sydney NSW 2016 Australia

^{a)}Corresponding author: fernando@sydney.edu.au

Abstract. The main aim of this report is to provide an analysis of Twin Towers of the New York City's World Trade Centre collapsed after attacked by two jet aircrafts. The approach mainly focused on the effect of temperature on mechanical properties of the building, by modelling heat energy in the south tower. Energy balance during the collapse between the energy inputs by aircraft petrol and the transient heat to the towers was conducted. Both the overall structure between 80 to 83 stories and individual elements was modelled. The main elements contributed to the heat transition includes external and internal columns. Heat applied in 2D and 3D models for single elements was through convection and conduction. Analysis of transient heat was done using Strand7.



Graphical abstract. Heat flow within the three-level model at 60s and 5400s and elements including internal and external columns and truss are attached.

INTRODUCTION

Framed Tube System Tower with multistories

Twin Towers were components of the World Trade Centre located in Lower Manhattan, New York City. They consisted of two 110-story with 6-level basement commercial office buildings: the 417 m North Tower, and 415 m South Tower. At 9:03 a.m. on September 11 in 2011, the Twin Tower collapsed after attacked by two jet aircrafts. This project was aimed to give a transient thermal analysis of the tower element in this process and a calculation of the entire energy flow in the building. We focused on the South tower, it collapsed within 1.5 hour after the attack. As a framed tube structure, it occupied approximately 63m x 63m with core of roughly 27m x 41 m (detailed dimensions shown below). There were 59 external columns on each side of the structure and 4 columns on the four corners, thus there was a total number of 240 external columns. The structure core consisted of 47 steel columns running from the bedrock to the top of the tower. The large, column-free space between the perimeter and core was bridged by prefabricated floor trusses. Trusses in between connected the core to perimeter wall with a spacing of 2.03 m centre to centre.

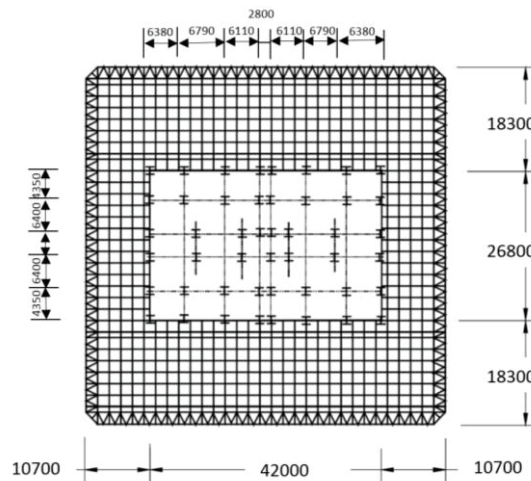


FIGURE 1. Structure Introduction: plan view of WTC (unit mm)
[Federal Insurance and Mitigation Administration, 2002.]

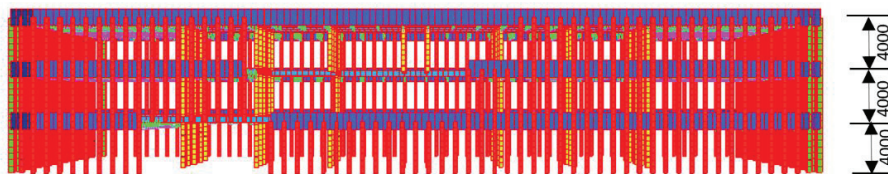


FIGURE 2. Structure Introduction: Elevation view of WTC from level 80 to 82 (dimension only refers to the strand7 model, for exact level heights for entire building please refer to the appendix)

This project aimed to investigate the temperature transfer and energy flow within the building after the attack till collapsing.

TABLE 1. Building Details

Location: New York City	The Year of Built: 1968
Architects: Yamasaki & Associates	Approximate Cost: \$450 million
Structural Engineers: Lesile E. Robertson Associates	Overall Height: 415m
Function: Commercial office	Floor Area: approximately 3,700 m ²
The Structure of the Plan: A square shaped floor space around an square core	
Number of Floors: 110 floors above ground, and 6 levels of basement	

STRUCTURAL MEMBERS

Below is the description of the members of the structure:

Perimeter walls: The perimeter wall was consisted of external Vierendeel trusses columns. The size of a single square-hollow-section external column was 365mm×365mm, with thickness varies from 6.35mm to 63.5mm. Three columns spaced in 1016mm are connected together by a 1320mm wide spandrel, and forms a piece of the perimeter wall (about 10m in length), as shown below. To ease the design, all of them was modelled in same size of 365mm×365mm, with thickness of 9.5mm.

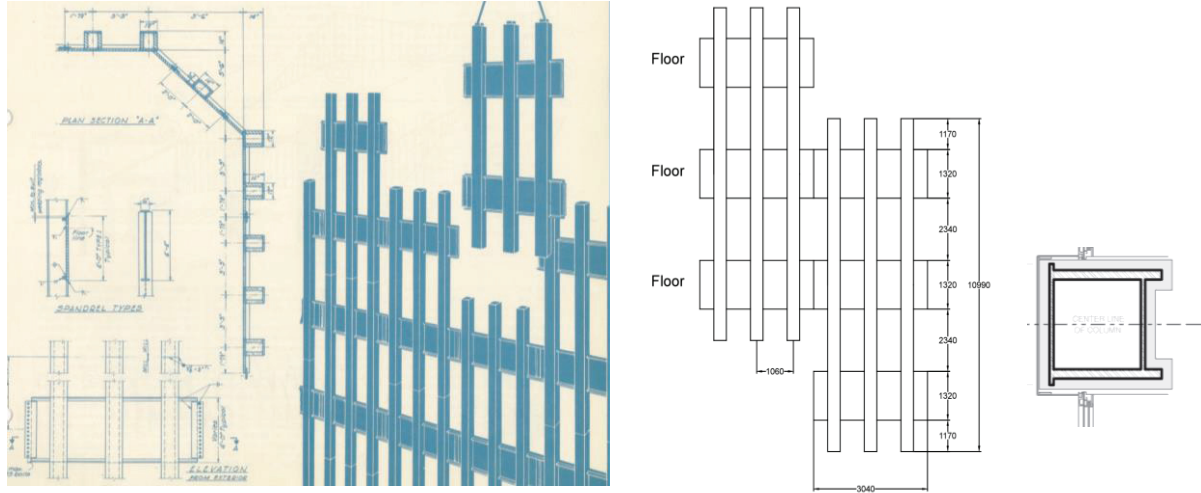


FIGURE 3. Schematic of contemporary steel design – perimeter columns with corss section (unit: mm)
[American Iron and Steel institute, 1964]

Core columns: Core of the framed tube was mainly supported by core columns, varied in both dimensions and shape. For lower floors of the structure, core columns were exclusively large box columns of roughly 300mmx1320mm, as the original design of 178mm thickness was not accommodated. From ground to 66 floors, there were 47 steel columns, among which 12 columns were 1400mmx560mm and 35 columns were 600mm x 460mm in size. For upper stories, some columns were replaced by an I-steel and for stories above 84 floors, all of them were I-shaped columns. Length of columns depended on the storey height varied from 3050 to 6710 mm (assumed a uniform length of 4000 mm when modelling).

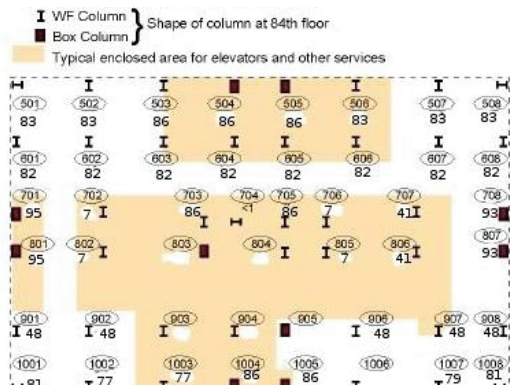


FIGURE 4. Structural plan view of core column in WTC towers on a typical level (Floor 84)
[Federal Emergency Management Agency, 2002]

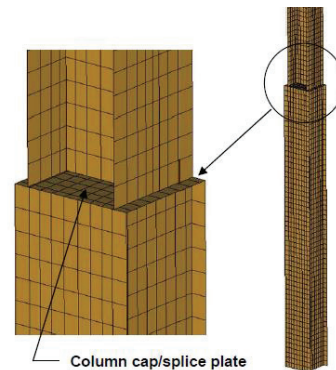


FIGURE 5. Details of box column-to-wide flange core column splice [Federal Emergency Management Agency, 2002]

Trusses: Trusses welded to the core and connected by 25mm diameter bolts to the external columns were spaced 2.03m both in transverse and longitudinal directions. They spanned 10700mm or 18300mm depending on the distance from the core to the edge of the tower and the main trusses were always in the longer span. It consisted of two layers of steel plates of roughly 100mm thick, beneath a fireproofed concrete deck. The top and bottom steel plates were 900mm apart and connected by a 28mm diameter cable.

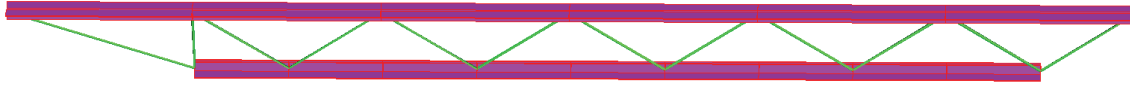


FIGURE 6. Trusses element in Strand 7 structural model

TABLE 2. Structural Element for the Level 1 (Building – Projects)

Details of the Structural Elements	Structural Element Sizes
Columns - Structural Systems	External:365*365*9.5
	Internal:300*900
Trusses - Structural Systems	1800*740

LOAD

Load applied to each column was calculated from data in reference 5. Assuming the core supported 53% of the buildings weight and the perimeter columns supported 47% referring to the NIST (National Institute of Standards and Technology) NCSTAR1 report. The load applied on each column was calculated by adding all the dead loads and live loads above level 83, dividing by the number of columns. Dead load was the sum of the weights of construction materials and the permanent non-varying loads from non-structural components such as wiring, plumbing, heating and cooling aggregates and elevators. Live load was assumed to be a quarter of maximum design loads. For more detailed calculation please refer to the appendix.

TABLE 3. Load Capacity and Applied Load on Columns

	Load Capacity	Applied Load			
	Buckling Load Capacity (kN)	Dead Load (kN)	Live Load (kN)	G + Q (kN)	1.2G + 1.5Q (kN)
External column	2817	912	327	1239	1585
Internal column	57079	3059	645	3705	4639

TEMPERATURE

The maximum flame temperature of hydrocarbons (jet fuel) in air is 1000⁰C. Consider to the diffuse flame and other energy loss, the fire temperature was set at 800⁰C. Though steel would melt at 1500⁰C, 800⁰C was sufficient enough for steel to lose more than 90% of its bearing capacity and cause the failure of a structure. Hence, it is realistic to assume the fire temperature as 800⁰C, and the initial temperature of the whole structure as 20⁰C.

The iso-fire diagram on buildings was considered in the first place. However, in iso-fire diagram, it was assumed that the temperature was increased from 0⁰C and hence not suitable to the project with actual initial temperature f around 20⁰C. Additionally, due to the uncertainty in thermal property of building materials and the limitation of fire temperature, it was not applicable to apply the diagram to this project in a suitable way. Thus the properties in iso-fire diagram was not adopted.

NUMERICAL ANALYSIS

Strand7 was used for the finite element numerical analysis. Two types of model were created to stimulate the heat flow. Structural model was utilized to analyses how heat propagated along the entire steel structure, meanwhile, the detailed element models would illustrate the temperature change as well as the energy flow in the affected elements. In this project, only Transient Heat solver was used for all models, and the period was chosen as 1.5 hours (5400s) ("Collapse Of The World Trade Center") which was the average time between collision and collapse of two buildings. Thermal material properties were assumed temperature independent and the problem only involved conduction and convection, consequently, only liner heat solutions were required.

For the structural model (shown in Fig. 7), considering the limitation in computational time, only four floors (80th to 83rd floors) struck by airplane were modelled. The beam elements were used in this structural model, the cross-sectional dimensions of each element were set in element property. As it was a steel structural building, Structural Steelwork (AS 4100-1998) was chosen as the material for all, concrete cover was neglected. Damaged parts from collision to the building were simplified as a hole, within the region, all the elements were removed. A fixed 800°C (Eagar and Musso 8-11) was applied to every element in contact with the surface of the plane-shaped hole left by the aircraft impact, in order to simulate the ignition.

While modelling the detailed elements, as the floors and walls were either protected by concrete cover or fireproof layers, considering the complexity and uncertainty of the material thermal properties, only steel columns were analysed. The energy flow in air was also neglected. Both two dimensional (2D) and three dimensional (3D) models were utilized, and the material property for all models were Structural Steelwork (AS 4100-1998) provided in Strand7.

In 2D models, plate element was used to create the cross section of both internal and external columns, the thickness of which was set to 4m in geometry to simulate the column height. Since the cross section of internal columns was rectangular, to be more precise, a fixed 800°C was applied to nodes at either long edge or short edge to do the analysis separately, with initial nodal temperature of 20°C at the other nodes.

Three connected columns were created with brick elements in 3D models with the middle one exposed to fire only, in order to obtain both heat flux and energy propagation along the columns. In 3D models, not only nodal temperature, but also air convection was considered. Similarly, the analysis was done by applying fixed 800°C to the surface nodes at either long edge side or short edge side along the column length. The rest of the nodes were set to initial 20°C. Under convection condition, instead of applying fixed nodal temperature, the ambient temperature at the surface of the brick element in contact with fire was defined as 800°C. Because the free convection coefficient for air, gases and dry vapor varies from 0.5 to 1000 (W/(m²C) ("Convective Heat Transfer")), to be more conservative, the $h_c=1000(W/(m^2C))$ was applied to the same brick surface together with the ambient temperature. The initial temperature of 20 °C was added in Load Case 1 and involved in Transient Heat solver.

In transient heat analysis, the governing equation is (based on Fourier law):

$$\nabla^T q + \rho C \frac{\partial T}{\partial t} = Q \quad (1)$$

Where q is the heat flow, ρ is the material density, C is the specific heat, T is temperature and Q represents the heat energy generated per unit of volume. In conduction analysis for both 2D and 3D models, the boundary condition is,

$$T = T_{ref} \quad (2)$$

When it comes to convection, the boundary condition is,

$$q^T n = h_c (T - T_{ref}) \quad (3)$$

Where T_{ref} is the ambient temperature.

RESULTS AND DISCUSSIONS

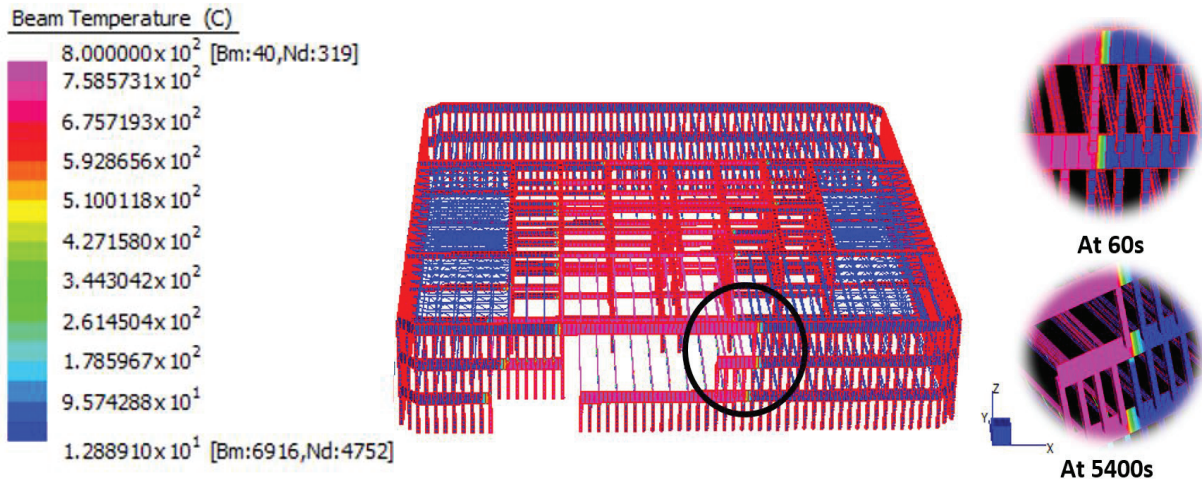


FIGURE 7. Result of temperature transfer after 1.5 hour using 3D model analysis (from level 80 to 82 of WTC)

Figure above shows the result of the structural model after burning for 1.5 hours. Temperature was illustrated by different colours as shown in the chart on the left. The temperature of the entire model was presented by colours on the right, with details of a typical connection (circled part) burning performances at 60s and 5400s. It can be observed that the temperature only changed a little along the element, which shows the heat propagation on steel was very slow. Along the connecting beams between two external columns, one metre away from the heat source column, the temperature was only around 200^oC after 1.5 hours. As steel would only change its bearing capacity at 700^oC or above, the result of 200^oC temperature increase would hardly change steel's property, which means the adjacent column was barely affected by the heat diffusion through structural elements only. According to this, the capacity reduction mainly happened to elements in contact with the heat source, and the energy was mainly absorbed by those elements as well.

2D Temperature at node model results

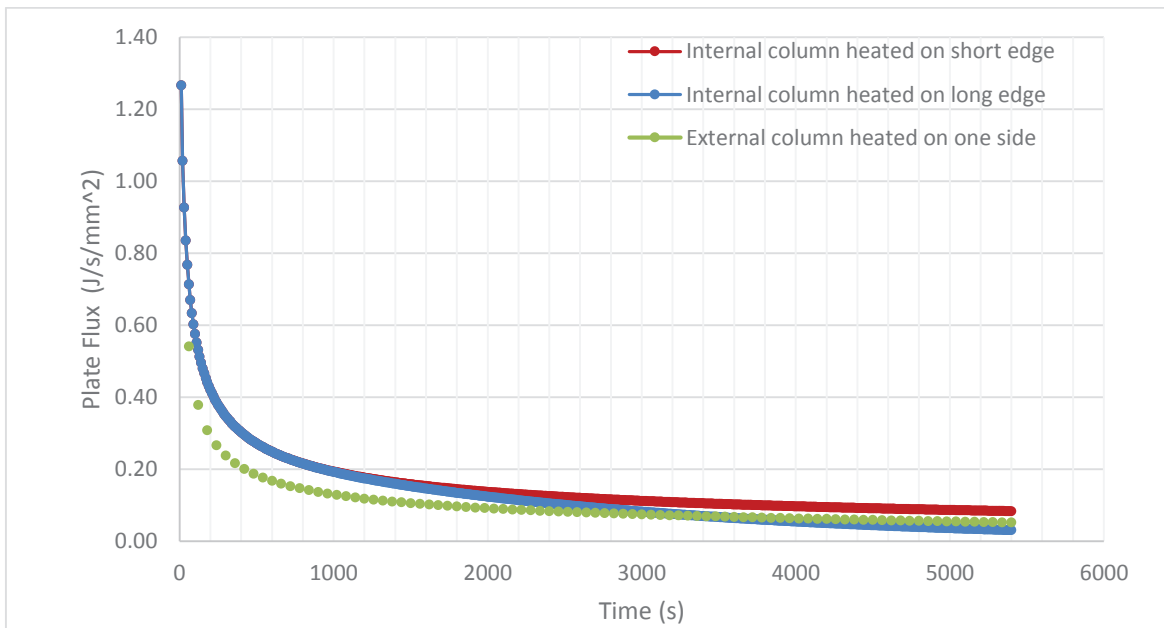
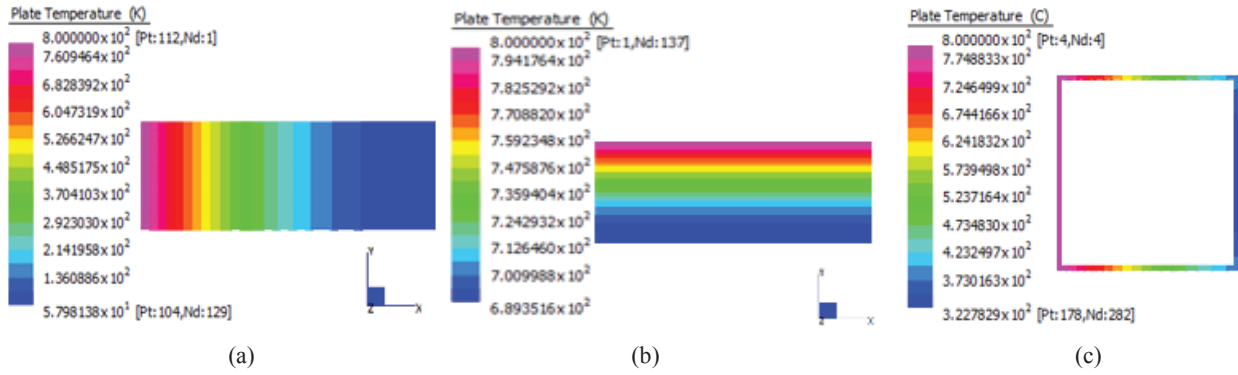


FIGURE 8. (a) Temperature applied on the long edge of internal column; (b) Temperature applied on the long edge of internal column; (c) External column heated on one edge; (d) Flux in columns

3D Temperature at node model results

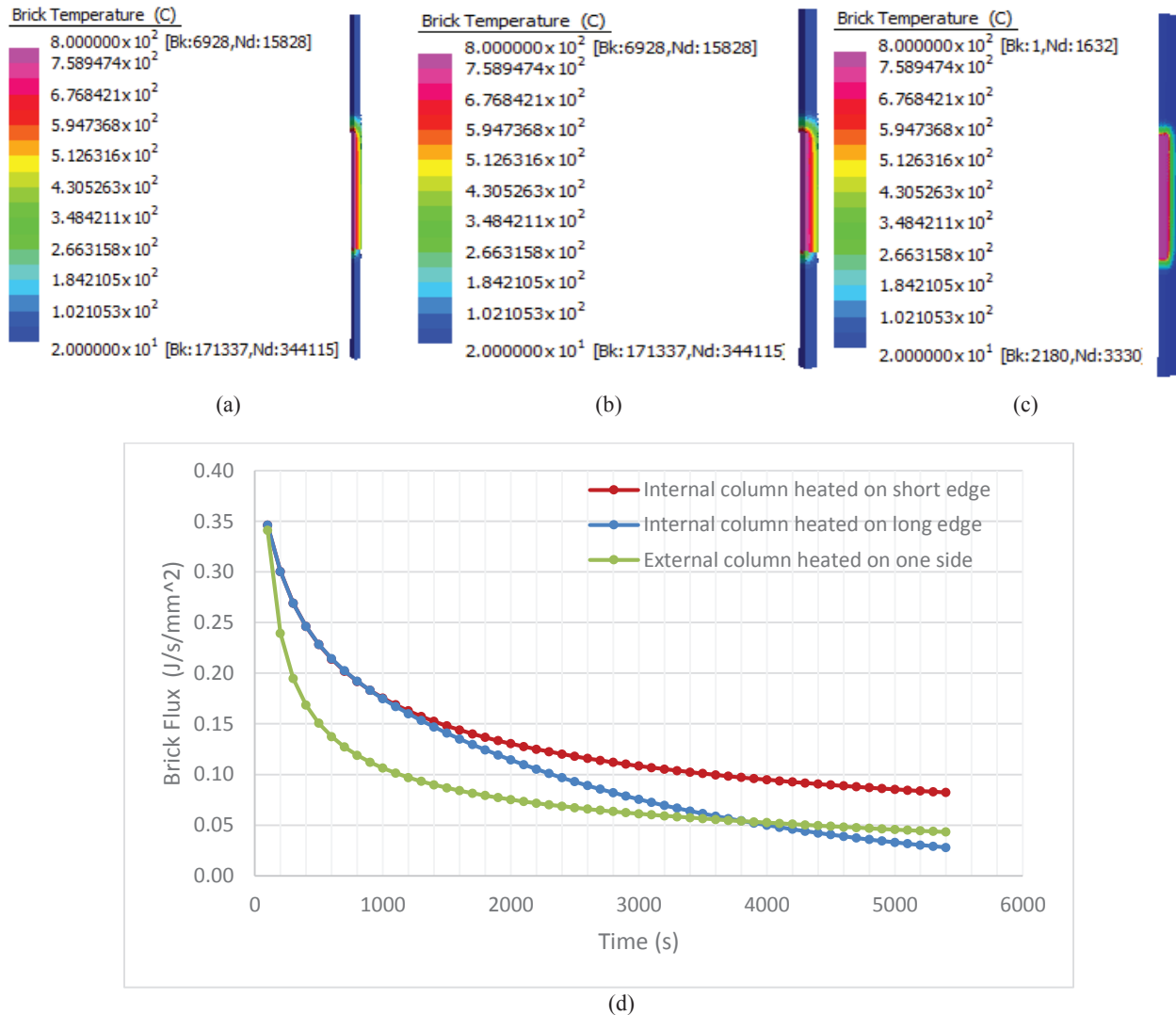


FIGURE 9. (a) Temperature applied on the long edge of internal column; (b) Temperature applied on the long edge of internal column; (c) External column heated on one edge; (d) Flux in columns

Results of heat conduction within column cross sections and between each floor during the fire due to the plane fuel leakage were done in 2D (Quad 4 elements) and 3D (Tetrahedral elements) models as shown above. The heat transits from the heated face to its adjacent sides then across the entire column member in the direction where the heat applies, or spread to its adjacent columns from middle column outwards. For both 2D and 3D models, the temperature of face on fire was assumed to be fixed at 800°C. Thus the highest temperature achieved is about 800°C for each model. For 2D models, the lowest temperature on the cross sections is around 60°C and 300°C, for core columns and external columns respectively. For 3D models, the lowest temperature stays at its initial value of 20°C, on the ends of upper and lower columns.

For flux analysis, generally, energy absorbed by core columns is higher than energy absorbed by external columns. In 3D models a smaller flux results generated than in 2D models. For interior columns, flux absorbed when heat applied on shorter edge of column is smaller than that when heat applied on longer edge of column. This may due to that for limited small area surface, the capacity of it to absorb the heat may be smaller than that for a large area surface. Thus

the flux is lower and slower spread across the column surface with shorter edge. Similarly, in external columns, the face area is smaller than the face area of long edge core column surface, thus the heat absorbed by external column face is smaller than the larger core column face. Moreover, as the external columns are hollow sections, the energy it can absorb is less significant compared to the solid internal columns.

In 3D models, the direction of heat transient is in 3 directions, which consumes longer time for heat to transfer compared with 2D models. Furthermore, when Strand7 plot the flux graphs it assumes the flux can only transit in one direction where heat applies and assumes no flux in other two directions. In reality the flux goes everywhere and thus the result from only one direction of flux may have been reduced. For 2D models the flux only goes in one direction and the result is not deducted hence larger. These may explain the reason for that 2D element flux is greater than 3D element flux.

Though there are some discrepancy between them, the results are overall very similar to each other.

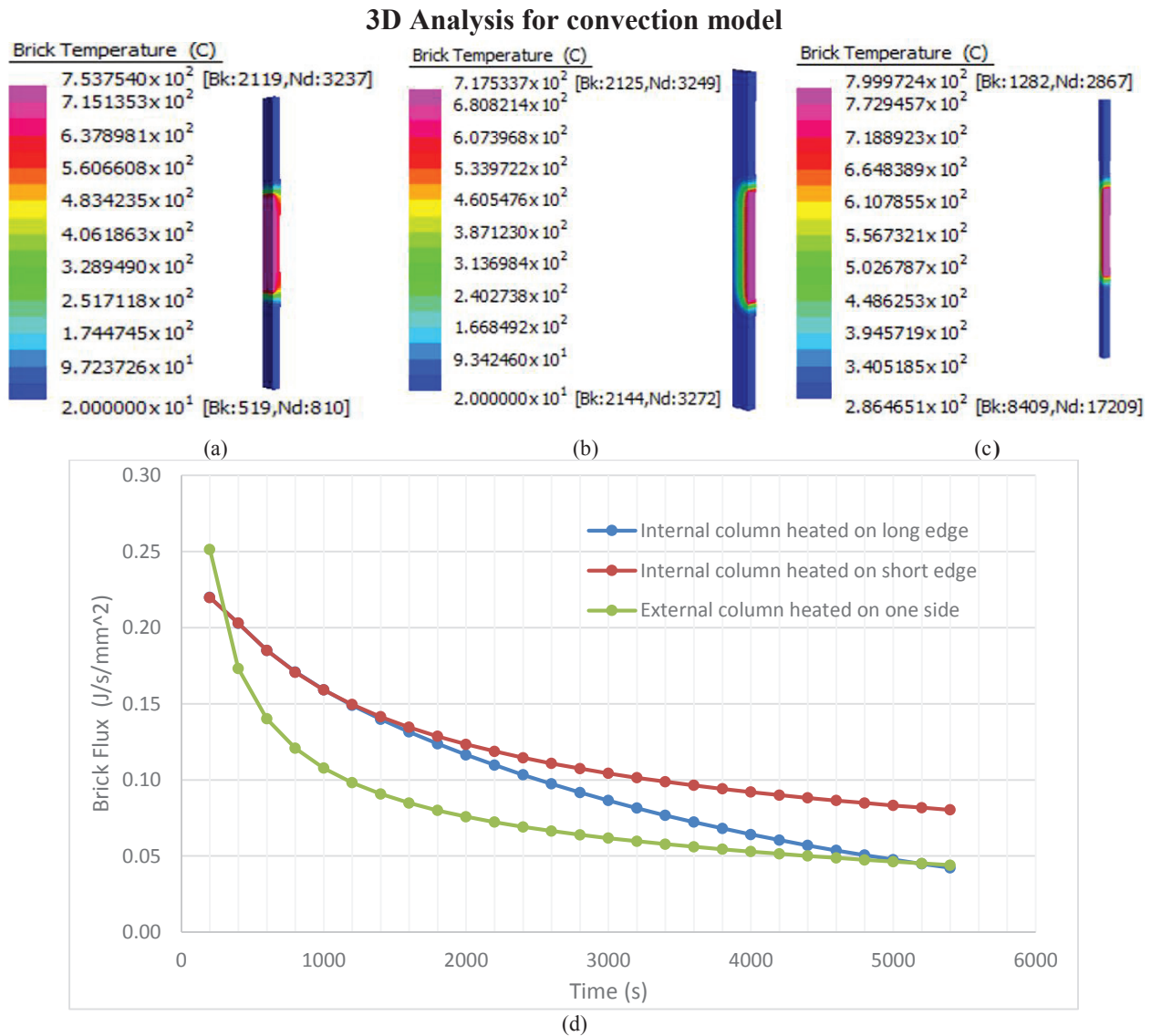


FIGURE 10. (a) Internal column heated on the long edge; (b) Internal column heated on the short edge; (c) External column heated on one edge; (d) Flux in columns

The convection analysis provided a more realistic comparison. In actual situation, fire burnt on jet fuel, the generated heat propagated to the structure via convection. Therefore, there were two stages of energy consumption, energy absorbed by air and transferred from air to structural elements.

From the results, after 1.5 hours, external column had the highest temperature among all which was nearly 800°C. This was due to its hollow cross-sectional geometry. According to the heat capacity of a body with constant volume, for temperature change only,

$$C_v = \frac{\Delta Q}{\Delta T} \quad (4)$$

Where C_v is the heat capacity at constant volume, which is different from the C value in Eq. (1), ΔT is the change in temperature and ΔQ is the amount of heat transferred. Compared with solid column (such as the internal column), the amount of steel volume reacting on convection was less. The difference in the amount of energy provided by air during a same period was neglected compared with the difference in volume. As a result, the increase in temperature was greater than internal columns. For internal columns, the one with long edge exposed to fire ended up with higher temperature. Since the interacting surface was three times bigger, it had more chance to absorb energy from the air.

According to the flux graphs, for all members, the flux decreased with time but the trend was getting smaller. Heat flux in multi-dimensional case is

$$\vec{q} = -k\nabla T \quad (5)$$

Where k is the coefficient of conductivity, T is temperature and ∇ is the gradient operator. The element temperature was increasing by time, therefore, the temperature gradient was reducing caused the decrease in flux. In this project, flux represents the speed of energy assimilation. Reduced flux would slow down the ascending in temperature. That could explain why the temperature changed fast at the beginning but slow in the final stages. Additionally, the highest temperature for each model did not reach 800°C This was also due to the feature of convection. The interaction between steel and air were becoming less active by time and getting more stable in the end. If the time period was long enough, the element temperature would probably become 800°C.

Results Summary

The heat energy could be calculated from the integration of flux and time, times the area of heated faces:

$$\text{Energy} = A \cdot \int_0^{5400} \phi(t) dt \text{ [J]} \quad (6)$$

Where ϕ is flux per second per mm², A is the area of heated column face in mm²; the kinematic energy on one face of column starts from 0 to 1.5 hours was calculated (results shown in the following section).

TABLE 4. Energy results per surface of column

		Face area [mm ²]	Heat Energy	Model heated by Convection	Model heated by Temperature on nodes	
				3D	3D	2D
Core column (300×600mm ² , solid)	Heat on short edge	1.20E+06	$\int_0^{5400} \phi(t) dt$ [J/mm ²]	6.20E+2	7.02E+2	8.48E+2
			Energy [J] /face A· $\int_0^{5400} \phi(t) dt$	7.44E+8	8.42E+8	1.02E+9
	Heat on long edge	3.60E+06	$\int_0^{5400} \phi(t) dt$ [J/mm ²]	5.35E+2	5.60E+2	7.20E+2
			Energy [J] /face A· $\int_0^{5400} \phi(t) dt$	1.93E+9	2.02E+9	2.59E+9
Perimeter column (365×365mm ² , ×9.5mm thk)	Heat on edge (same)	1.46E+06	$\int_0^{5400} \phi(t) dt$ [J/mm ²]	4.04E+2	4.26E+2	5.39E+2
			Energy [J] /face A· $\int_0^{5400} \phi(t) dt$	5.90E+8	6.22E+8	7.87E+8

TABLE 5. Total energy based on assumption

NO. of faces on fire per column	Type of column		No. of Columns	Energy from Convection [J]	Energy from Temperature on nodes [J]	
				3D	3D	2D
Four	External		180	4.25E11	4.48E+11	5.67E+11
	Internal		34	1.82E11	1.94E+11	2.45E+11
Three	Internal	2×Short+1×long	43	1.47E11	1.59E+11	1.99E+11
		2×long+2×short	86	3.95E11	4.19E+11	5.33E+11
One	External		44	2.60E10	2.74E+10	3.46E+10
			SUM	<u>1.17E+12</u>	<u>1.25E+12</u>	<u>1.58E+12</u>

The aircraft fuel energy could be calculated by multiplying the unit petrol energy density by assumed fuel volume:

$$\text{Fuel Energy} = U \cdot i \cdot V \quad [J] \quad (7)$$

Where U is the unit petrol energy density in J/m³, i is the assumed percentage full of petrol container; V is the total volume of aircraft petrol in m³ when the container is full (results shown in the following section).

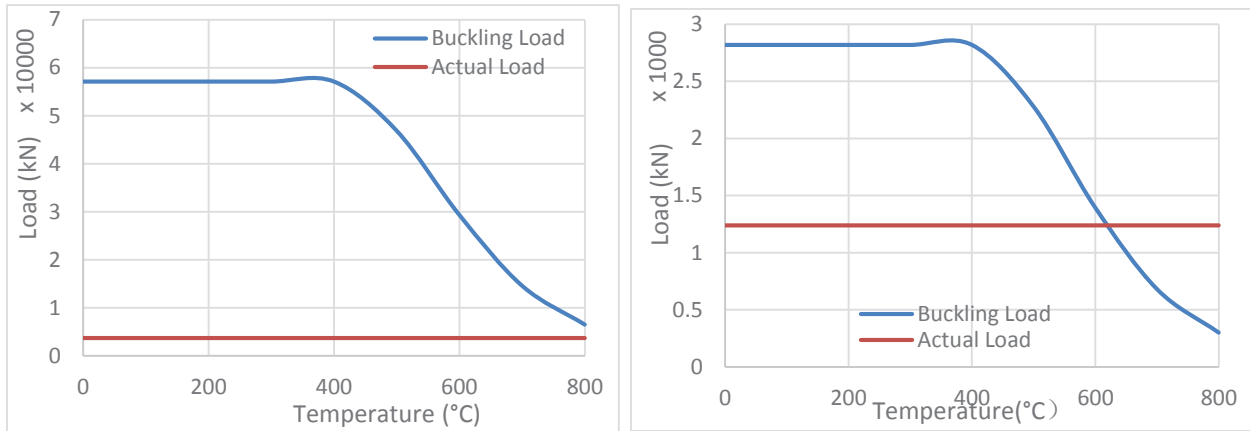
TABLE 6. Energy comparison with aircraft fuel

	Unit energy density (J/m ³)	Volume (m ³)	Assumed % full	Sum of Energy by aircraft fuel [J]
Aircraft petrol	3.53E+10	90	90%	<u>2.86E+12</u>

For all elements, the total energy calculated from 3D models under convection was the smallest, while 2D model gave the biggest value. It can be explained by various reasons. In convection process, the column surface was heated up by the air first, which meant the temperature difference between the surface nodes and the other nodes was less than it was in the fixed temperature cases. Referring to the flux equation, it would lead to a reduction in flux, which was also proved by the flux charts above. Consequently, the energy based on the least flux value was the smallest. In 3D models, the heat propagated through x, y, and z directions at the same time. However, only the flux in main direction was captured and analysed. On the other hand, in 2D models, the heat flowed in one direction only, therefore, the flux was fully recorded. So with the same heat source, 3D models should have smaller flux than 2D models.

Compared with the overall energy from the plane fuel (90 m³ (Eagar and Musso 8-11)), the energy values based on numerical analysis in those three types of models were all a bit smaller than half of the fuel energy. This phenomenon could have been explained in several ways. First of all, the plane flew for a while before it crashed into WCT, therefore, the fuel tank was not full. Secondly, due to the complexity in calculation, heat in the air and surrounding building materials (such as walls and slabs) was ignored. Thirdly, the crashing hole in the building was generated from personal assumptions referring to reality, hence the position and affected area was not that accurate. Additionally, as the fire could travel with air or flue leakage, columns outside of the hole would also be affected, which was not considered in the model. Moreover, the fuel was assumed to be burnt fully, it was hard to achieve in reality due to insufficient oxidizer. Further energy loss in explosion and radiation was excluded as well.

Considering the connection between material property and temperature, the compression capacity of both internal and external columns was calculated based on different temperature conditions. The capacity was compared with the actual loading condition (G+Q) in **FIGURE 11**. (Detailed calculation was in Appendix B.)



(a) Buckling Load in internal column

(b) Buckling Load in external column

FIGURE 11. Buckling Load vs Actual Load

It was clear in the chart, the buckling load in internal column was very big due to its solid cross section. With 800°C, when the yielding stress reduced to 10% of it was in room temperature, the compression capacity was close to the actual load but still a little bit greater than the actual load. In reality, the internal column at the collapsing floors were actually with I cross-section instead of solid rectangular cross-section. Hence the bearing capacity should be way less than it was calculated. The internal columns might fail due to the temperature change. However, for external column, the buckling and actual load intersected at around 620°C. As the maximum temperature on external columns was about 800°C after 1.5h, those columns would collapse within this period. As calculated above, the aircraft fuel could provide enough energy to heat the external column up to about 800°C, so it was sufficient to fail the columns. Because the failure of floors caused the collapse of the whole building (Kotsovinos and Usmani 741-765), as the floors were supported by columns only, the heat flow in columns could lead to the collapse of the building.

As the elements' buckling capacity are still larger than the actual loads, the collapse may due to various reasons other than the reduction in element capacity from fire. The tower under attack was experiencing gravity loads, impact load of aircraft head, fuselage cutting force of aircraft wings, wind force and so on. Portion of main structural elements was damaged by the collision that no longer support the upper stories, and the balanced elements' buckling resistance strength was reduced during the fire. Moreover, the fire can burn the office furniture and other flammable materials, and extend to other stories, hence reduce the element strength of the entire building. As a result of all these factors, the levels damaged or on fire cannot withstand the loads, the entire building collapses.

CONCLUSIONS

In this project, the process of WTC Twin Tower collapse was analysed. Influence of heat through structural elements was illustrated through entire structural model and single element models in 2D and 3D. Heat applied on models was tested in two ways through temperature at nodes and convection. In addition, various loads on structure was calculated and compared with the buckling load capacity of elements. The energy mainly transferred into structural elements where exposed to fire as it was found that the propagation of heat through elements was small enough to be neglected. Then, from single element Strand7 results, it was found most of the heat energy from fire was due to the fuel leakage from the airplane. Despite that 3D models give a more precise analysis, the results from 2D model were closer to the fuel energy. This may due to the uncertainty of fire, imperfections in assumption and the limitations of Strand7. The energy from aircraft fuel could cause a significant reduction in column loading capacity therefore led to the buckling of the structure. The whole structure collapsed as a result of both the buckling collapse of columns during the fire and experiencing gravity loads, impact load of aircraft head, fuselage cutting force of aircraft wings, wind force and so on. Consequently, the entire building collapsed.

ACKNOWLEDGMENTS

We would like to express our very great appreciation to Dr. Peter Ansourian, and Dr. Faham Tahmasebinia for their valuable and constructive suggestions during the planning and development of this project work. Their willingness to give their time so generously has been very much appreciated.

REFERENCES

1. J. Holusha (January 6, 2002). "*Commercial Property; In Office Market, a Time of Uncertainty*". The New York Times. Retrieved November 21, 2008.
2. American Iron and Steel Institute (1964). "*The World Trade Center – New York City*". *Contemporary Steel Design* (American Iron and Steel Institute) 1 (4)
3. Convective Heat Transfer (2016). "*Convective Heat Transfer*", Engineeringtoolbox.com. N.p., 2016.
4. Eagar, Thomas W. and Christopher Musso (2001). "*Why Did The World Trade Center Collapse? Science, Engineering, And Speculation*". *JOM* 53.12 :8-11.
5. Kotsovinos, Panagiotis and Asif Usmani. "The World Trade Center 9/11 Disaster And Progressive Collapse Of Tall Buildings". *Fire Technol* 49.3 (2012): 741-765.
6. Gregory H. Urich, *Analysis of Mass and Potential Energy in the World Trade Center Twin Towers*, B.S. Electrical and Computer Engineering
7. EFCA (May 22-May 25, 2004), Keynote Lecture, *Conference and Gam*, Istanbul, Turkey, Massachusetts Institute of Technology Cambridge, MA, USA
8. Massachusetts Institute of Technology Cambridge, (May 25, 2004), "*Keynote Lecture of EFCA 2004 CONFERENCE AND GAM*". Massachusetts Institute of Technology Cambridge, MA, USA
9. G.H.Urich, "*Analysis of Mass and Potential Energy in the World Trade Center Twin Towers*". B.S. Electrical and Computer Engineering.
10. Irfanoglu, Ayhan and Christoph M. Hoffmann. "*Engineering Perspective Of The Collapse Of WTC-I*". *J. Perform. Constr. Facil.* 22.1 (2008): 62-67.
11. Federal Insurance and Mitigation Administration, 2002. *World Trade Center Building Performance Study*. Washington: Federal Emergency Management Agency.
12. 911research net (May 8, 2016). "*World Trade Center Demolition.*", Retrieved from <<http://www.911research.wtc7.net>>
13. 911research net (May 8, 2016). "*Collapse of the World Trade Center Towers*". Retrieved from <<http://www.911research.wtc7.net>>
14. Ken Doc (May 8, 2016), "*15 hard facts about 911*". Retrived from <<https://kendoc911.wordpress.com/>>
15. 911research net (May 8, 2016). "*9-11 research WTC Master Plan*". Retrieved from <<http://www.911research.wtc7.net>>
16. "Convective Heat Transfer". Engineeringtoolbox.com. N.p., 2016. Web. 7 June 2016
17. "Collapse Of The World Trade Center". Wikipedia. N.p., 2016. Web. 4 June 2016.

APPENDIX A – Actual Floor levels

TABLE 1. Floor height at each level [data from 911 Research Net, access in 2016]

	sub-level no 4-5	sub-level no 1-3	service level 1	1-concourse	2-6-storage
Height (m)	3.53	3.05	4.88	6.71	3.53
	7-lower mechanical	8-upper mechanical	9-39	40-44 sky lobby	45-73
Height (m)	4.27	3.05	3.66	4.27	3.66
	74-76 upper mechanical	77 upper esc floor	78 sky lobby	79-105	106 typical
Height (m)	4.27	3.66	4.27	3.66	4.27
	107 restaurant	108 lower mechanical	109 upper mechanical	110 roof to top of roof panels	
Height (m)	5.33	4.27	3.56	4.67	

APPENDIX B – Load calculations

Buckling load (External column in room temperature):

$$A = 13510 \text{ mm}^2, I_x = 2.85 * 10^8 \text{ mm}^4, I_y = 2.85 * 10^8 \text{ mm}^4,$$

$$E = 200\text{GPa}, L = 4\text{m}, f_y = 270\text{MPa}, k_f = 0.9$$

$$r_x = r_y = \sqrt{I/A} = 145\text{mm}$$

Nominal section capacity N_s (AS4100 6.2)

$$N_s = k_f * f_y * A = 3283\text{kN}$$

Nominal member capacity N_c (AS4100 6.3)

$$\lambda_x = \left(\frac{L_{ex}}{r_x} \right) \sqrt{k_f \frac{f_y}{250\text{MPa}}} = 27 = \lambda_y$$

$$\alpha_b = 0$$

$$\lambda = \lambda_n + \alpha_a \alpha_b = 27$$

$$\eta = 0.0032(\lambda - 13.5) = 0.045$$

$$\xi = \frac{\left(\frac{\lambda}{90} \right)^2 + 1 + \eta}{2 \left(\frac{\lambda}{90} \right)^2} = 6.23$$

$$\alpha_c = \xi \left[1 - \sqrt{\left(1 - \left(\frac{90}{\lambda \xi} \right)^2 \right)} \right] = 0.953$$

$$N_c = \alpha_c N_s = 3130\text{kN}$$

Assume $\varphi = 0.9$,

$$\therefore \varphi N_c = 0.9 * 3130 = 2817\text{kN}$$

TABLE 2. Capacity reduction for external columns [Irfanoglu and Hoffmann, pp 62-67]

T	E(Mpa)	fy(Mpa)	$\phi N_c(kN)$
0	200000	270	2817
100	198000	270	2817
200	180000	270	2817
300	160000	270	2817
400	140000	270	2817
500	120000	216	2277
600	60000	130	1393
700	26000	62	681
800	20000	27	300

Calculations for the internal columns followed the same sequence, and were done by excel. The results were listed in table below.

TABLE 3. Table of results

λ_y	48	λ_x	16	α_b	0	η	0.112	ξ	2.46	α_c	0.87
$N_s(kN)$	72900		$N_c(kN)$	63421		$\phi N_c(kN)$	57079				

TABLE 4. Capacity reduction for internal columns [Irfanoglu and Hoffmann, pp 62-67]

T(°C)	E(Mpa)	fy(Mpa)	$\phi N_c(kN)$
0	200000	270	57079
100	198000	270	57079
200	196000	270	57079
300	190000	270	57079
400	190000	270	57079
500	168000	230	46847
600	152000	197	29329
700	128000	97	14606
800	100000	49	6524

Design load per area

TABLE 5. Summary of dead load [Gregory H. Ulrich, 2016]

	Foundation	Structural steel /floor:	Concrete	Superimposed
DL	4,330 tons	91.6 tons (top)	Above grade (Floor 1-110): 467 tons outside, 242 tons inside core	145 tons above grade
		1,464 tons (bottom)	Below grade (Floor B1 – B6): 1315 tons	7.92 tons below grade
Max. DL pressure	<u>28.7 kN/m²</u>			

TABLE 6. Summary of live load [Gregory H. Urich, 2016]

LL = larger of	Most predominate	¼ the design load
	244 kg/m ²	56,177 tons in sum
Max. LL pressure	4.35 kN/m ²	
Maximum design load	1.2G + 1.5Q = 1.2 x 29.0 + 1.5 x 4.35 = 41.33 kN/m ²	

Design load applied on each column:

TABLE 7. Calculation spreadsheet of design load applied on each column

<u>DL</u>						
Steel	7797	short tons	69365.568	kN		
		Numbers	Loads			
	Ext` col	240	<u>135.8409</u>	kN		
	Core col	47	<u>782.20747</u>	kN		
Concrete	outside light concrete					
		Area	28,225	sq ft		
		Thk	4	inch		
		Density	150	lb/ft ³		
	thus	Mass	1411250	lb	6277.551	kN
	hence	Ext` col	<u>706.22451</u>	kN	x27 floors	
	inside normal concrete					
		Area	11,745	sq ft		
		Thk	5	inch		
		Density	150	lb/ft ³		
	thus	Mass	734062.5	lb	3265.272	kN
	hence	Int` col	<u>1875.7945</u>	kN	x27 floors	
Superimposed DL	total	4000	short tons	35585.77	kN	
	outside	240	No.	<u>69.68881</u>	kN	
	inside	47	No.	<u>401.2864</u>	kN	
<u>Sum of DL</u>	outside	912	kN			
	inside	3059	kN			
<u>Sum of LL</u>	outside	8830	short tons	<u>327</u>	kN	
	inside	3409	short tons	<u>645</u>	kN	
1G+1Q	outside	<u>1239</u>	kN			
	inside	<u>3705</u>	kN			

APPENDIX C – Summary of changes

TABLE 8. Summary of final changes based on lecturer & tutors reviews

Changed parts	Description of changes
Gramma & Spelling	all marked out points in review and other grammar/spelling mistakes corrected
text/ symbol format	all texts changed to identical format, x changed to multiple symbol, equation number format: "1)" changed to "(1)"
Graphical Abstract	Updated table with units and proper scientific notation, add charts
Introduction	problem and the aim
Table 4	units and proper scientific notation
Figure 1 & 2	Specified the plan and elevation view are acting as introduction purpose
Structural model	added the substantial elaboration
Governing equations	Eq. (3) & (5) are removed, the calculation of q is explained, variables are defined
Equation 6	Cv value explained
Results summary	The collapse of the building in connection with column heat flow is explained.
Conclusion	included entire achievements of the current report
Reference	added extra reference for numerical analysis part
Appendix	added Appendix C: summary of changes